Thermometry below 1K

Sergey Sheludyakov

Master's thesis

Physics

Department of physics and astronomy

Univeristy of Turku

Supervised by:

Dr. Sergey Vasiliev

Prof. Kurt Gloos

University of Turku

Department of Physics and Astronomy

Sheludyakov, Sergey: Thermometry below 1K

Master's thesis, 73 pages

Physics

October 2011

Progress in low temperature physics requires new more precise and practically convenient thermometry methods. The significant change in properties of matter at low temperature limits an application of conventional high-temperature devices and makes them totally ineffective below 1K. Nevertheless a number of primary and secondary thermometry methods are available. Although a dozen of comprehensive reviews on thermometry below 1K exist, there is a lack of information about the most recently developed methods and advances in conventional techniques.
The introductory part of the thesis elucidates physical principles and the most recent innovations in thermometry below 1K. The main emphasis is put on the ^{3}He melting curve thermometry, superconductive fixed-point devices and resistance thermometry. Resistance thermometry and especially RuO_2 sensors are known to be the most suitable and popular for temperature measurements below 1K. They can operate down to 10-20mK, have a good interchangeability for sensors from the same batch, moderate magnetoresistance and low price. At the same time, commercially available uncalibrated resistance thermometers cost about several hundred dollars for a bare chip whereas calibration increases their price up to one order.

In experimental part of the work, temperature measurement in a range from 600mK down to 6mK was carried out by three separate thermometers: ^{3}He melting curve thermometer, SRM 768 Fixed-point device and RuO_2 resistance thermometers of various design and packaging. A number of precautions were fulfilled in order to provide a proper performance for thermometers such as magnetic shielding of FPD and electrical grounding and shielding for resistance sensors. A new perspective 16-chip RuO_2 Dale RCW575-based resistance thermometer for application from several Kelvin down to 15mK was developed. This sensor can also be used even beyond this range up to 30K with reduced accuracy. Low price, reliable thermal contact, ease of packaging, interchangeability of sensors from the same batch and good reproducibility upon thermal cycling make it a very convenient thermometer for routine measurements. The thermometer was calibrated against ^{3}He melting curve thermometer and SRM-768 Fixed-point device. Calibration acquired by these two methods coincided in the whole range of measurement within error bars. As a result, our sensor can be used in a wide spectrum of low-temperature laboratories and successfully compete with available commercial resistance thermometers.

Key words: Thermometry, ^{3}He melting curve thermometry, Superconductive fixed-point device, resistance thermometry.

Acknowledgements

I would like to express my sincere gratitude to Dr. S.A.Vasiliev for support, vital discussions and supervision of the thesis. I also would like to thank Dr. J.Ahokas, Mr. O.Vainio and Dr. S.T.Boldarev for their enormous help in experimental part of work and tolerant introducing into world of low-temperature physics and practical cryogenics.

Contents

Introduction

Rapid progress in low-temperature physics is tightly bound to the advances in deep cooling. At the same time, a proper interpretation of any low-temperature experimental data requires an accurate temperature measurement. As it is known, an internationally adopted scale, ITS-90, spreads only down to 0.65K which keeps a lower range uncovered, whereas plenty of important researches are carried out at substantially lower temperatures. However, significant changes in properties of matter make conventional thermometry means, such as gas, vapor or platinum resistance thermometers not any more applicable [1]. Therefore, thermometry must rely mainly on other physical qualities of condensed matter, such as magnetic or nuclear properties, whose characteristic energies lie in the millikelvin range [2]. Additional problems related to poor thermal contact due to Kapitza boundary resistance (especially below 10mK), thermometer susceptibility to electrical or magnetic interference, make temperature measurements of the same difficulty as cooling itself [3].

A low-temperature thermometer should satisfy a number of requirements: wide operating range with simple and monotonic dependence on temperature, low self-heating, fast response and measurement time, ease of operation, immunity to external parameters (in particular, magnetic field), small size and small thermal mass [4]. Plenty of techniques with various physical backgrounds are exploited. Primary thermometers, or those which do not need a preliminary calibration, are noise thermometers using SQUIDs, gamma-ray anisotropy (nuclear orientation), Coulomb blockade, shot noise, second-sound or osmotic pressure in ^{3}He–^{4}He mixtures. The others, such as paramagnetic (Curie law) susceptibility of dilute salts, magnetic alloys or nuclear spins; ^{3}He melting curve, NMR and resistance thermometers, are secondary and should be calibrated before use.

Unlike the higher temperature devices, all sub-Kelvin range thermometers have their advantages and disadvantages, but none has all the necessary features for defining an International Temperature Scale: sensitivity, reproducibility, practicality (convenience of realization or calibration), and universality.

The majority of thermometers are suitable only as secondary devices, and the ranges of usefulness of many are limited. However, a thermometer using melting pressure of ^{3}He, which was first proposed by Scribner and Adams in 1970 [5], almost entirely meets the requirements. ^{3}He is a well-defined substance with sufficient availability, and the melting pressure, p_m, is sensitive to temperature over most of the range of interest. Provisional Low Temperature Scale PLTS-2000 based on p_m-T relation for the range 0.9mk-1K was formally adopted in October 2000 [6], [7]. PLTS-2000 has only a provisional status because of differences in opinions regarding the p_m–T

relationship at the lowest temperatures. These differences have not yet been resolved. Moreover, a discrepancy between ITS-90 and PLTS-2000 in the overlap region led to intermediate PTB-2006 scale used to make a smooth transition from one scale to another.

Although ^{3}He melting curve thermometry is much more convenient than primary methods, it still does not suit for everyday use. However it may provide a reliable reference for calibration of other secondary devices, such as resistance thermometers. As a result, calibration of a secondary thermometer for routine measurements is an important experimental task. The most reliable calibration can be achieved in case if several thermometry means are used simultaneously.

Although a number of comprehensive reviews on low-temperature thermometry exists, the most recent innovations in the conventional methods as well as new means, such as the shot noise thermometry are discussed there only in brief. That is why the first aim of the thesis is a detailed review of modern low-temperature thermometry from 1K down to several mK. The emphasis is made on the ^{3}He melting curve method, superconductive fixed-point devices and resistance thermometry which we used in the experiment.

It was of primary interest for us to investigate the characteristics of RuO_2 RCW575 Dale chips from the large batch we have recently purchased. The main practical characteristics of resistance chips such as operational range, interchangeability of chips form the same batch and reproducibility upon thermal cycling are studied.

Moreover, a new resistance thermometer design with sixteen RuO_2 chips had been developed and it was important for us to clarify whether this innovation gives any advantage in the sensor performance at low temperatures.

A number of precautions were fulfilled to provide a proper performance and coincidence of MCT and FPD in the whole range of measurements. A 16-chip RuO_2 resistance thermometer was calibrated against MCT and showed reliable performance at least down to 25mK within error not larger than 2%. Reliable thermal contact, ease of manufacturing and low price makes it competitive with other available commercial resistance thermometers. The majority of commercial dilution refrigerators operate down to 40-50mK although the best units are able to reach temperatures of a few mK. Therefore, our calibrated sensor may also be used in a wide spectrum of low-temperature laboratories where a range of interest is limited by a few tens of mK. As a result, a new reliable temperature reference for routine measurements with a resistance thermometer was established.

This thesis consists of three chapters: the review of modern low-temperature scales, the review of modern thermometry methods below 1K and experimental results. The first chapter includes the guideline of international temperature scale ITS-90 and provisional low-temperature scale PLTS-2000.The second chapter is devoted to the most important and widely used primary and secondary

thermometry methods for measurements below 1K. Physical backgrounds, recent innovations as well as the main experimental principles are described for each method. Primary methods described are nuclear orientation thermometry, Johnson noise thermometry, Coulomb blockade thermometry and shot noise thermometry. More specific and rarely used methods, such as osmotic pressure thermometry and Mossbauer thermometry are considered in brief. The secondary methods reviewed are ^{3}He melting curve thermometry, superconductor fixed-point devices and resistance thermometry. The other methods, like Curie law magnetism thermometry and semiconductor non-resistance thermometers are only shortly described. The third chapter elucidates the main stages of the experiment: preparation, temperature measurement and data analysis. As a result we present convenient fitting functions for calibrations of RuO2 resistance thermometers, which can be suggested for wide use in low-temperature community.

Chapter 1. Low-temperature scales.

1.1 ITS-90

Temperature is one of the most important among physical entities, but our ability to measure temperature accurately is much less than that for time, frequency or voltage. As it is known, all physical quantities can be separated into two categories: extensive quantities such as length, energy or mass which have a property of additivity, and intensive quantities that do not have such a property (density, pressure and temperature). It is surprising that people have been almost totally ignorant about heat and temperature until 18th century and the main difficulty associated with the concept of temperature results from its being an intensive quantity [8].

The definition of any temperature scale can be obtained from the Carnot cycle which is based on the Second law of thermodynamics.

$$\oint T^{-1} dQ = 0,$$

in other terms $\frac{T}{Q} = const$, where Q is the amount of thermal energy transferred in the process.

Carnot cycle or any other process gives the temperature only as a ratio, whereas the absolute values in a temperature scale should be fixed by a definition. By using an absolute zero as a starting point one can in principle carry out experiments which are related to the Carnot cycle to establish the temperature scale. In practice, a number of fixed temperature points are established and further used to calibrate the chosen thermometric method, which makes use of some temperature dependent property of a suitable material in the desired temperature range [9].

A commonly adopted scale, ITS-90, serves as an approximation of the thermodynamic temperature and spreads from 0.65K to the highest temperature practically measurable in terms of the Planck radiation using monochromatic radiation. One Kelvin, a unit of thermodynamic temperature, has been defined as a 1/273.16 fraction of the water triple point absolute temperature.

ITS-90 includes a number of ranges and sub-ranges and 17 fixed (triple and melting) points. Four instruments are used to define temperature: ^{3}He and ^{4}He vapor pressure thermometer (0.65-5K), ^{3}He and ^{4}He constant volume gas thermometer (3.0-24.5561K (triple point of neon)) and platinum resistance thermometer (13.8033(triple point of hydrogen) - 1234.93K (triple point of silver). For each range the most suitable polynomial is offered. Several of these sub-ranges overlap however these differing definitions have equal status. ITS-90 has been constructed in such a way that, throughout its range, for any given temperature the numerical value of T_{90} is a close approximation to the numerical value of T according to best estimates at the time the scale was adopted [1].

There is still substantial work going on to improve the ITS-90 and check its thermodynamic consistency. Moreover, a work to provide a new definition of Kelvin and relate temperature to fundamental constants like it is done for voltage or frequency is in process.

1.2 Provisional Low Temperature Scale PLTS-2000.

ITS-90 provides a reference only down to 0.65K, whereas a lower temperature range is kept uncovered. As a result, provisional low temperature scale was adopted in October 2000 after long international discussions. The melting pressure of ^{3}He serves to provide a basis for temperature measurement in range from antiferromagnetic transition in solid ^{3}He ($T_{Néel}$=0.902mK) up to 1K.

Point	pm/MPa	T_{2000}/mK	ΔT/μK	δTr/μK
Minimum	2.93113	315.24	360	10
A	3.43407	2.444	48	0.7
A-B	3.43609	1.896	38	2.8
Néel	3.43934	0.902	18	1.1

Table 1. Values of pm/MPa and T_{2000}/K for the ^{3}He melting-pressure features, with estimated standard uncertainties (1-sigma) with respect to thermodynamic temperature, ΔT/μK, and the standard uncertainties of the current best realization, δTr/μK [2]

The melting pressure of ^{3}He is a thermodynamic property that is usable over a very wide temperature range, almost unsusceptible to ^{4}He impurities and can be relatively easily realized in laboratories around the world. In addition, liquid and solid ^{3}He provide four unique fixed points along the melting curve: minimum of the melting pressure at P_{min}=2.93113 MPa, two low-temperature transitions: to the superfluid A-phase and from A- to superfluid B-phase and nuclear antiferromagnetic transition in solid ^{3}He.

The adopted equation for PLTS-2000 is as follows.

$$P = \sum_{i=-3}^{+9} a_i T^i$$

a_{-3}=−1.3855442·10^{-12}	a_{-2} = 4.5557026 ·10^{-9}	a_{-1}=−6.4430869·10^{-6}	a_0 = 3.4467434 · 10^0	a_1=−4.4176438 · 10^0
a_2 = 1.5417437 · 10^1	a_3 =−3.5789853 ·10^1	a_4 = 7.1499125·10^1	a_5=−1.0414379·10^2	a_6 = 1.0518538 · 10^2
a_7=−6.9443767 · 10^1	a_8 = 2.6833087 · 10^1	a_9 =−4.5875709 ·10^0		

Table 2. PLTS-2000 polynomial coefficients for the ^{3}He melting curve

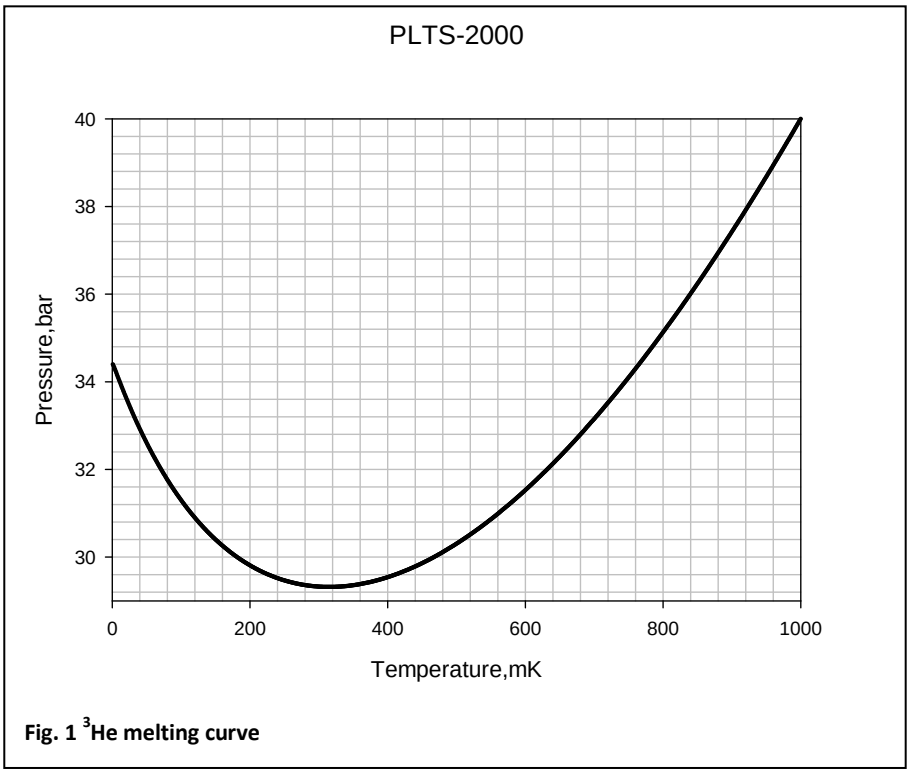

Fig. 1 ^{3}He melting curve

On the other hand PLTS-2000 has only a provisional status due to disagreement in the values of the low-temperature fixed points T_A,$T_{A\text{-}B}$ and T_N. The compromise was found as an average of several scales obtained by groups in Berlin (PTB), Florida (UF) and NIST[1] with a help of noise and nuclear orientation thermometers. However, the disagreement is not still resolved and a 2% divergence in the lower part of a polynomial exists that is why the scale has only a provisional status [2].

Although PLTS-2000 is not defined below T_N, ^{3}He melting pressure scale may be extended down to about 0.5mK by using equation given by Ni et al. [10]. They used ^{60}Co nuclear orientation thermometry as a primary reference for temperature and found that the melting pressure can be represented as a polynomial

$$P(T) - P_N = B_0 - B_1 T^4$$

with B_0=0.1987kPa and B_1=0.2611kPa/(mK)^4.

PLTS-2000 and ITS-90 overlap from 0.65 to 1K, where in principle they should coincide. Comparison of ^{3}He vapor pressures and melting pressures had been performed at PTB and it was found that the difference between two scales rises from about 0.6mK at 1K to 1.5mK at 0.65K. It is recommended to use melting pressure (PLTS-2000) for preference. A smooth crossover was proposed by PTB in 2006 (PTB-2006) for the range of 0.65-3.2K which is used to erase the discrepancy between ITS-90 and PLTS-2000 in the overlapping region. Temperatures according to PTB-2006 are equal to those of PLTS-2000 in the range from 0.65K to 1K. The temperatures T_{2006}

[1] Physikalisch-Technische Bundesanstalt (Germany), University of Florida (USA), National Institute of Standards and Technology (USA)

in the range from 1K to 2K are thermodynamically sound as they are calculated using thermodynamic vapor-pressure relations and are in agreement with T_{2000} at 1K and with T_{90} at 2K. The ^{3}He vapor-pressure polynomial of PTB-2006 has exactly the same definition range and form as that of the ITS-90, users can replace the coefficients and there is no need for a correction function [11]. Where it is desired to use vapor pressures, new more accurate equations [12] are now available as alternatives to the equations specified in ITS-90.

Chapter 2. Review of thermometry below 1K.

Review of primary thermometry.

Primary thermometers are based on the well-defined theoretical knowledge and may provide a standard for secondary methods. There are several types of such devices that can be applied to the range below 1K where the use of conventional "high-temperature" thermometers is strongly limited. The capability of the constant volume gas thermometer (CVGT) is limited by liquefying of He, whereas the ^{3}He saturated vapor thermometer can work, in principle, down to 0.3K, where its vapor pressure is only 250Pa [14]. For lower range a number of other methods can be used. Some of them exploit Boltzmann population of magnetic sublevels where temperature is contained in a factor of $\exp(\Delta E/k_B T)$, some are based on electrical or thermodynamical properties of matter. The nuclear orientation (NOT) thermometer relies on the temperature dependence of γ-ray spatial radiation anisotropy, Johnson noise thermometers use the Nyquist relation for the voltage appearing in the resistive element due to Brownian motion of conduction electrons. Recently developed Coulomb blockade thermometers utilize the temperature dependence of electrical conduction in arrays of metal-insulator-metal junctions. The shot noise thermometer is based on the temperature dependence of the noise spectral density crossover from Johnson to shot noise regime in a single tunnel junction. Osmotic pressure thermometry employs temperature dependence of osmotic pressure in ^{3}He/^{4}He dilute mixtures. However, the use of primary thermometers is practically inconvenient because of slow response time and limited operation range. Moreover, primary thermometers require special equipment and knowledge and therefore are available mostly in National standard or metrological laboratories.

2.1 Nuclear orientation thermometry.

A radioactive sample decays via emission of a α,β- or β+ particle, or by a capture of an orbital electron. A by-product nucleus of a stable element relaxes to the ground state emitting a γ-quant (Fig. 2). If one deals with an ensemble of radioactive nuclei, the mean value for emission probability is equal for all directions. On contrary, in a case if nuclei are oriented (e.g. by magnetic field), radiation anisotropy for each of 2I+1 nuclear sublevel can be observed. The anisotropy is a result of the Boltzmann population of sublevels and therefore depends on temperature [3].

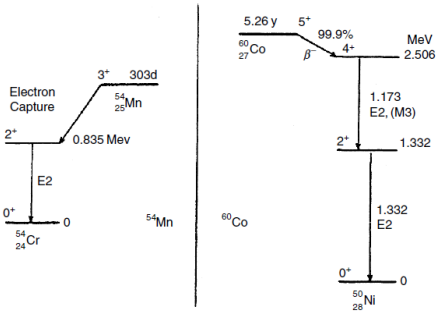

Fig. 2 Energy level diagrams for ^{54}Mn and ^{60}Co (slightly simplified) [9]

The normalized intensity of γ-quant emission

$$W(T,\Theta) = 1 + \sum_{k=2,4} B_k(T) u_k F_k Q_k p_k(cos\Theta)$$

Θ – angle between the γ-quant emission and orientation axis; $p_2(cos\Theta)$, $p_4(cos(\Theta))$ – Legendre polynomials, u_kF_k are the numbers dependent on the transition, $B_k(T)$ – coefficients connected with initial spin system orientation. Q_k – experimental correction dependent on the detector type and solid angle where the radiation is registered [3]. For ideal detector, Q_k=1. If all nuclear and hyperfine properties of a nucleus are known, it can be used as a primary thermometer. As it can be seen, the most significant temperature dependence of radiation anisotropy corresponds to $\Theta=0$ (and $\Theta=90$), $\frac{\partial W(T,\Theta)}{\partial \Theta} = 0$ (Fig. 3,Fig. 4).

Detector should be placed along the direction where the change of γ-ray intensity is maximal as a function of temperature. The background and geometry correction is carried out at high temperature when $W(T,\Theta)=1$.

The most widely used isotopes for NOT are ^{60}Co and ^{54}Mn with the half-lives of 5.2 years and 300 days respectively [3]. Their nuclear and decay parameters are well-known and life times at γ-active levels are small. There are a number of other suitable radioactive isotopes but a lack of information about their decay characteristics degrades them to secondary devices [8].

The nuclear sublevel splitting may have various physical background: either magnetic hyperfine interaction (^{60}Co) or mixed magnetic-electric HFI for heavy rare-earth as well as pure quadrupole interaction, e.g.^{190}IrRe (QI-NO). Pure brute force (BFO) thermometers have also been suggested, for example ^{54}Mn in Al. The advantage of the last two types of NO thermometers is that they can be used at very low temperatures, in 1mK region; the BFO devices have an adjustable temperature range, but applied magnetic field is required, while QI-NO thermometers have a fixed temperature range for a given system but require no external magnetic field [13].

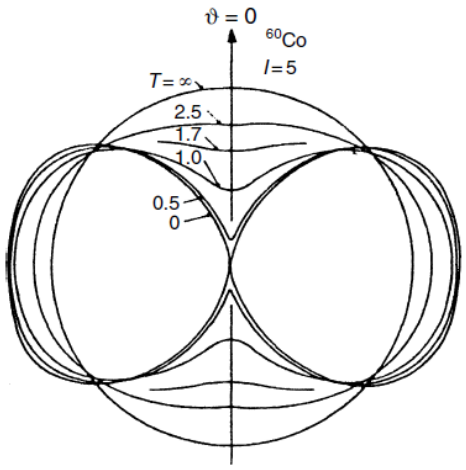

Fig. 3 Angular radiation pattern of ^{60}Co for several values of $k_BT/\mu\mu_B B$ [9].

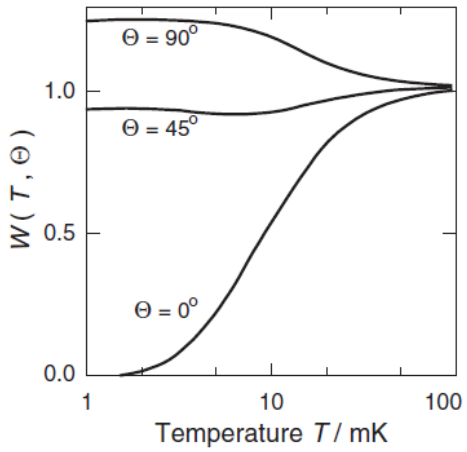

Fig. 4 Emission probability $W(T,\Theta)$ as a function of temperature for three different angles Θ. Calculated for ^{60}Co in a ^{59}Co matrix [9].

The cobalt thermometer recruits ^{60}Co nuclei produced by neutron activation of the only stable cobalt isotope, ^{59}Co, single crystal that is spontaneously magnetized [8]. The main drawback of a ^{60}Co thermometer is self-heating resulting from the β-decay and γ-ray emission that may lead to errors, especially for temperatures below 20mK. That is why the use of ^{54}Mn is preferable because it decays via the electron capture and produces less heating [3]. In fact, thermometers based on this isotope have been used down to tens of μK without noticeable heating [13]. Another solution may be a use of less active sample that on the other hand increases the counting time. The disadvantage of a Mn thermometer is that a radioactive isotope cannot be used in situ and should be introduced into a ferromagnetic host matrix (Co, Ni or Fe single crystal). For these purposes radioactive element is deposited on matrix material and then diffuses into it at high temperature. ^{54}Mn in Fe thermometer requires an external magnetic field of 1T to orient the matrix domains that leads to effective field of 10-30T for dopant atoms [14].

Another disadvantage of nuclear orientation thermometers is a limited range of sensitivity (from a few mK to several tens of mK). Moreover, the method relies on statistical measurements that also may cause an additional error.

$$\frac{\Delta T}{T} = (2/n)^{1/2},\ n \text{ is a number of counting pulses}$$

Measurement is a time-consuming process: one point can be acquired from several minutes to half an hour for weak samples. At the same time, high sample purity is not required and a reliable thermal contact (metal-to-metal) to the object under measurement can be established. Energy of emitted γ-quants is enough high to penetrate through the cryostat walls and no special windows is needed (like for Mössbauer thermometry). A nuclear orientation thermometer has also a small size, low specific heat and does not require any electrical wires going to the cryostat. The most widely

used ^{60}Co in ^{59}Co thermometer allows temperature measurements in the range from a few mK to 50mK.

The use of radioactive samples, large acquisition time per point and other practical inconveniencies allow using them only in specialized metrological laboratories. The accuracy of a method depends on the acquisition time and 1% uncertainty requires from several minutes to half an hour per point. NOTs are mostly suitable for calibration of secondary systems like ^{3}He melting curve thermometers. However a high precision and possibility of working in a few mK range makes a nuclear orientation thermometer a very important means for primary measurements.

2.2 Johnson noise thermometry.

The Brownian motion of conduction electrons in metal leads to statistical fluctuations of voltage across a resistor. This phenomenon was predicted by Einstein (1906), first experimentally observed by Johnson (1927) and then theoretically explained by Nyquist (1928) [15]. The RMS (root mean square) Johnson (thermal) noise voltage can be estimated by the formula

$$d < v^2(f) >= 4k_B TRdf \text{ (only for } f \ll \frac{k_B T}{h})$$

At 1K $k_B T/h \approx 20$ GHz and it is not a serious limitation in practice. However, if $\frac{k_B T}{h} \to 0$, a generalized quantum mechanical relation should be used [9].

Only fundamental constants are needed to calculate temperature and therefore the noise thermometry can be used in a primary mode if all other parameters are known. The main experimental difficulty appears from the extreme weakness of the effect, for example, at R=1kOhm, df=1kHz and T=10mK, the corresponding "useful noise" power is only 10^{-22} W [9], that is why none of conventional semiconductor amplifiers can be used. The low-temperature noise thermometry became possible only after SQUIDs with their ultra-low intrinsic noise have been invented.

Resistive SQUIDs (or so-called V-devices) have been first proposed by Zimmerman et al. [16]. They imply a noise resistor to be directly connected to the Josephson junction and the AC-Josephson effect is in use. There are several possible designs, i.e. an RSQUID by Menkel et al. contained an evaporated silver film (R=$10^{-5}\Omega$) noise resistor and two shunted (R=1Ω) junctions connected in parallel [17]. The SQUID acts as a very precise voltage-to-frequency converter. Relation between frequency and voltage is as follows: $f_J = \frac{2e}{h}V$. Since the Josephson oscillations cannot be measured directly, the signal is amplified using a resonance circuit. Afterwards frequency that is measured by a counter and temperature is determined by measuring the variance σ^2_f of the oscillation frequency [15].

$$T = (\frac{h}{2c})^2 \frac{\sigma_f^2 \tau}{2k_B R},\ \tau \text{ is a frequency counter gate time}$$

In practice junction shifts the frequency to the megahertz region. For example, 484MHz corresponds to 1μV noise voltage [9]. This method allows working in a primary regime because the result does not depend on the circuit parameters (bandwidth and gain). Total uncertainty in the temperature measurement is about 0.1% at 10mK and 1% at 1mK [9].

The second type is a so-called current sensing (I-device) noise thermometer, first realized by Webb et al. [18]. A noise resistor is inductively coupled to a SQUID which works as a very accurate low-noise amplifier for a signal generated in the input coil. The rms of the noise current in this case is

$$< I^2 >= \frac{4k_B T}{R}(\frac{1}{1+(2\pi f\tau)^2})\Delta f$$

with $\tau = L_{tot}/R$ being time constant. L_{tot} denotes total inductance of the input circuit and bandwidth. The noise resistor is usually chosen to be small (0.1-1mΩ) to couple it to the SQUID.

Bulk resistive RF-SQUIDs with one Josephson junction have been used in early works however two Josephson contact DC-SQUIDs are more widespread nowadays. They have a lower noise and higher sensitivity that leads to a more accurate temperature measurement [4]. The SQUID noise can be represented by the energy equivalent sensitivity, which corresponds to a minimal current possibly detected in the input coil. It is expressed in units of the Planck constant, *h*, and is about *500h* for commercially available SQUIDs and *~10h* for the best devices [4]. The equivalent noise temperature, or amount of noise that added by an amplifier is expressed as $T_N \approx \frac{\varepsilon_c}{2k_B\tau}$. It is of order of K for semiconductor amplifiers and μKs for SQUIDs. The rough estimate of the precision in a given measuring time t_{meas} can be evaluated by relation: $\frac{\Delta T}{T} \approx (\frac{2\tau}{t_{meas}})^{1/2}$ which is independent of temperature as long as $T>>T_N$ [19]. Counting time of about 10s may provide 1% precision at T=1mK [9].

A novel non-wired DC-SQUID thermometer, so-called magnetic field fluctuation thermometer (MFFT), has been recently proposed [20], [21]. In the I-device a metallic temperature sensor with resistance R is directly inserted into the superconducting input loop of the SQUID, whereas in a case of MFFT, no electrical connection to the input loop of the SQUID is required (Fig. 5, Fig. 6). The noise current inside the temperature sensor causes magnetic-field fluctuations above its surface. These fluctuations are inductively detected by a SQUID-magnetometer as a thermal flux noise. A test resistor is made of very pure non-magnetic material, i.e. copper with a very low ferromagnetic impurity (not more than a few ppm of Fe impurity) to avoid errors. Engert et. al [20] used their MMFT thermometer from 4.2K to 7mK with less than 1% uncertainty and counting time of 10s.

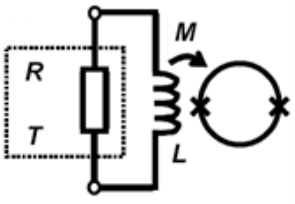

Fig. 5 I-device [20]

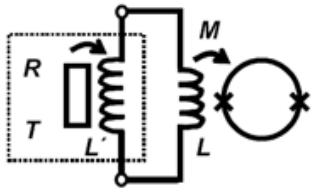

Fig. 6 MMFT [20]

As a result, a Johnson noise thermometer can be used down to 1mK with an uncertainty of 1%. An upper limit for the SQUID-noise thermometry is defined by the junction critical temperature. A number of practical difficulties, such as detection of very weak signals, large counting time, high sample purity (for I-devices and MMFT), precise information about gain and bandwidth restricts from using them in daily experiments. However they are successfully used along with NOTs to build a thermometric fundament for secondary devices.

2.3 Coulomb blockade thermometry.

The Coulomb blockade method is one of the most promising recent advances in primary thermometry [22]. It is based on temperature dependence of the electrical conduction dip width in an array of a large number (N>30) of tunnel junctions if low bias voltage is applied (Coulomb blockade effect). Each array consists of small islands made of normally conducting metal with typical dimensions of 1mm – 100nm – 30nm[2] separated from each other by a layer of insulator. According to classical physics, there will be no current in such a circuit due to potential barrier, but laws of quantum mechanics allow tunneling process to occur. In a first order, current through a junction is proportional to applied bias voltage like for a resistor. The second order process appears when the voltage is small. Metal islands and the insulator layer form a capacitor and insulator layer plays a role of dielectric. Every electron which tunnels through a barrier, charges the capacitor with energy $E_c = \frac{1}{2CV^2} = \frac{e^2}{2C}$. This energy is required for an electron to tunnel through a barrier and it is supplied by bias voltage. Tunneling takes place until bias voltage is larger than $V = \frac{e}{C}$. As it is known, every additional charge dq which is transported through dielectric to a conductor is hindered by the field of already present charges residing on the conductor. If the bias voltage is less than $V = \frac{e}{C}$, fewer electrons will have enough energy to tunnel. Moreover each tunneled electron increases the island potential and prevents the tunneling of other electrons. In such a weak tunneling regime only one electron is able to tunnel per a time that leads to a drop of electric conduction through a junction at low bias voltages that is known as the Coulomb blockade effect.

[2] Length-width-height

In a limit of high charging energy $\frac{e^2}{2C} \gg kT$, conduction approaches zero and is almost independent of temperature. In opposite limit of the partial Coulomb blockade regime, when $E_c << k_B T$, electrical conduction G of a junction circuit has a minimum when the bias voltage is zero. Temperature can be sensed through measurement of the conduction dip width.

In practice, normalized conductivity G/G_T is measured. It is defined as a ratio of the actual value $G \equiv \frac{dI}{dV}$ to the asymptotic conductivity at high bias voltages, G_T (Fig. 8) and can be measured by a lock-in amplifier with AC-excitation at frequency of a few tens of Hz. The full width of a dip at half of maximum, $V_{1/2}$, of the $G/G_T(V_{bias})$ curve is approximately proportional to temperature. However, Bergsten et. al. proposed to measure the zero point of the third derivative, $\frac{d^3 I}{dV^3}$, and showed that it can be used for primary thermometry, because it scales linearly with temperature [23] (Fig. 9).

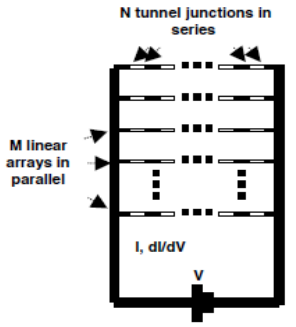

Fig. 7 Schematic of a sensor based on several one-dimensional arrays of tunnel junctions [22].

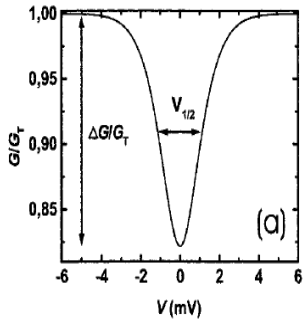

Fig. 8 A typical conduction curve of a CBT [22].

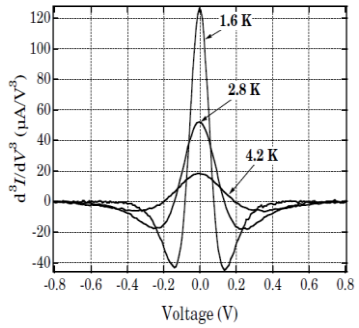

Fig. 9Third derivative as a function of bias voltage [23].

The shape of the normalized conductance curve obeys equation:

$$\frac{G}{G_T} = 1 - \frac{e^2/C}{k_B T} \frac{v sinh(v) - 4 sinh^2(\frac{v}{2})}{8 sinh^4(\frac{v}{2})}$$

where $\equiv \frac{eV}{2k_B T}$, V is bias voltage.

The full width of the conduction dip at half maximum can be found as

$$V_{1/2} \cong 5.439 N k_B T/e$$

The barrier resistance should be chosen larger or of the same order as so-called quantum resistance $R_q = \frac{h}{e^2} \approx 25.8 K\Omega$ to maintain weak tunneling. A choice of R<25.8KΩ leads to strong tunneling effects and large heat release. At the same time, Farhangfar et al. showed that blockade effect survives even with 1-2KΩ junctions, but this regime is totally unfavorable for thermometry [24]. The relation is highly accurate for high ($R_j \sim R_q$) junction resistances but a certain disagreement

appears when R_j is smaller than R_q. Half width of the dip, $V_{1/2}$ depends only on fundamental constants and a number of junctions, therefore T can be found absolutely, without calibration.

The device can also operate in a secondary mode, where the depth of the dip ΔG/GT is measured. It is found to be proportional to inverse temperature:

$$\frac{\Delta G}{G_T} = \frac{1}{6}\frac{E_C}{k_B T}$$

Unfortunately $\frac{\Delta G}{G_T}$ value is also dependent of charging energy (E_C) and thermometry based on the dip height has to be calibrated (e.g. by using the half width of the conductance peak). However, Holmqvist et al. suggested secondary mode of the CBT to provide a faster readout [25].

A schematic layout of a typical sensor is presented on Fig. 7. A sensor consists of Al\Al_2O_3\Al junctions and is fabricated by electron-beam lithography. Thermometer is usually supplied with a strong (0.05-0.2T) constant magnet to suppress superconductivity in aluminum (T_c=1.1K) [26], [27].

Serial connection of junctions results in a one-dimensional array. Long arrays efficiently suppress errors due to finite impedance of the electromagnetic environment and high-order tunneling effects. Parallel arrays decrease the sensor impedance to a convenient value [28]. It is more favorable to use an array of junctions as far as the dip width is linearly proportional to number of junctions. It leads to wider dip width, $V_{1/2}$ at lower T and therefore increases the thermometer resolution. Larger number of junctions also decreases the probability of high-order tunneling effects.

However non-uniform distribution of tunnel resistances is a main source of uncertainty in CBT. Thermometer can also suffer from the background charges which can spoil its performance in the low temperature range. In order to avoid the non-uniformity errors, a single junction thermometry is under development. The objective is to measure the conductance of a single tunnel junction, embedded in a four-probe configuration through lines consisting of arrays of tunnel junctions [29]. On the other hand, problems with all nanofabricated thermometers include non-equilibrium effects and a general lack of robustness: aging and destruction of a sensor due to electrostatic discharge [26].

In practice, the present working range of CBTs is from about 20mK to several tens of K. As far as a CBT measures an electron temperature, at T<20mK an electron-phonon decoupling causes thermometer saturation. CBT performs better than 1% accuracy in the range of 50mK – 4K, and about 3% down to 20mK. The temperature range can be adjusted by fabrication parameters. Coulomb blockade effect has an electrostatic nature and CBTs are highly insensitive to ambient

magnetic field that is proven for fields up to 27T [30]. It should also be emphasized, that CBTs are already commercialized and available on the market [31].

2.4 Shot noise thermometry.

Another recent innovation can be attributed to the shot-noise thermometry. The phenomenon of shot noise arises from random fluctuations of current or voltage caused by the discrete nature of the charge carriers. It was firstly described by Schottky in 1918 and found to be either temperature or frequency independent with a current spectral density $S_I = 2eI$, with I being current.

The Johnson noise prevails in equilibrium, in a case of zero external bias current or voltage. However shot noise dominates in the opposite limit. Shot noise thermometry relies on a temperature dependence of the noise current spectral density crossover from the shot to Johnson noise limit as a function of applied DC-bias voltage in a single tunnel junction [32]. In general, the spectral noise current density is a sum of corresponding Johnson and shot noise terms:

$$S_I(T) = 2\frac{eV}{R}coth(\frac{eV}{2k_BT})$$

$S_I(T)$ transforms to $S_I = 4k_BT/R$ for zero bias voltage, that corresponds to the Johnson noise. In the opposite limit when $eV \gg k_BT$ the spectral noise density is approximated by $S_I = 2eI$ as it is promised.

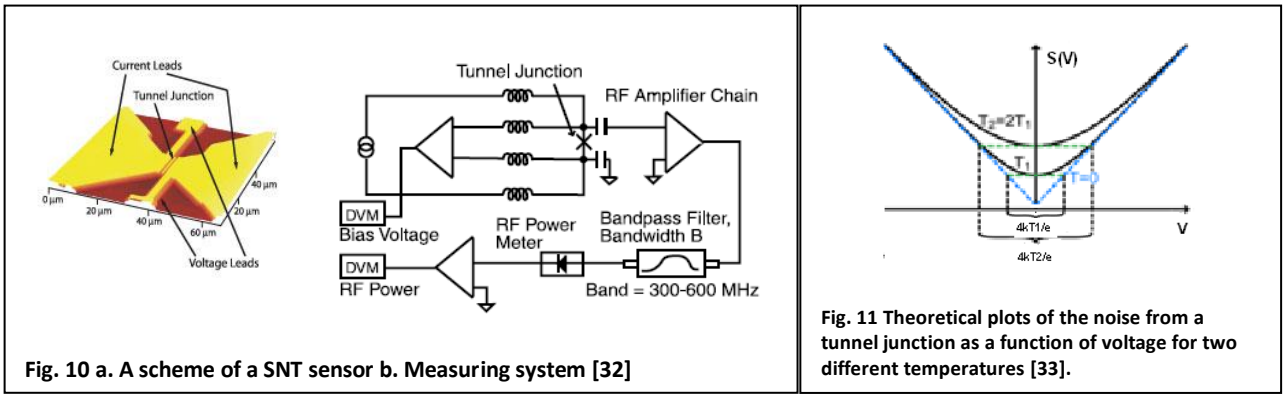

Fig. 10 a. A scheme of a SNT sensor b. Measuring system [32]

Fig. 11 Theoretical plots of the noise from a tunnel junction as a function of voltage for two different temperatures [33].

An SNT has similar structure as a CBT device but requires only one tunnel junction for operation. Sensor consists of two normal metal electrodes usually made of aluminum (current leads) and separated by an insulator barrier (Al_2O_3). The voltage readout leads should be closely situated to a junction to minimize inaccuracy due to voltage drop in there (Fig. 10a). The junction resistance is chosen to be 50Ω to match the impedance of the microwave devices. In order to suppress superconductivity in aluminum an external magnetic field of 0.5T should be provided. The current leads are used for sweeping of bias voltage while DC voltage through the junction and RF-noise power are simultaneously acquired by the voltage leads. In principle, two points in the shot (high bias) and Johnson (V=0) limits are enough to determine temperature, which can be found after

fitting with the theoretical curve with T as a fit parameter. Theoretical curve of a noise current spectral density versus voltage is shown on Fig. 11. The horizontal dotted lines indicate the Johnson noise level at each temperature, and diagonal lines indicate shot noise.

The measuring apparatus is shown on Fig. 10b. Inductively coupled leads are used to block high-frequencies and allow the junction to be current biased by a pair of leads. Capacitively coupled leads allow noise to be measured simultaneously. The noise signal is amplified by a cryogenic high electron mobility transistor amplifier chain and a chain of RF-amplifiers. The output of the chain is measured by a Shottky diode, which converts noise power to DC voltage [30].

SNT is free of limitations like gain or bandwidth because the object of interest is a crossover between two white noise (with frequency independent current spectral densities) regimes and the gain is the same for both of them [33]. As a result, one can use microwave devices with the bandwidth of hundreds MHz to increases the overall noise signal and accelerate the readout process.

A shot-noise thermometer can operate in a very wide temperature range with a modest uncertainty in results. It has a 2% uncertainty at room temperature, 0.5 % at 3K, 0.2% at 300mK and 2% at 37mK.

An appropriate quantum correction to the fitting curve should be applied at lower temperatures where the thermal energy becomes lower than the energy of measuring microwave photons. The net error of SNT is about 10% at 10mK [34]. A non-zero voltage drop in the readout leads also causes a systematic error in the temperature measurement that can be corrected by a more careful sensor design. An estimate showed a 0.4% deviation from the actual temperature at 4K [35]. Moreover, DC voltage measurements require a high-stability bias source, i.e. at 10mK k_BT/e ratio is only 1μV that demands at least the same stability for the bias voltage.

An SNT should be insensitive to magnetic field due to a certain similarity to a CBT but it has not yet been tested. The main advantage of the SNT is an opportunity to fabricate a more accurate sensor with smaller uncertainty in resistance than for CBT due to a single junction configuration. It is also geometrically easier to thermalize the junction area by cooling fins than for CBT sensors [28]. As a result, Spietz et. al. claimed that self-heating is out of concern at least down to 10mK in spite of large Joule heating due to smaller than for CBTs junction resistance [33].

As it was mentioned before, all nanofabricated thermometers suffer from static electricity and their performance can change with aging. But in general, SNT can be successfully used as a primary thermometer down to 40 mK with a very modest uncertainty. At the same time it cannot still compete with the conventional methods like nuclear orientation, Johnson noise or ^{3}He melting curve thermometry at lower temperature.

2.5 Other primary thermometers.

A number of other primary methods are also used. Gas and vapor pressure thermometry are in use for the ITS-90 definition in its lowermost range. The Mössbauer thermometry is based like nuclear orientation thermometry on measuring of Boltzmann population of nuclear sublevels of a radioactive nucleus. However its realization is very complicated from the practical point of view in spite of a well-defined physical background. The low-energy γ-rays ($E \leq 100$ keV) require in most cases special thin windows to let the γ-rays escape from the cryostat. In addition, corrections for finite sample thickness, long counting times, specialized equipment and motion of source or absorber are necessary [3].

The osmotic pressure thermometry relies on a pressure difference between superfluid ^{4}He and ^{3}He/^{4}He dilute mixture when they are separated by a superleak. In this case temperature can be found from the Van't-Hoff relation: $\pi = xRT/V_m$, π is the osmotic pressure, x is a molar concentration of ^{3}He, R is the gas constant, V_m is the ^{4}He molar volume. This thermometer can be used in the temperature range between 10mK and 700mK and is particularly suited for investigations of dilute ^{3}He/^{4}He mixtures [36]. Moreover, it is insensitive to high magnetic fields [3], [9].

Review of secondary thermometers.

Although primary thermometers may provide vital information about temperature in the investigated system, their use is limited by a number of practical inconveniencies. First of all they are usually bulky, have a limited operation range, slow response time and usually require special measuring instrumentation. Therefore even with the recent development of new nanofabricated devices, primary thermometry is still mostly spread in special metrological and national standard laboratories.

By a definition, secondary thermometers are all that are not primary. The most popular secondary devices are resistance thermometers with either positive (normal metal) or negative (semiconductor) resistance coefficient, magnetic susceptibility (either nuclear or electron), superconductor fixed-point devices which provide a temperature reference by a measurable superconductor transition and thermocouples, where thermal EMF is measured. A ^{3}He melting curve thermometer should be considered separately because of its special importance. It relies on a melting pressure measurements along the $p_m(T)$ curve and provides an internationally adopted PLTS-2000 scale. Lounasmaa [14] classifies ^{3}He melting curve thermometers and superconducting fixed-point devices as the secondary standards because once calibrated, all same type devices are also considered to be calibrated. PLTS-2000 serves as a calibration for ^{3}He melting curve thermometers.

In practice, each FPD has its own calibration provided by a manufacturer due to slight difference in the transition temperatures caused by features of the nucleation process. Secondary standards are the most wide-spread instruments for calibration of practical secondary devices.

All secondary thermometers are relatively easy in use, have fast response times and sensitivity that make them (especially resistance sensors) "work-horses" in low-temperature laboratories throughout the world.

2.6 ^{3}He melting curve thermometer

Being proposed in 1967 by Scribner and Adams [5], ^{3}He melting curve thermometry (MCT) still plays an important role and serves as a basis for current internationally adopted Provisional Low-Temperature Scale PLTS-2000. It exploits a possibility to determine temperature by measuring the pressure of ^{3}He two-phase (co-existed solid and liquid) mixture.

An extraordinary $P_m(T)$ curve shape with a set of internal fixed points make ^{3}He melting curve thermometry one of the most powerful instruments for sub-Kelvin measurements. The melting pressure strongly depends on temperature in a wide range (at least 0.9mK-1K) and even at T=1.2mK the melting curve slope is 2.7×10^3Pa mK^{-1}[3]. Therefore, it can be used for precise temperature measurement for three decades of T with the vicinity of $T=T_{min}$ as the only exception where thermometer's sensitivity, $\frac{dP}{dT}$, approaches zero.

2.6.1 ^{3}He Melting curve.

The history of MCT starts from prediction made by I.Pomeranchuk (1951) that ^{3}He should have a minimum in its melting curve [37][3]. This can be understood with an assumption that thermal kinetic energy and phonon excitation negligibly contribute to the overall entropy of solid ^{3}He and therefore it is mainly determined by mutual nuclear spin disorder and S remains constant with temperature, $S=Rln(2I+1)$, where I is the ^{3}He nucleus spin. Whereas liquid ^{3}He behaves like a dense Fermi gas and can be described with the same principles as a gas of conducting electrons in metal with entropy being linearly dependent on T ($S \approx 3RT$). A high temperature range of the melting curve is out of practical interest whereas the range below 1K attracts one's attention due to extraordinary behavior. In the range down to 0.315K melting curve obeys a normal $dP/dT>0$ dependence with $S_l>S_s$, whereas at T=0.315K and pressure of 29.3 bars the entropies of both phases become equal which causes a minimum point of a $p_m(T)$ curve.

[3] At that time ^{3}He has not yet been liquefied and even enough available

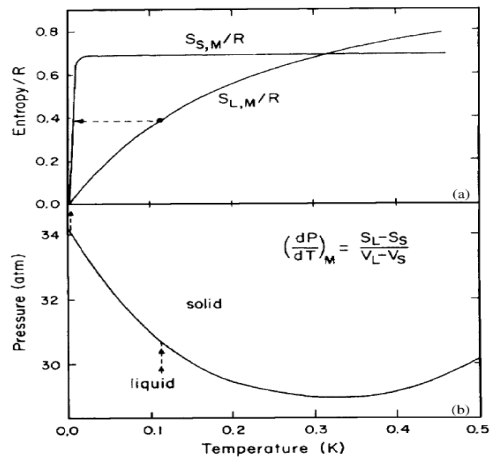

Fig. 12Entropies of liquid and solid 3He (a) and melting curve (b) [37]

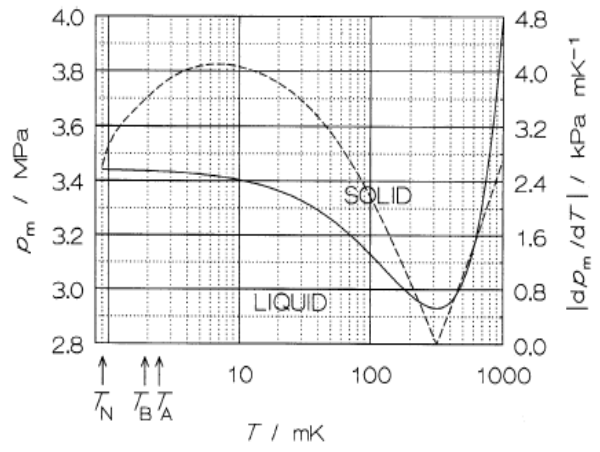

Fig. 13 ^{3}He melting curve [5]

The melting curve can be obtained from the Clapeyron-Clausius relation

$$\frac{dp_m}{dT} = \frac{S_l - S_s}{V_l - V_s}$$

with S_l and S_s, V_l and V_s being molar entropy and volumes of liquid and solid. Because molar volume of liquid is always larger than that of solid ($\Delta V=1.31 cm^{-3}mol^{-1}$ at T=40mK) an unusual situation with $\frac{dP_m}{dT} < 0$ implies $S_s > S_l$. However, at temperature of 0.9mK the entropies become equal again (as it should be at T=0) when a nuclear spin ordering in solid occurs. It corresponds to a flat maximum on the melting curve (Fig. 13). In principle, a melting curve thermometer could be used in a primary way if a satisfactory ^{3}He entropy theory existed.

Along with the minimum point at 315mk three more fixed-points exist at T<3mK: two superfluid transitions at T=2.44mK (A-transition), 1.90mK (A-B transition) and a nuclear spin ordering in solid (Néel transition) at 0.9mK. Unfortunately the low-temperature fixed points are not reachable with a dilution refrigerator and therefore the minimum point has a primary importance.

At the same time a number of factors such as ^{4}He impurity or external magnetic field may cause a deviation from the theoretical curve. The impurity effect is caused by a sample contamination with a small amount of ^{4}He. It is recommended for supplied sample to contain no more than 10 ppm of ^{4}He and in this case the impurity effect on the melting curve will be very small. However, ^{4}He is expected to be preferentially absorbed on the wall of the cell or on the sinter, and below 50mK the impurity effect should be unobservable as the solubility of ^{4}He in liquid or solid ^{3}He is less than 1ppm [2]. At the same time, the experiments by Ganshin et. al. with 2.1% of ^{4}He impurity showed a hysteresis in the melting pressure by tracing back and forth within 0.1bar error in the minimum point which was shifted to a higher temperature (T=333mK). The relative error increased at lower

temperatures and achieved 15% at 60mK. The ^{4}He impurity contribution to the P_{min} shift can be estimated by relation

$$\Delta P_{min} = \alpha x T$$

where x is the ^{4}He concentration, $\alpha=7\times10^6$ Pa/K and T is the temperature, and the corresponding change in the T_{min}

$$T'_{min} = T_{min} + \frac{ax}{2b}$$ where $b=3.8\times10^6$ Pa/K^2 [38].

At lower concentration no change within $\pm$0.3mK in the T_{min} happened for 0.1% impurity of ^{4}He [39].

The influence of external magnetic field on the melting curve can be found as an effect on the entropy difference S_l-S_s. The liquid phase at low temperatures achieves spin ordering and is almost insensitive to magnetic field; therefore the change of the slope is proportional to the entropy of solid ^{3}He. This can be explained by using a magnetic version of the Clapeyron-Clausius equation

$$\frac{dP}{dB} = M_{sat}\frac{m_{sol} - m_{liq}}{v_{sol} - v_{liq}}$$

where M_{sat} is the ^{3}He molar saturation magnetization and m_{liq} is the relative magnetization of the liquid. Because $m_{sol}>>m_{liq}$ and $\Delta v<0$, $\frac{dP}{dB} < 0$, hence one should expect a pressure depression when an external magnetic field is applied. As a result, a 0.5bar depression was observed at B=15T and T=5mK [40].

On the other hand, MCT is insensitive to RF-interference because of the large pressure transducer AC-impedance. In fact, there is no heat dissipation in an MCT as far as its impedance is contributed only by an imaginary component.

2.6.2 Cell design and temperature measurement.

In spite of a number of possible MCT cell designs the main principle remains the same: temperature is measured by a melting pressure change that is detected by a sensitive transducer. The first basic cell design was proposed by Scribner and Adams where the Straty -Adams thin-diaphragm pressure transducer was utilized [5].

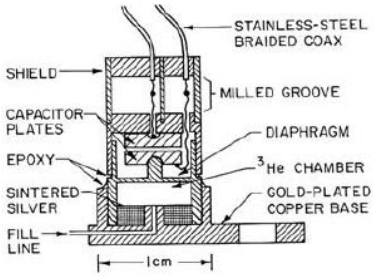

Fig. 14 Cylindrical Greywall's cell design [41]

The first electrode of the capacitor is fixed to a movable diaphragm, whereas the second one is static and fixed to the cell body. Therefore the melting pressure can be sensed via the diaphragm displacement which is measured capacitively. Nowadays the most spread design is that proposed by Greywall and Bush [41] with round flat electrodes (Fig. 14), another variant is to use a concentric configuration with cylindrical electrodes, e.g. Mikheev et. al. [42].

In a case of the conventional Greywall design, where the first plate is static and the second one is fixed to the diaphragm with epoxy, the displacement as a function of pressure may be estimated by relation

$$y = 3a^4(m^2 - 1)P/(16Em^2t^3)$$

Here, y is the displacement, P is the pressure, and a is the radius of the diaphragm, m is the reciprocal of the Poisson ratio, m~3 for metals, t is the thickness, and E is the Young's modulus of the material [43]. Therefore a lower plate thickness should lead to larger deflection and higher gauge sensitivity. On the other hand, it limits the absolute working range of a device by shortening of the cell electrodes and possibility of inelastic diaphragm movement or even breaking the gauge by high pressure.

A classical Greywall cell had a diaphragm diameter d=0.64cm and thickness t=0.025cm [39]. For a parallel plate capacitor with spacing l between the plates, the resolution of a gauge obeys a relation

$$\frac{dC}{C} = 3a^4\frac{dP}{16Et^3l}$$

Therefore a small gap between the plates is preferable. The Greywall cell had a 4.3pF capacitance at vacuum that corresponds to the gap of 3.6×10^{-3} cm [39].

Beryllium copper (BeCu) is usually chosen for the diaphragm construction because of good mechanical properties. Other materials such as titanium or tungsten are also possible but their use is limited due to machining difficulties [2].

The recent design by Sebedash et al. considers the use of a two-volume system, a usual ^{3}He volume and a reference volume, one inside another and separated by a flexible membrane that also acts as a

first electrode [44],[45]. The second electrode is built in the reference volume which provides a counter pressure to the main volume, therefore the working pressure (on the diaphragm) becomes lower and a very flexible membrane can be used. The working pressure can be calculated as a difference between the actual and the reference values.

$$\Delta p = p - p_r$$

They obtained less than 10mPa pressure resolution during experiments with ^{4}He melting curve at temperatures 0.08-0.3K A use of MCT with such design can allow a temperature measurement down to 0.1mK with uncertainty of 10%. A certain modification of the cell design, such as a use of a very thin membrane and only one filling line is expected to provide even better results [46].

Two basic methods are used for capacitance measurement: an AC-bridge measurement or using a cell transducer as a circuit element with the tunnel diode oscillator. A bridge measurement becomes possible only when none of the electrodes is grounded; otherwise the cell capacitor can be used as an element of a tunnel diode oscillator circuit. The first method is more accurate, i.e. Sebedash et. al. had less than 10^{-6} resolution in capacitance by using Andeen-Hagerling AH2700A ultra-precision capacitance bridge, whereas the electrode grounding makes the cell easier to manufacture but the possible resolution is of order of magnitude less [47].

The bridge method is more wide-spread and is based on the comparison between unknown and reference capacitor. The main problem in this case arises from the stray capacitance in the coaxial leads. It can be overcome by three-terminal measurement with one being common either for the reference or unknown capacitor. The main element in such a circuit is the precise ratio transformer that is used for comparing the capacitance to be measured and a reference capacitance. A variable resistor is placed in one side of a bridge in order to balance the resistive part of a signal. A lock-in amplifier is used as a balance (null) detector.

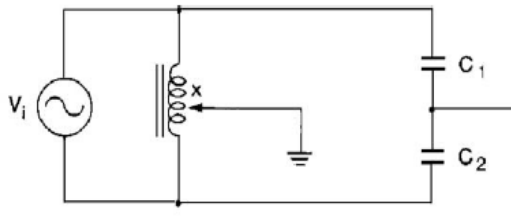

Fig. 15 Diagram of the ratio-transformer-based capacitance bridge. Ideal case [2]

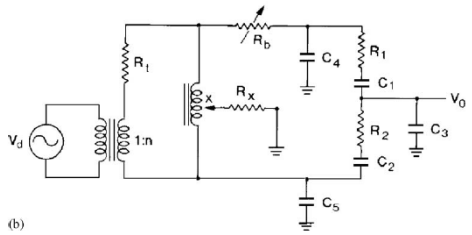

Fig. 16 Realistic scheme including resistances and other caps [2]

In an ideal case, the output/input voltage ratio, V_0/V_1 is

$\frac{V_0}{V_1} = ((x-1)C_1 + xC_2)/(C_1 + C_2)$ where x is a ratio transformer setting, C_1 and C_2 are reference and unknown capacitance respectively. At the balance, V_0=0

$$\frac{C_1}{C_2} = x/(1-x)$$

In a case of realistic circuit C_3 capacitance (common coaxial) has the largest stray contribution

$$\frac{V_0}{V_1} = \frac{((x-1)C_1 + xC_2)}{(C_1 + C_2 + C_3)} - jwR_x(C_1 + C_2)\frac{((x-1)C_4 + xC_5}{C_1 + C_2 + C_3}$$

As it can be seen, C_3 can decrease sensitivity by the factor of $\frac{C_1+C_2}{C_1+C_2+C_3}$

For this reason a common (ground) lead should be chosen of minimal capacitance while the others are out of primary concern.

The other important point is to provide stability to a reference capacitor. It is preferably to place it to the same temperature as the thermometer. The efficiency of the method also strongly depends on the measuring equipment. High-quality capacitance bridges are very expensive.

The second method of the capacitance measurement is to use a pressure transducer as an element in the oscillator circuit. As the capacitance changes, the oscillation frequency also changes and it can be measured by a precision frequency counter. If the oscillator is placed outside the cryostat, the necessary stability cannot be achieved because of variations in lead resistance. This problem has been solved by the use of a tunnel diode oscillator with the diode located in the cryostat. Usually a circuit proposed by van Degrift [48] is most widely-used. In principle, it can provide a resolution as good as 10^{-9}, but there are certain difficulties with the heat disspation and tuning the circuit.

There exists one more parameter that should be known during measurement - thermometer thermal relaxation time. Thermometer response to the temperature change obeys a first order differential equation

$$\tau\frac{dy(t)}{dt} + y(t) = kx(t)$$

with input, *y(t)*, output, *x(t)*, of a thermometer and τ is a time constant which characterizes thermometer reaction delay. A decrease of the thermometer time constant can be reached by reducing Kapitza boundary resistance at the metal-liquid interface. This is done by filling ~50% of the gauge volume by sintered silver powder. The Kapitza resistance can be evaluated as

$R_K = \frac{a}{A}T^{-3}$, with $a \cong 0.05$ for liquid ^{3}He, and A – contact area in m^2,

To get lower boundary resistance, powder with a high specific area should be chosen. Usually it has a submicron particle size and specific surface area of 1-2 m^2/g [49]. A thermometer time constant, τ, can be estimated by the following relation (like for a capacitor discharge on a resistor)

$$\tau = R_k C_{th}$$

where R_K is the liquid-metal interface Kapitza resistance and C_{th} is the thermometer heat capacity that can be simply estimated by $C_{th} \cong C_{liq}$ due to large specific heat of liquid ^{3}He in comparison with that of BeCu. Therefore τ is proportional to T^2 and for T>10mK

$$\tau = \frac{13.4n}{AT^2}$$, n is a number of mol of ^{3}He [50]

At T<10mK the behavior of the Kapitza resistance is found to be proportional to $\sim T^{-1}$, but this behavior is not well understood. Such a behavior has been observed only for pure ^{3}He-metal interfaces whereas even a small impurity of ^{4}He or impurities on sinter degrades it [68].

At very low temperatures time constant becomes very large, i.e. at 2mK according to Pollanen et.al. τ=490s with the total MCT heat exchanger surface area of 2.9 ± 0.2 m^2 [51].

2.7 Fixed-point Devices.

Superconducting transition in metals is the most common critical phenomenon at low temperatures. If appropriate materials with the sharp transition and small hysteresis are chosen, a very convenient temperature reference can be found. Nevertheless, a number of factors, such as the sample purity and ambient magnetic field can distort the expected performance and should be taken into account.

The first such a practical device, SRM-767, was proposed by National Bureau of Standards and relied on five superconducting transitions in metals [9].

T_c(Cd),K	T_c(Zn),K	T_c(Al),K	T_c(In),K	T_c(Pb),K
0.520	0.851	1.180	3.415	7.20

Table 3 SRM-767 fixed points [9]

It had a limited usefulness as far as thermometry at a few Kelvin is not a great practical problem and can be realized by other means. At the same time, its successor, the SRM-768 device for sub-Kelvin measurements was found to be very convenient for practical use. It provides five fixed points in a range of 15-208 mK [55].

Material	Transition temperature, mK	Typical transition width, mK	Typical reproducibility upon thermal cycling, mK
W	15.0 – 17.0	0.7	0.20
Be	21.0 – 24.0	0.2	0.10
$Ir_{0.8}Ru_{0.2}$	98.5 – 99.5	0.8	0.10
$AuAl_2$	160.0 – 161.0	0.3	0.10
$AuIn_2$	205.0 – 208.0	0.4	0.15

Table 4 SRM-768 characteristics [55]

The SRM-768 device consists of two sets of coils, each set contains a primary and secondary coil, with secondary being wounded on top of the primary. In order to protect coils from the ambient magnetic field the device is placed into the niobium shield. Thermal contact between the samples and the copper body is provided by Cu wires welded to the body and connected to the sample by varnish. Two primary coils are used to generate small AC magnetic field

$B = 0.0158I$, where I is the current through the coil in amperes, and resulting field in teslas, and two secondary coils to measure the AC-magnetic susceptibility, χ, of the samples [55]. The sets are interconnected with each other that is why only four leads are required for measurement. The uniformity of a pair of primary and secondary coils is such that although a pair has a mutual induction of 3mH, the mutual inductance of a combination is generally less than 100μH [55]. The superconductive transitions are observed as a change in the coil mutual inductance which occurs when the magnetic field generated by primary coil is expelled from the interior of the sample, or χ becomes -1, as it enters the superconductive state. According to Lenz's law, the voltage induced in the secondary coil, V_s, in response to a magnetic field generated in the primary coil is given by

$$V_s = M_{12} d\Phi/dt$$

where M_{12} is the mutual inductance between two coils and Φ is the magnetic flux linking them. Since $M_{12} \sim \chi$, the change in the sample magnetic susceptibility causes a change in the coil mutual inductance [52].

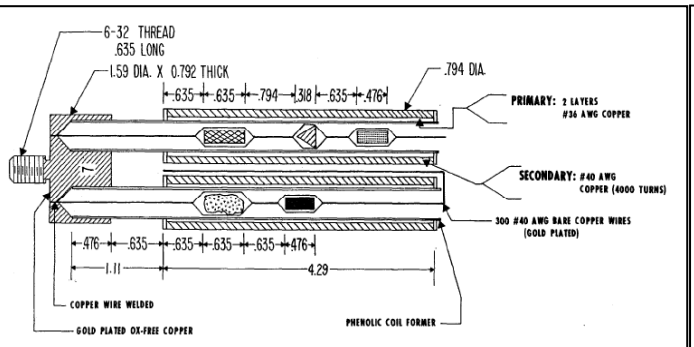

Fig. 17 SRM-768 fixed-point device [55]

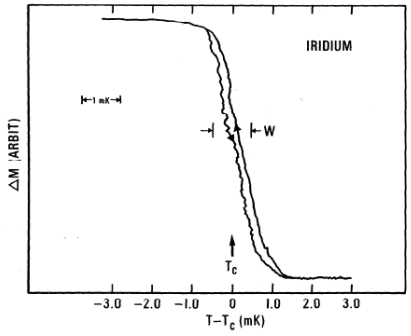

Fig. 18 Typical superconductive transition [55]

A change in mutual inductance typically can be measured by using a lock-in amplifier with AC-excitation. The lock-in input is used for measuring voltage induced in a secondary coil. The width, W, of the transition is defined as the temperature range over which 80% (between 10 and 90%) of the change in mutual inductance occurs, while critical temperature, T_c, is defined as the midpoint of the mutual inductance change. Two traces of the transition are generally obtained, one as the sample is slowly warmed through the transition, and a second one as the sample is cooled back through T_c. The hysteresis could be due either to lack of thermal equilibrium or to supercooling effect.

It should be emphasized that transition temperature depends on the sample composition and crystal defects and can vary for different devices. That is why each fixed-point device has a special serial number and its own calibration. The SRM-768 devices were calibrated in NIST either by nuclear orientation ^{60}Co or Josephson noise thermometer [55]. A later calibration of serial 7 device in NIST has found an inconsistency with the earlier one of 0.2% for W and Be and 0.1% for 3 high-temperature fixed points. The authors advised to use this data to correct all previous calibrations [53].

There are several factors than can distort the device performance, such as an ambient magnetic field, Joule heating or heating due to eddy currents. Therefore one should follow the experimental precautions developed by NIST:

- ambient magnetic field is less than 1μT
- peak-to-peak field in primary coil is less than 2.3μT for tungsten, 0.40μT for the other superconductors (Joule and eddy current heating 1.8 and 0.08nW respectively) [55].

The reproducibility and the T_c shift in a 1μT field are about 0.1mK. The transitions should be swept with low enough speed, especially for Be and W, to avoid hysteresis effect.

The ambient magnetic field is the most important factor that defines the shape and position of superconductive transition. First of all, magnetic field $H_c(T)$ can completely suppress superconductivity at temperature T in a sample according to approximate formula

$$H_c(T) \cong H_c(0)\left(1-\left(\frac{T}{T_c}\right)^2\right)$$

The second problem due to magnetic field is that it can cause a supercooling effect which introduces hysteresis into transitions. In other terms, an ambient magnetic field shifts the transition temperature T_c to lower values

$H_{sc} = H_a = 2.4kH_c(T)$ where *k* is the Landau-Ginzburg parameter [55].

The relative supercooling is small for high-temperature samples, whereas the situation changes for pure metals whose critical temperatures are below 0.1K. Their small *k* and extremely small critical fields H_c result in extensive supercooling. As it was pointed out by Buhrman and Halperin, placing of specimen of interest in a good electrical contact with another superconductor which has a much higher T_c can sufficiently decrease or even defeat supercooling (so-called proximity effect) [54]. That is why the small Al buttons which act as the nucleation centers to induce superconductivity were spot-welded to W and Be samples in SRM-768.

Near critical temperature T_c, the amount of supercooling can be evaluated as

$$\Delta T_s = T_s - T_c = \frac{1}{2.4k}\left(\frac{dH_c}{dT}\right)^{-1}_{T=T_c} H_a$$

This expression gives only the maximum supercooling which can occur. Sample imperfection will cause the sample to enter the superconducting state anywhere between T_s and T_c [55].

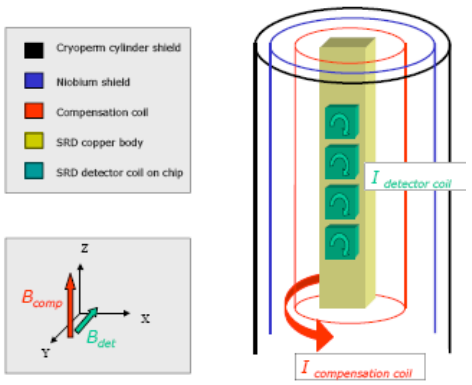

Fig. 19 SRD1000 [57]

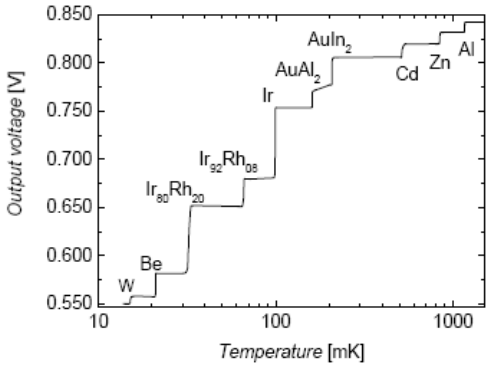

Fig. 20 Output voltage control unit as a function of the temperature of SRD1000 [59]

Since SRM-768 was developed and commercialized in late seventies, its fabrication was discontinued in nineties [9]. As a substitution, a new SRD1000 fixed point device is produced by Dutch consortium of institutes [9]. The principle of the device has not changed, however SRD1000 contains 10 superconducting samples in a range between 15-1200mK that allows using it almost in the whole range of adopted PLTS-2000 scale. In comparison with the NIST SRM-768 device, two more samples were added to the range below 0.1K as well as "high-temperature" Cd, Zn and Al points. The technique used to detect the superconducting transitions is almost the same as for SRM-768, based on the familiar principle of magnetic flux exclusion in a superconducting state. But the change of magnetization is detected by a planar microcoil system, realized by a thin-film niobium structure on a silicon wafer substrate [56].The SRD1000 sensor is contained within a Cryoperm 10 magnetic shield and a Nb superconducting shield, to prevent shifts of T_c due to magnetic flux. In order to suppress residual magnetic field, an additional compensation coil is used. It was found that in most cases due to geometry of shielding, the X,Y-components are significantly smaller than the Z-component, that is why the chosen coil configuration allows suppressing of residual field (Fig. 19)[57]. The device is also commercialized [58] and all appropriate measurement electronics can be purchased with the device.

Material	W	Be	$Ir_{80}Rh_{20}$	$Ir_{92}Rh_{08}$	Ir	$AuAl_2$	$AuIn_2$	Cd	Zn	Al
Nominal Tc (mK)	15	21	30	65	98	145	208	520	850	1180
90/10% transition width (mK) <	0.2	0.3	0.5	0.5	0.5	0.5	1	4	3	4

Table 5 SRD1000 fixe points [57]

A more careful preparation of cadmium and zinc samples led to the transition width narrowing to 3 and 2mK respectively [59]. In period from 2003 to 2006, several systems were built and then calibrated at PTB. The evolution of the SRD1000 devices can be found in [60].The systems are now in use by several ultra-low temperature research laboratories in Europe and Japan.

Thus, a superconducting fixed-point device can serve as a convenient temperature reference if all the precautions are fulfilled. However the lowermost points are very vulnerable towards the residual magnetic field and moreover should be traced out very slowly in order to acquire a proper data about their critical temperatures.

2.8 Resistance thermometry.

Resistance thermometry is the simplest and most widespread method for routine temperature measurement. A resistance thermometer has a small size, fast response, high sensitivity and does not require any special equipment for measurement. At the same time, a number of practical problems, such as RF-heating, self-heating, heat conduction of the leads and lack of thermal contact may become a pain for an experimentalist. As far as low-temperature sensor resistance may depend on temperature in a rather complicated way, a resistance thermometer is a secondary one and must be calibrated.

All resistance thermometers may be divided into two categories according to their $\frac{dR}{dT}$ dependence: metals have a positive resistance coefficient, while semiconductors obey $\frac{dR}{dT}<0$.

As was mentioned earlier, platinum resistance thermometer is used in ITS-90 to approximate thermodynamic temperature between fixed points. Pt thermometers are in use down to $T \cong 10K$ with a linear *R(T)* dependence [7]. They can be bought as 100Ω or 1KΩ cheap thin-film sensors with a price of several euros per item. In order to shift the lower limit for the metal sensors, a small fraction of magnetic element is usually embedded. So-called Kondo alloys allow operating down to 0.1K. The most vivid example is Rh with 0.5% (atomic) of Fe. At T>30K it behaves like an

ordinary Pt sensor, whereas at T<10K it remains sensitive to temperature due to electron scattering on the iron atom impurities [9].

The second type is semiconductor thermometers. The most popular are doped Ge, carbon, RuO_2 and ZrN (Cernox) based sensors. An ideal semiconductor has a following R(T) dependence

$$R(T) = \alpha \exp\left(\frac{\Delta E}{k_B T}\right)$$

ΔE is a band gap. Real sensors have much more complicated dependences which should be found empirically. In general, semiconductor sensors are operable in 10mK-10K range, although the lower limit is mostly defined by reliability of thermal contact, grounding and shielding.

Doped Ge sensors are rather widespread and work in the range of 0.3-40K, but different amount of doping may allow using them down to 0.03K.

The following functions may be used for calibration [9]

$$\ln(R) = \sum_{n=0}^{m} \alpha_n (lnT)^n \text{ or}$$

$$\ln(T) = \sum_{n=0}^{m} \beta_n (lnR)^n$$

Ge sensors are very stable and calibration does not drift with time. At the same time they are very susceptible to magnetic field and mechanical stress, their magnetoresistance increases with decrease of temperature and one should avoid using them in fields more than 1T. ZrN-thermometer have a very small magnetoresistance and it is suggested to be the best variant for measurements in high magnetic fields at T>1K [9].

Speer carbon resistors were the most popular resistance thermometers in milli-Kelvin range from sixties but now are out of production; however they are still available at Leiden Cryogenics [61]. They are suitable for every-day measurements (in principle down to 0.01K) if a very high precision is not required. Their characteristics may vary for samples from the same batch and also change with time. The main problems with the carbon sensors are calibration drift, difficulties with thermal contact and high heat capacity. However Samkharadze et al. have recently shown that a carbon sensor can operate down to 5mK if a good thermal contact is established and proper filtering is applied [62].

Carbon chips have almost disappeared from market being substituted by the thick-film ruthenium-oxide resistors. These resistors are commonly used in room-temperature electronics and produced by many companies throughout the world. RuO_2 sensors are made of ceramic composite which consists of conducting RuO_2 and Bi_2RuO_2 in $PbO\text{-}B_2O_3\text{-}SiO_2$ glass matrix. The main advantages of a RuO_2 sensor are reproducibility, stability upon temperature cycling, reasonable magnetoresistance, compact size and low price. All these features ensure the popularity of Ru-based

sensors, for example, they are used for a critical temperature control of the superconducting magnets in CERN's Large Hadron Collider [64].

Dramatic increase of resistance at low temperatures for semiconductor sensors may induce errors in measurement. For 0.05-4.5K measurements a 1kΩ room-temperature resistance is usually chosen that leads up to several tens of KΩ at temperatures below 50mK [62].

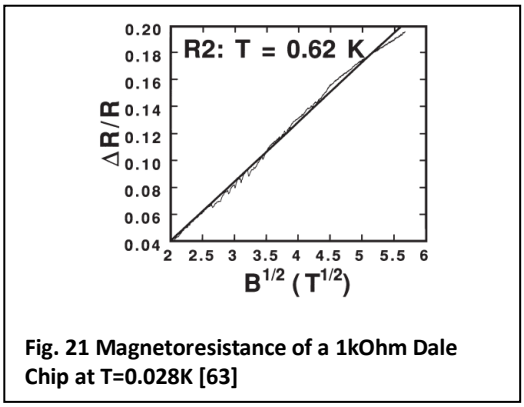

Fig. 21 Magnetoresistance of a 1kOhm Dale Chip at T=0.028K [63]

A use of high, e.g. 100kΩ resistors necessitates a high impedance measuring device and the use of a large voltage to overcome the effect of Johnson noise. RuO_2 chips from the same batch may have small differencies in R(T) dependencies (in order of a few percents) which may also vary with thermal cycling. RuO_2-chips temperature cycling down to 4.2K showed an initial increase in resistance of about 30Ω (~0.2K), but after 60 cycles the value became stable. Magnetoresistance measurements showed a small decrease in resistance at T<0.15K and B<4T, whereas at higher fields a $B^{1/2}$ dependence occurred. Magnetoresistance above 0.2 K is entirely positive and decreases as the temperature is increased. At all measured temperatures the resistance measured above 4 T is a monotonically increasing function of applied field, and is directly proportional to $B^{1/2}$ for all temperatures for several chips from the same batch [63]. Zak et. al. compared commercially available sensors and showed that at 0.4K and field B=5T relative resistance change by 4.3% for Lakeshore ROX-102 and 5.8% for Dale RCW575 sensors [64]. The best currently available Lakeshore Rox 103A sensor has a +0.58% temperature error at T=2K, B=2T and +1.5% at B=8T [65]. However the characteristics of RuO_2 sensors may vary depending on the model and manufacturer.

The fitting function for a RuO_2-thermometer is [9]

$$lnR = \sum_{n=0}^{m} A_n (lnT)^n$$

For a limited temperature range

$$R = R_0 \exp\left(\frac{T_0}{T}\right)^{1/4}$$

A cryogenic resistance thermometer should be properly packaged for a better performance at low temperatures. The main aim of packaging is to enhance thermal contact between thermometer and an object to be measured. That is why resistance element is glued to a pure copper base with a highly heat conducting epoxy, usually Stycast 1266 or Stycast 2850 FT [66][4]. Sensor leads should be wrapped around the copper base and glued as well to avoid sensor heating from certain wire heat conductivity. The second reason of packaging is to decrease sensor's heating due to noise pick-up as much as possible. Poor thermal contact and noise pick-up cause sensor saturation (overheating and deflection from proper performance) at temperatures below 100mK. Noise pick-up is usually decreased by proper filtering and placing a thermometer into a copper full-metal jacket. An example packaging of a Lakeshore sensor is shown on fig. 22 [67].

Commercially available sensors can be purchased either calibrated or not. A typical price of an uncalibrated sensor is about hundred dollars and depends on model; however calibration increases the price up to one order. Lakeshore provides calibration down to 20mK with accuracy of ±2mK and ±4mK at 50mK for their RX-102B-CB thermometer, but the price of a bare sensor changes from 400$ to 4000$ after calibration [68].

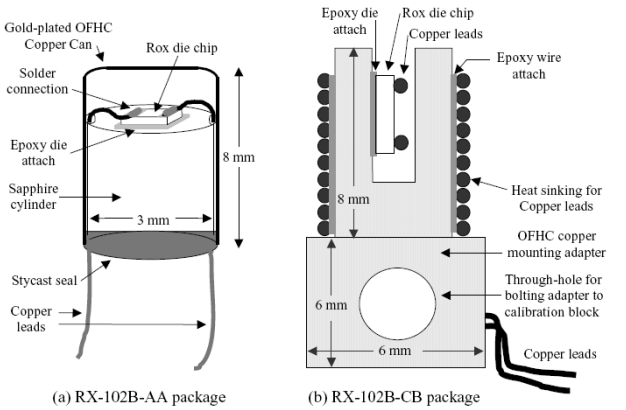

Fig. 22 Lakeshore sensor packaging for applications down to 20mK [67]

Every resistance measurement leads to a sensor heating according to the Joule law, $P=I^2R$. A certain thermal resistance leads to a raise of the sensor temperature above the surroundings after excitation, so-called self-heating. Thermal resistance for infinitesimal change of T can be expressed as $R_{th} = \frac{\delta T}{\delta Q}$, where δT is the sensor temperature increase over ambient temperature after applying a certain amount of heat, δQ. Thermal resistance strongly increases at low temperature that is why a self-heating power that one can afford is reduced. At 10mK an acceptable sensor heating does not exceed 1fW. The 100pA excitation produces a voltage drop of 10μV across a 100KΩ sensor. At the

[4] Stycast 1266 has five times larger heat conductivity than Stycast 2850 FT for 0.05K<T<2K, while at room temperature the heat conductivity of Stycast 2850 FT greatly exceeds that of Stycast 1266

same time, stray thermal EMF appears from the temperature gradient between the end (at room temperature) of a copper (manganin) wire and a solder joint (at low temperature) like in a thermocouple. An ordinary copper-to-tin/lead solder joint produces thermal EMF of 5μV/K. This is one of the reasons to use an AC-excitation bridge for measurements in millikelvin range. The use of low-frequency (10-20Hz) excitation cancels the DC-related effects like thermal and electrochemical EMF, while low frequency is kept to reduce reactance effects. Moreover, AC-bridges are more stable and faster. A sine AC-excitation that is used in Lakeshore and Stanford systems is less sensitive to stray capacitance, but requires a fast CPU unit to generate smooth sine waves and should be very well shielded. Square wave (in AVS systems by RV-Elektroniikka Oy) signals are more sensitive to stray capacitances but does not require any advanced circuitry [69].

Proper grounding and shielding can broaden the possible working range for a semiconductor resistance thermometer. Shielding the leads and if necessary filtering the signals coming into cryostat should be used in order to decrease heating due to RF-noise pick-up. The information about shielding, grounding and filtering can be found for example in [69] or [70].

Thus, calibrated resistance thermometer can be reliable instrument for temperature measurements. A vulnerability of resistance sensors at low temperature caused by poor thermal contact, RF-noise pick-up and self-heating limits their effective operational range. At the same time, the most popular RuO_2 resistance thermometers can successfully operate down to 10-20mK if all the necessary precautions are fulfilled.

2.9 Other secondary thermometers.

Other popular secondary devices are magnetic thermometers using either electron or nuclear magnetism. The principle is based on the Curie law for paramagnetic dilute salt (CMN or LCMN) and alloys (PdFe). Magnetic susceptibility that is usually measured, depends on temperature as $\chi = C/T$ where C is the Curie constant. $C = \mu_0 n g^2 \mu^2 \frac{I(I+1)}{3k_B}$, n is the density of magnetic dipoles, μ is either Bohr or nuclear magneton that defines a thermometer type. The Curie law can be used with an assumption that $T >> \Theta$ (magnetic ordering temperature) and magnetic moments do not interact. The possible working range for nuclear-magnetism thermometers is almost 3 orders larger [9], [3]. NMR methods are frequently used for nuclear susceptibility measurement. NMR nuclear susceptibility thermometers allow measuring down to a few μK with uncertainty of 2%.

There are also diode (1-500K) thermometers and thermocouples (3-1144K), but they are out of use at temperatures below 1K [71]. Capacitance thermometers are sometimes used for temperature measurement in high magnetic fields. Currently available commercial $SrTiO_3$ thermometers are

insensitive even to high magnetic fields and can operate down to 10mK, but they have a shift in calibration after thermal cycling.

Chapter 3. Experiment.

The second part of this work is devoted to the experimental temperature measurements in a range from 0.6K down to 6mK. Three independent thermometry methods were used: ^{3}He melting curve thermometer, SRM-768 fixed-point device and five resistance thermometers.

The main aims of the experiment were providing reliable performance and coincidence between the MCT and fixed-point device that can be used for calibration of a resistance thermometer. Broadening of the effective operational range as well as the calibration of resistance sensors from the large batch we have purchased were the most important practical goals of the experiment.

3.1 Setup and thermometers

The experiment was carried out with the Oxford 2000 commercial dilution refrigerator. The preceding runs showed its ability to reach 16mK without step heat exchangers; however no tests with the installed discrete heat exchangers have been done before. Three different thermometry means were used: a ^{3}He melting curve thermometer, an SRM-768 superconductive fixed-point device and five resistance thermometers with different packaging and wiring. All thermometers were placed on a high-purity copper mixing chamber plate to measure the fridge lowermost temperature. A 0.25KΩ MC heater regulated the temperature and provided an active temperature stabilization.

All wires from room temperature are thermally anchored at several temperature levels of the cryostat: 4.2K, 1.5K, 0.7K and 0.1K. A bulky copper connection board was set at 0.1K plate for heat sinking. Copper wires were used for heaters, however high-resistance and therefore low thermal conductive manganin wires were chosen for the thermometers.

3.2 Melting curve thermometer.

The melting curve thermometer consists of three parts: pressure transducer cell, capacitance bridge for the transducer response measurement and gas handling system to supply ^{3}He at high pressure. The melting curve thermometer we used (Fig.24) was manufactured by Dr. S.T.Boldarev [72]. It has a classical cylindrical Greywall-Bush design with Straty-Adams-type flat electrodes. The main parts are made of hardened beryllium copper; however a pure copper bottom was built in order to provide a better thermal contact to the object under measurement. As it is known, the rapid growth of the Kapitza boundary resistance dramatically worsens the thermometer dynamic characteristics at low temperatures. That is why a part of the cell volume is occupied by 100Å silver sintered powder. The sinter adheres to the silver plated copper base and greatly increases the contact area between

^{3}He and metal base. Unfortunately the amount of sinter is unknown for our MCT which complicated the choice of the thermometer starting pressure.

The electrodes are of 8mm diameter: the lower plate is fixed to a movable diaphragm while the upper one is static. In order to achieve small electrode spacing, the cell transducer plates were cured with epoxy while the cell pressure was 40bars and plates were in contact.

The capacitor plates are electrically isolated from the cell body which allowed capacitance bridge measurement. As it was mentioned before, a high coaxial lead capacitance to the ground can suppress the cell signal; therefore a three terminal method was used during measurements. A reference 22pF silvered Mica capacitor was placed on the mixing chamber in proximity of MCT for better stability.

The CuNi filling line of our MCT is thermally anchored at several temperature levels of the cryostat in order to decrease the heat transfer to the thermometer. It also allowed a hydrostatic head calculation for absolute pressure measurement. The capillary is of 0.6mm outer diameter from room down to 4.2K level, whereas it is two times narrowed at the still temperature level. High price of ^{3}He as well as the desire of making a device with a small specific heat explains such a design.

The gas handling and pressurizing system (Fig. 23) includes a ^{3}He storage reservoir, charcoal dipstick, a set of valves, pressure meters and calibrated commercial pressure transducer. The 99.996% purity gas is stored in a 5l reservoir at pressure of 600Torr in order to prevent an occasional gas release to atmosphere. A liquid nitrogen sorption cold trap was used to protect the low-temperature lines from small leaks of air and other contaminations that can block the capillary. The charcoal dipstick serves for cell pressurizing up to 35bars. It absorbs a significant amount of gas from the storage reservoir while immersed in a dewar with liquid helium, whereas the gas is released to the cell when the dipstick is warmed up. The high pressure gauge is needed to follow the pressure while the thermometer filling is in process.

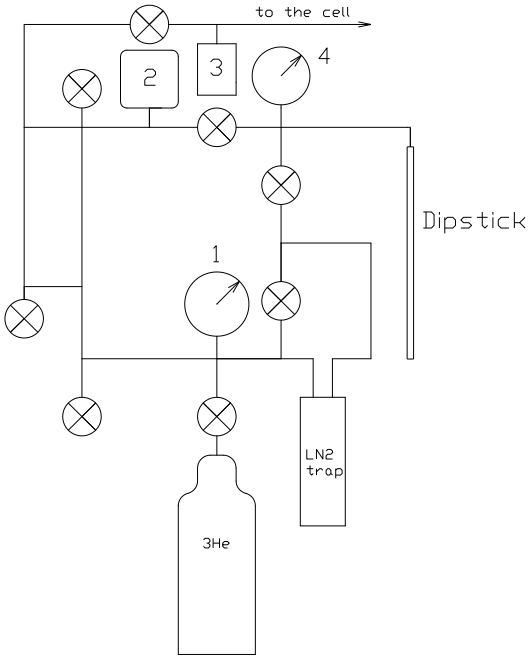

Fig. 23 Gas system: 1. Vacuum meter 2. Digiquartz pressure transducer 3. Emergency volume 4. High pressure meter

A valve on the top of cryostat separates cryogenic parts from the room-temperature line. A special emergency volume has been built if a rapid growth of pressure in the cell occurred, e.g. during the fast warming of the cryostat. All lines as well as the thermometer cell were carefully checked with the leak detector and tested by high pressure.

In order to calibrate the cell pressure transducer and define starting pressure, an auxiliary pressure meter, Paroscientific Digiquartz 2900 AS-002, was used. It has a working range of 0-62 bars with repeatability and hysteresis of 0.005% [73]. Pressure is converted into frequency in the 30-38 KHz range. The manufacturer calibration of Digiquartz is as follows:

$$p = 509.874 - 13.532f$$

The use of a frequency counter makes a fast frequency-to-pressure conversion possible. According to the calibration, 73.9 Hz of a frequency counter corresponds to 1 bar pressure change. The counter we used measured frequency with accuracy of 0.1Hz, which corresponds to 1.4mbars of pressure resolution.

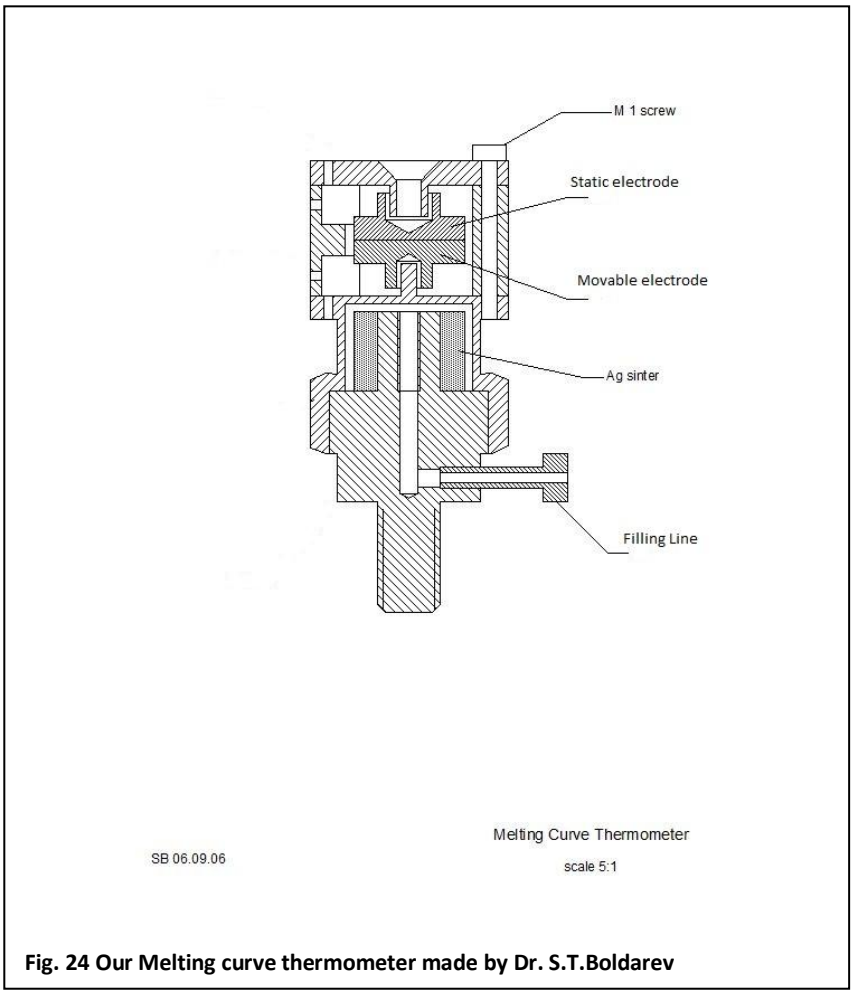

Fig. 24 Our Melting curve thermometer made by Dr. S.T.Boldarev

The cell capacitance measurement was organized by typical bridge system with the ratio transformer (Fig. 15, Fig. 16 and Fig. 25). For this purpose, a Model DT 72A Dekatran Decade ratio transformer was used. In principle, it is an auto-transformer with a variable tap. The tap position is indicated by the dial reading. A real part and phase of balance voltage was measured, however as we figured out, it does not make any difference if one measures X and Y values which were minimized to balance the bridge. The capacitance ratio can be estimated according to

$$\frac{C_1}{C_2} = x/(1-x)$$

On the other hand, one does not need to measure capacitance in absolute units, and ratio transformer dials were simply calibrated versus Digiquartz frequency and then converted to pressure.

An SR-530 lock-in amplifier served as a null detector and as a generator of 1 KHz sine voltage with V_{rms}=1V excitation. However, a lower excitation has also been checked, but no observable change in the thermometer performance has been noticed. The bridge balance was detected as a minimum in the lock-in input signal. In our experiments, the bridge balance occurred from 60μV at a few hundred of mK down to several μV at 10mK. At 1V excitation the 10^{-5} change of the transformer

ratio corresponded to 14μV change of the lock-in signal. Taking into account that we were able to measure bridge balance with 1μV accuracy, an approximate capacitance resolution is $\frac{\Delta C}{C} \sim 10^{-6}$.

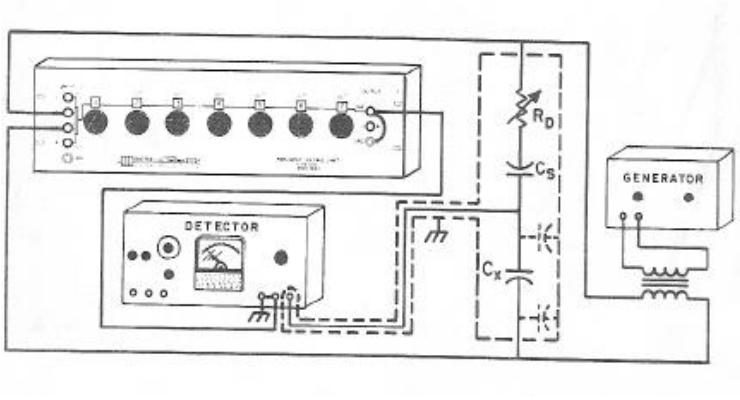

Fig. 25 Capacitance bridge with Dekatran ratio transformer. Lock-in amplifier works simultaneously as a generator and detector. The Dekatran dials were used to set the transformer ratio

3.3 The fixed-point device.

The second thermometry means we have used is a serial #18 NBS SRM-768 fixed-point device (Fig. 17). The mutual inductance of the secondary and primary coil was measured by a SR-830 lock-in amplifier with AC-excitation at 300Hz.

Two home-made magnetic shields were used for FPD protection from ambient magnetic field because Earth's magnetic field of 0.6 gauss can totally distort the device performance. First of all, FPD was shielded using degaussed mu-metal and superconducting niobium shields. The degaussing coil had a few tens of wounds around the hollow metal cylinder and supplied by an auto-transformer in order to provide high AC-current. The demagnetizing current was 10 amps at maximum and then slowly decreased. This procedure was repeated several times.

Material	Tc (mK)	Typical transition width, mK	Typical reproducibility upon thermal cycling specified by NIST, mK	Corresponding pressure uncertainty, mbar
$AuIn_2$	202.78	0.7	0.15	1.4
$AuAl_2$	160.38	0.2	0.10	1.3
Ir	99.27	0.8	0.10	2.2
Be	22.84	0.3	0.10	3.7
W	16.34	0.4	0.15	7.9

Table 6 Serial 18 SRM-768

The primary coil excitation voltage was set of the order of 0.1V whereas the induced signal in the secondary coil was in the μV range for high temperature transitions and decreased down to hundreds nV for tungsten. Data acquisition was organized via self-written Labview program.

3.4 Resistance thermometers.

The resistance thermometers we used are based on RCW575 RuO_2 Dale-electronics-type chips bought from Vishay Inc. The RCW575 chips are known as reliable low temperature sensors and are in use from eighties. Although Dale electronics does not exist anymore, Vishay Inc. fabricates them for common applications in electronics as very accurate 1KΩ resistors. All sensors are from a large, 5000 pieces, batch which was purchased only for 300 euro. Therefore, calibration and proven reliability and interchangeability of sensors from the same batch can make them a very convenient and cheap thermometer. A commercial Lakeshore Rox 102-A chip was also used for comparison. The first two sensors, S_0 and S_1 are the home-made thermometers of a new advanced design (Fig. 26). Each thermometer consists of sixteen Dale chips. The chips were divided into four sets connected in series, whereas each set consisted of four chips with parallel connection. The chips were glued with Stycast 1266 epoxy to high-purity copper base that has a bolt-type connection. In order to suppress an expected heating of sensors at low temperatures, S_0 and S_1 thermometers were placed into metal enclosures with the LC-filters and extra feed-through capacitors. The room temperature resistances of the sensors were 1010Ω and 1007Ω respectively. The dissimilarity in the RT-resistances appears due to slight difference in connection wire resistance.

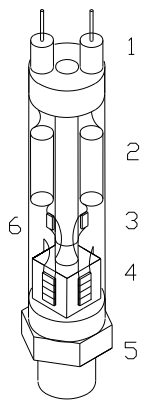

Fig. 26 Packaging of a 16-chip sensor: 1. Feed-through capacitors. 2. Inductive coils. 3. Capacitors to ground. 4. Sets of chips. 5. Bolt-type connection. 6. Metal enclosure

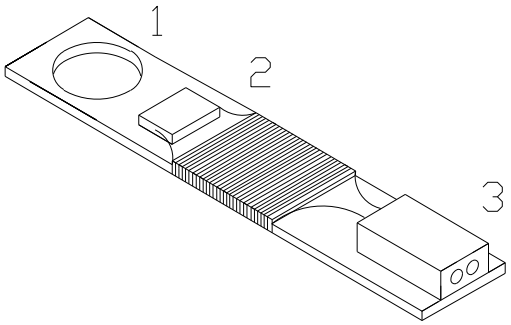

Fig. 27 Single-chip configuration: 1. Hole for the bolt connection 2. Chip with wound wires 3. Connector

The second pair of thermometers, S_2 and S_3, has a single-chip configuration (Fig. 27). A RuO_2 resistor was glued to a small copper plate with Stycast 2850 epoxy as well as the wires that were wound around. The room temperature values are R_2=999Ω and R_3=1006Ω. The fifth thermometer is a commercial single-chip Lakeshore RuO_2 102-A sensor with the same packaging as the first two

sensors. However, it has a slightly higher RT value, 1037Ω. It should also be marked that the Lakeshore sensor sensitivity at T<100mK is much higher than that for other thermometers and at T<50mK its resistance grew above 100KΩ.

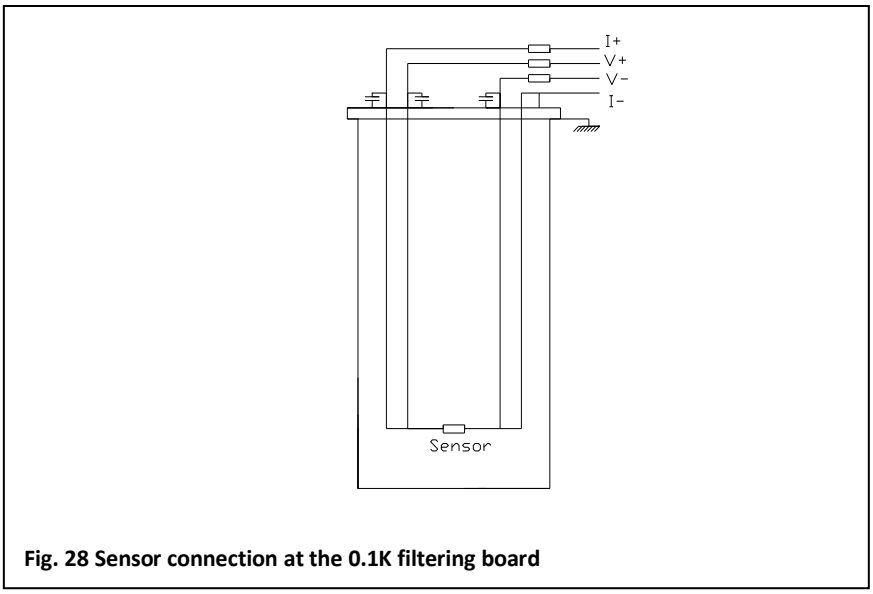

Fig. 28 Sensor connection at the 0.1K filtering board

All leads from the sensors to the 0.1K board were connected with the twisted pairs of Lakeshore manganin cables. The additional RC-filtering board for up to six thermometers had been made and placed on the 0.1K plate. 50Ω and 4.7nF elements were used for filtering which provides low-pass filters with cut-off at 4.3 MHz. The sensor 4-wire connection was performed as recommended by the AVS-47 resistance bridge manual (Fig. 28). All sensors except S_0 had the following connection: I^+,V^+,V^- leads were connected to the filtering board while the I-return lead was grounded. S_0 I^- lead remained floating for comparison.

The resistance measurement was carried out with the SIM-921 AC-resistance bridge embedded in the SIM-900 mainframe by Stanford Research Instruments. In order to switch between the sensors, SIM-925 Octal 4-wire Multiplexer was used. On some stage of experiment an isolation transformer was connected to defeat the mains interference which caused jumps in the sensor resistance. In order to eliminate ground loops, the cryostat was electrically isolated from the pumping system and only one common grounding point was used either for cryostat or for the resistance bridge. The cable connection from sensors to SIM-921 was carefully checked and shields were grounded from both sides, either to the bridge or to the cryostat.

3.5 MCT filling and calibration.

The MCT room temperature test should be performed as the first experimental stage. Linearity of the cell pressure transducer was tested after the MCT had been installed and connected to measurement circuit. The MCT was pressurized with nitrogen only up to 3.7bars and the lock-in

response on the pressure change was measured. We observed linear bridge reaction on pressure change. This was considered to be enough for the preliminary tests.

After the setup had been closed and cooled down to temperatures below 1K and all mixture was condensed to the dilution fridge, the MCT filling was implemented. First of all, the MCT room temperature filling lines were cleaned with the charcoal dipstick in liquid helium. Afterwards, some amount of ^{3}He was allowed to come to the dipstick through a sorption LN_2 trap. In our case 200Torr (NPT) of gas from reservoir was used to fill the MCT cell up to approximately 30 bars. This corresponds to only 50mmol of ^{3}He being consumed. The filling pressure was monitored by a Digiquartz output with the frequency counter.

After filling the cell, the pressure transducer was calibrated against Digiquartz. During the calibration the temperatures of all parts of MCT gauge and filling lines inside vacuum can were kept above 0.85K, so that there could not occur any solidification, even at highest pressure of 35bars. As was mentioned before, there is no need to know the absolute values of the cell transducer capacitance. That is why the ratio transformer dials were calibrated against Digiquartz frequency. The calibration procedure was performed several times during experimental run to detect possible drifts of the gauge capacitance or sensitivity.

The pressure range of interest was 29.3-34bars which corresponds to 5-700mK possible operating range. It was important to clarify whether the calibration depends on the MCT temperature in the range above 0.85K and way of calibration (growing or lowering the pressure). In our case no temperature dependence was noticed, however a small (a few mbar) hysteresis in first runs was observed between the calibration directions.

A slow linear drift of MCT calibration was observed from day to day (Fig.29). That is why it is recommended to exercise the cell transducer by tracing the pressure along whole range back and forth to reduce the hysteresis. Total calibration shift was 130mbar for 2 weeks and only 10mbar shift occurred in last 4 days.

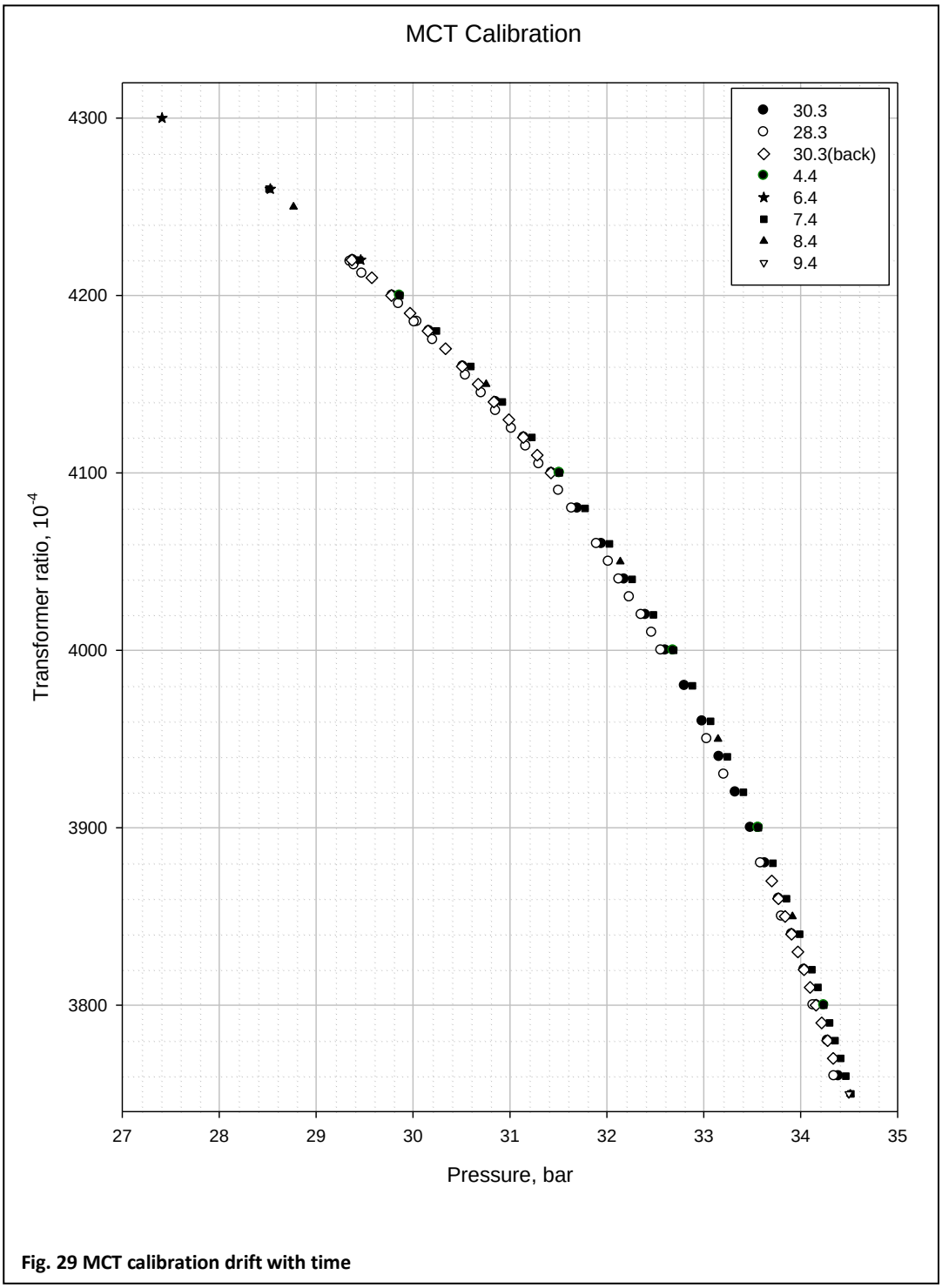

Fig. 29 MCT calibration drift with time

3.6 Choice of starting pressure.

The choice of a proper starting pressure is a cornerstone of successful MCT performance. It should be determined according to the temperature range of interest. Starting pressure defines the density and total amount of ^{3}He in the cell. If the initial pressure is too low, all solid will melt at low temperature, in an opposite limit, if the starting pressure is too high, it will be impossible to find the minimum due to ^{3}He solidifying in sinter. The recommended value is 33.8bars for 55% sinter

design (Fig. 30) [2]. However we were unaware of real amount of sinter for our thermometer. That is why several starting pressures were tried.

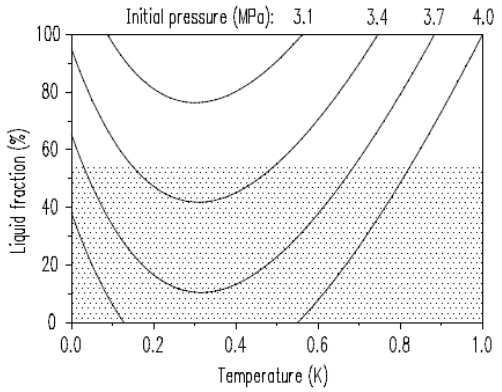

Fig. 30Co-existence curves of solid and liquid ^{3}He, expressed as liquid fraction, for four different initial pressures. The dotted area shows that about 55% of the volume of the cell contains sinter, and hence indicates the temperature ranges over which this is penetrated by solid ^{3}He [2]

Once the starting pressure is supplied, a solid plug should be formed by so-called blocked capillary method. The plug in the filling capillary is created at the still temperature level. The mixing chamber temperature is kept well above the temperature which corresponds to ^{3}He solidifying at chosen starting pressure. In our case, the MC temperature was stabilized by a PID controller at 1K for starting pressure of 34bars. At the same time, the still was rapidly cooled down by acceleration of a turbo pump allowing capillary to become blocked with solid. The capacitance bridge showed no reaction to any dipstick manipulation once the plug had been formed. Another method is to keep the still at temperature which corresponds to desired starting pressure and then start supplying ^{3}He to the cell.

There was no MCT signal while mixing chamber temperature was higher than it should be at starting pressure according to melting curve. However, the melting curve reaching can be confirmed by the MCT reaction on the MC temperature change.

3.7 Search of the melting curve minimum.

Melting curve minimum is the only fixed point attainable with the dilution refrigerator. A precisely found value can be used for the cell transducer calibration and correction of possible systematic error in pressure. However, an accurate minimum pressure measurement is a rather difficult experimental task. First off all it is caused by zero MCT sensitivity around it. In our case, ±3mK deviation from the minimum corresponded to only 2.5μV change of the lock-in detector signal.

Several minimum searches were done. As mentioned before, an unknown amount of sinter complicated the choice and several pressures from 34.2 to 31.2 bars were tried. Solidifying of ^{3}He

in the sinter did not allow us to find the minimum when 34.2 bars and 33.8 bars were tried. However at latter pressure solidifying of ^{3}He in the sinter occurred almost at the minimum pressure. On the basis of this we concluded that our cell contains 55-60 percents of sinter. The choice of 31.2 bars as the starting pressure allowed observing the minimum. Our value for p_{min}=29.362bar that is 55 mbar larger than the accepted one. A hydrostatic head contribution is only $p = \rho g h = 7\text{mbar}$ which slightly decreases the error down to 48mbar.

3.8 Fixed point device transitions.

An accurate study of the SRM-768 transitions can verify the MCT performance. In principle, FPD provides five fixed points and each of them can be used for MCT pressure calibration check if the search of minimum was unsuccessful. However one needs to fulfill a number of important precautions in order to acquire proper FPD transition temperatures.

First of all, the hysteresis either due to supercooling or to lack of thermal contact should be reduced as much as possible. The mu-metal shield degaussing and the use of additional niobium shield as well as the spot-welded buttons of Al should reduce the stray effect of residual magnetic field. The problems related to the slow response of MCT can be avoided by enough slow transition sweeping. Tracing speed for low-temperature transitions should be chosen as low as possible because of the increasing MCT time constant. One should keep in mind, that only T_{warm} should be used to obtain the transition temperature because it is not affected by supercooling.

All transitions were traced out by changing circulation rate of the dilution refrigerator. No electrical heating was applied; mixing chamber temperature was regulated only by varying turbo pump speed. MC warming without electrical heating becomes complicated at high temperatures, T>200mK, that is why we managed to trace $AuIn_2$ transition slowly only while cooling. Either imaginary or real part of the voltage induced in the FPD secondary coil was monitored. It was found that phase also has a well observable jump in a moment of transition, but only a real part of the induced voltage was taken into account. An MCT response was simultaneously acquired in order to refer the readings of these devices to each other. MCT and FPD signals were synchronized in time that made possible to recalculate the FPD signal against MCT temperature.

The first issue was to compare temperatures given by MCT with the fixed-point transitions. The data analysis indicated a certain proportional deviation in MCT temperatures from FPD: MCT showed higher temperatures than FPD and the difference increased from +1.2mK for tungsten up to +4.5mK for $AuIn_2$. Applying the pressure correction, -48mbars, which we figured out from the search of the minimum, led to larger discrepancy between thermometers.

However, one may use one of the FPD transitions in order to eliminate the MCT error. In principle, one may use any of them; however the best way is to find such pressure correction, which gives the smallest deviation of MCT temperature from the FPD reference values for all five transitions. The second factor that should be taken into account is a reproducibility of the FPD transitions specified by the manufacturer. Each of SRM-768 transitions has an uncertainty of reproducibility upon thermal cycling that appears from the features of the nucleation process. At the same time, the uncertainty in transition temperature of a potential reference point leads to an uncertainty in pressure to be chosen for correction of other fixed points. That is why it is more favorable to choose a higher temperature point, because the derivative, |dP/dT| decreases when approaching minimum. It is 37mBbar/mK at 22mK and only13mbar/mK at T=160mK. It means that although beryllium and $AuAl_2$ have the same typical reproducibility of 0.1mK (Table 3), the choice of $AuAl_2$ is more preferable because it provides almost three times smaller uncertainty in pressure correction for other transitions.

In order to find a proper point for making the pressure correction all transitions were analyzed. Each of them was tested as being a reference. Correction was calculated for each case and the deviation of MCT temperature from FPD for each other transitions were evaluated. The use of tungsten transition as a reference is the least favorable because it gives the largest divergence between FPD and MCT, whereas Ir and $AuAl_2$ provided almost equal results. Taking into account the aforementioned speculations about typical FPD transition reproducibility given by manufacturer, the choice of $AuAl_2$ is more preferable because it leads to almost two times smaller (than for Ir) uncertainty for corrected temperatures of other transitions.

Two ways of possible MCT temperature correction were analyzed. The first approach was to correct all transitions by a constant offset according to $AuAl_2$, +40.2mbar. However it gave a certain deviation from the FPD that increased for the low temperature points.

It indicates that one should use a proportional correction for each transition, $\Delta p = \frac{\Delta p_{AuAl2}}{p_{AuAl2}} \times p_{trans}$, where Δp_{AuAl2} is a pressure correction according to $AuAl_2$, +40.2mbar, p_{AuAl2} is an absolute pressure at temperature that corresponds to $AuAl_2$ transition, 30.26bars, and p_{trans} is the absolute pressure at temperature of transition to be corrected. This corresponds to ≈0.13% error in pressure determination, much larger than 0.005% specified in the Digiquartz manual. This much larger error may be explained by aging of the Digiquartz (it is 30 years old). As a result, the following pressure corrections were applied: Δp_W=+44.9mbar, Δp_{Be}=+44.5mbar, Δp_{Ir}=+41.6mbar, Δp_{AuAl2}=+40.2mbar and Δp_{AuIn2}=+39.6mbar. It corresponds to following temperature corrections: ΔT_W=-1.15mK, ΔT_{Be}=-1.20mK, ΔT_{Ir}=-1.93mK, ΔT_{AuAl2}=-3.1mK and ΔT_{AuIn2}=-4.4mK.

Now we present in more details experimental data on each of the SRM768 transitions observed in this work. All transitions are plotted using two x-scales: the upper one expresses the raw experimental MCT temperatures we have acquired, and the lower one contains corrected temperatures, as described above.

a. Be transition (22.84mK)

The hysteresis due to supercooling is more significant for pure metals such as beryllium or tungsten which have their transitions at lowermost temperatures. However, a proper value of the residual magnetic field can be defined if the second factor, delay of MCT, is minimized. In order to estimate residual magnetic field and possible amount of supercooling, beryllium transition was analyzed. It was swept back and forth with enough slow cooling and warming rates, 2.3μK/s and 2.4μK/s respectively (Fig. 31) which cancels the effects of slow MCT response and only supercooling contributes to hysteresis.

The cooling transition width was about 0.01mK, whereas the warming one is more broad, with W=0.1mK. However, it is even narrower than 0.2mK specified by Soulen and Dove [55].

Critical temperature was corrected against $AuAl_2$ and was about 22.62mK versus 22.84mK specified by NIST.

The residual magnetic field can be estimated according to relation

$$H_a = 2.4k\Delta T_s(\frac{dH_c}{dT})_{T=T_c}$$

by using experimental values for Landau-Ginzburg parameter from SRM-768 manual [55], k_{Be}=0.13 and $(\frac{dH_c}{dT})_{T=T_c}^{expt}$=7.0μT/mK. The amount of observed supercooling is not larger than 0.01mK. However, spot-welding of Al decreases transition temperature shift due to supercooling approximately up to 10 times [55]. The use of the formula gives an ambient magnetic field not larger than 0.2μT that is well below than that is recommended by NIST (1μT) [55].

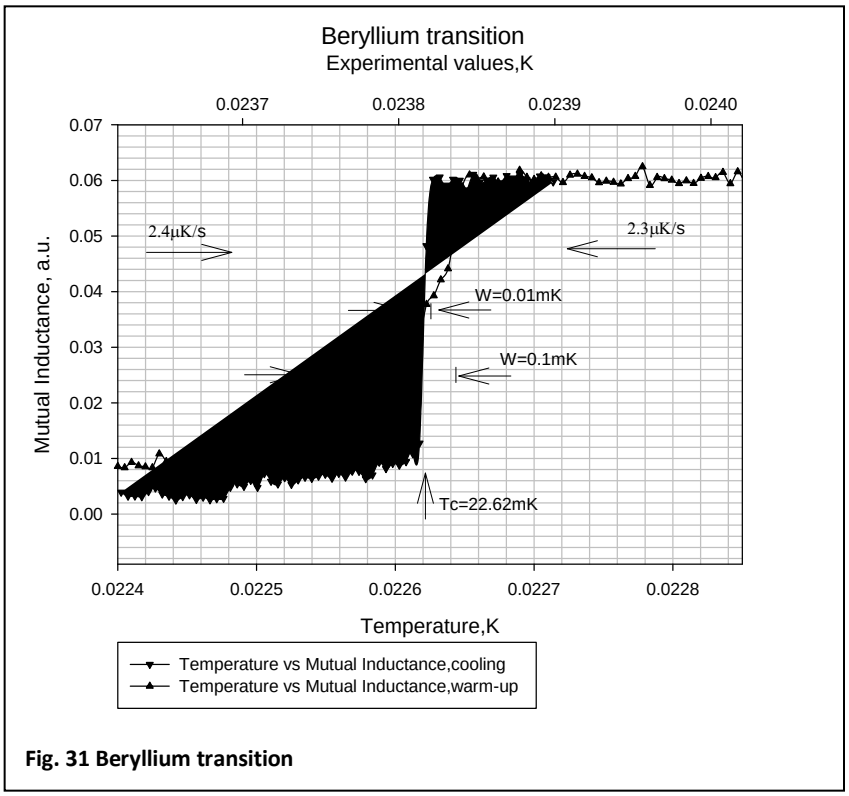

Fig. 31 Beryllium transition

b. $AuAl_2$ transition (160.38mK)

The sweeping speed for $AuAl_2$ transition during warming was 3.9μK/s. The T_c value obtained during this tracing was accepted to be the reference. The back tracing was carried out with speed of 15μK/s (Fig. 32). A certain hysteresis can be explained by a fast transition sweeping during cooling and slow MCT response. Critical temperature was assumed to be 160.38mK according to FPD reference. The observed transition width is 0.2mK which is 0.1mK less than a typical value.

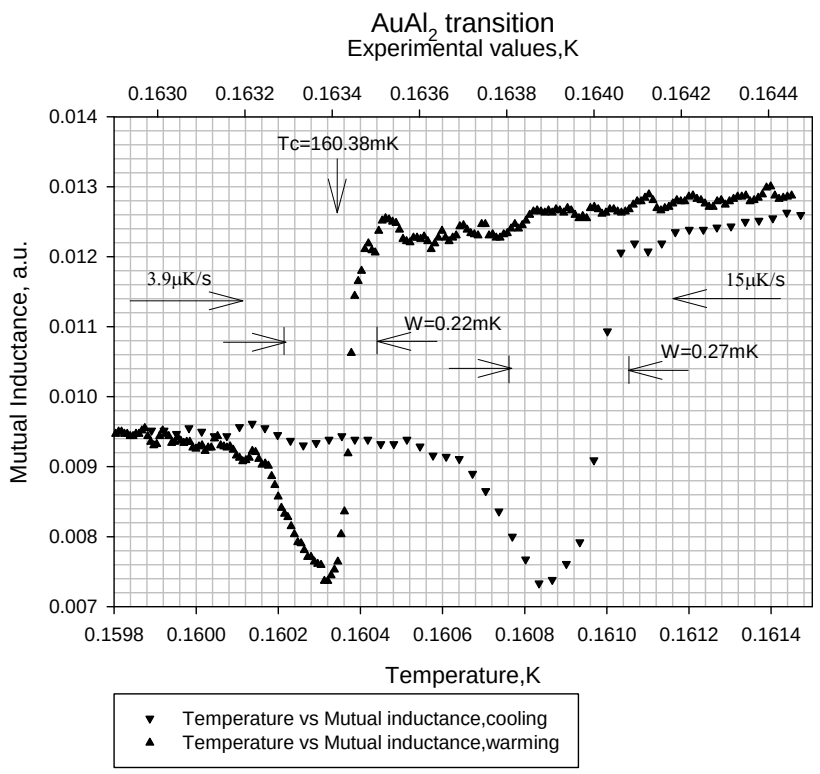

Fig. 32 $AuAl_2$ transition

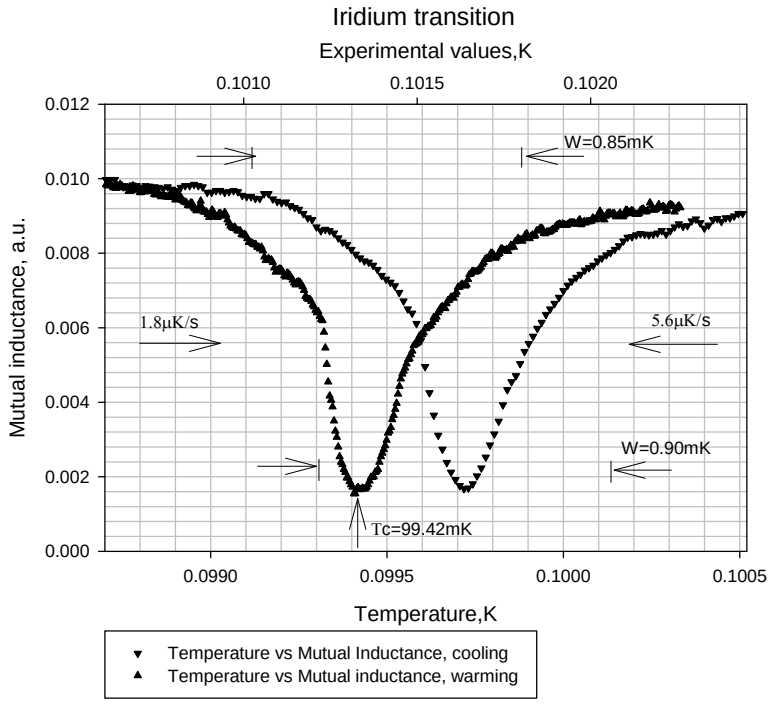

Fig. 33 Iridium transition

c. Ir transition (99.27mK)

The iridium transition was traced out with a cooling rate of 5.6μK/s and warmed with 1.8μK/s (Fig. 33). The transition critical temperature was corrected from 101.34mK to 99.42mK with 0.15 mK deviation from the FPD reference value. The width of 0.85mK is in a good agreement with the NIST value (0.8mK). The hysteresis is about 0.3mK within 0.1mK for typical transition reproducibility given by the manufacturer. The iridium (actually it is $Ir_{0.8}Ru_{0.2}$) sample is a type II superconductor and supercooling only negligibly contributes to hysteresis, it is specified as 0.02mK for 1μT. Therefore, observed hysteresis is again caused by a fast transition tracing during cooling.

d. W transition (16.34mK)

The change of mutual inductance for tungsten transition was an order of magnitude smaller than for other points, with induced voltage of order of hundreds nanovolts. The tracing speed was 3.3μK/s during cooling and 5.7μK/s while warming (Fig. 34). The transition width was 0.5mK and 0.2mK for warming and cooling transitions respectively. The critical temperature of 16.7mK deviates from the NIST value of 16.34mK. However, tungsten transition has a reproducibility provided by a manufacturer of 0.2mK. The supercooling contribution to hysteresis is about 0.02mK for field of 0.2μT. Therefore, hysteresis arises from the MCT large time constant at this temperature.

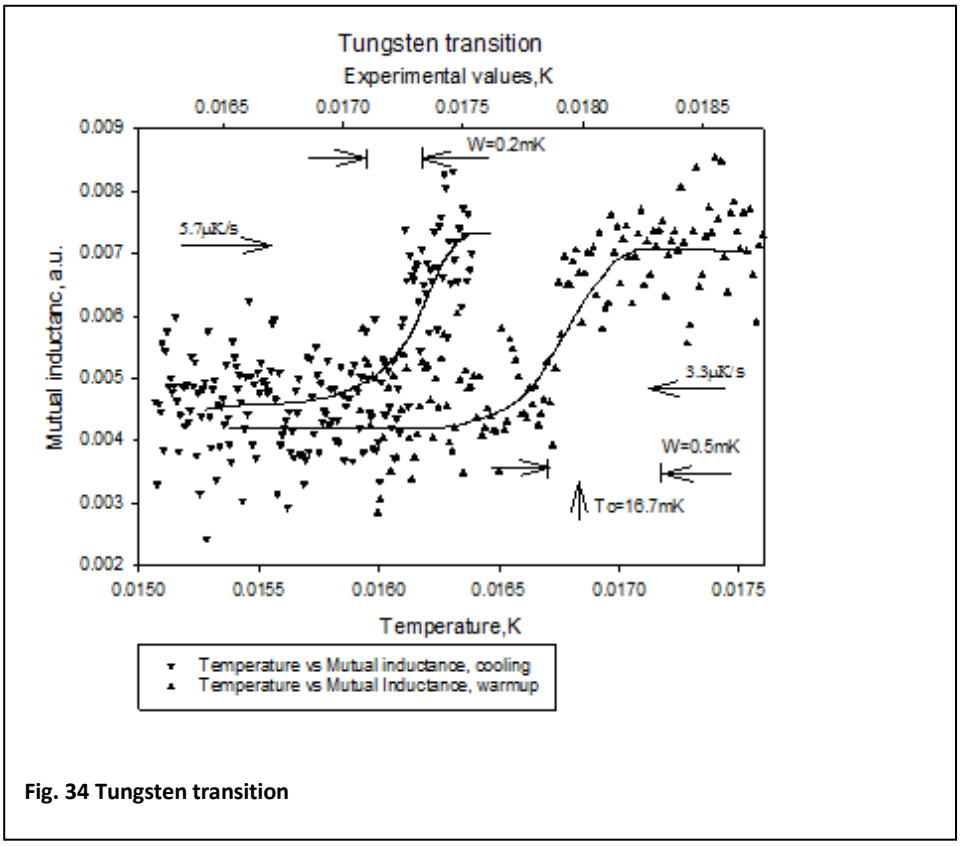

Fig. 34 Tungsten transition

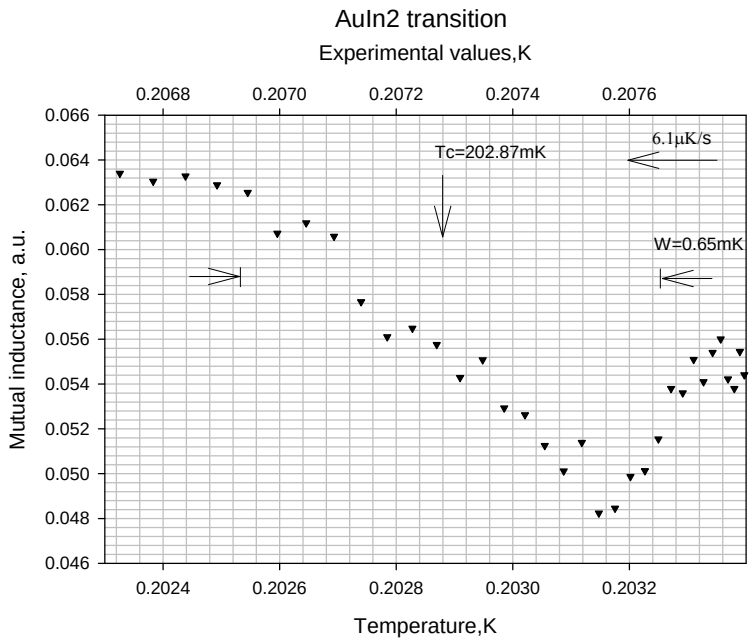

Fig. 35 $AuIn_2$ transition

e. $AuAl_2$ transition (202.78mK)

The $AuIn_2$ transition (Fig. 35) was observed only while cooling because as it was mentioned before, the slow warming is difficult to achieve without applying any external MC heating. That is why the value for critical temperature should be modified because of supercooling. The transition temperature is 202.87mK and for 0.2μT of residual field T_c should be increased by 0.1mK. The transition width is 0.65mK. The values specified by NIST are 202.78mK for critical temperature and 0.4mK for a typical transition width.

3.9 Hysteresis due to slow MCT response.

Since the residual magnetic field is small, the hysteresis appears mainly from slow MCT response to the temperature changes.

The hysteresis due to slow MCT response was studied on the example of the $AuAl_2$ transition which was traced with different speeds (Fig. 36). On the basis of this transition the choice of the tracing speed for other transition is analyzed.

The amount of supercooling which also contributes to hysteresis is not larger than 0.01mK for 0.2μT. As one can see, the largest deviation from the transition temperature appears with the highest tracing speed and it decreases for more moderate tracings. The transition temperature is

shifted from 160.38mK to lower temperatures for fast warming and to higher temperatures for fast cooling.

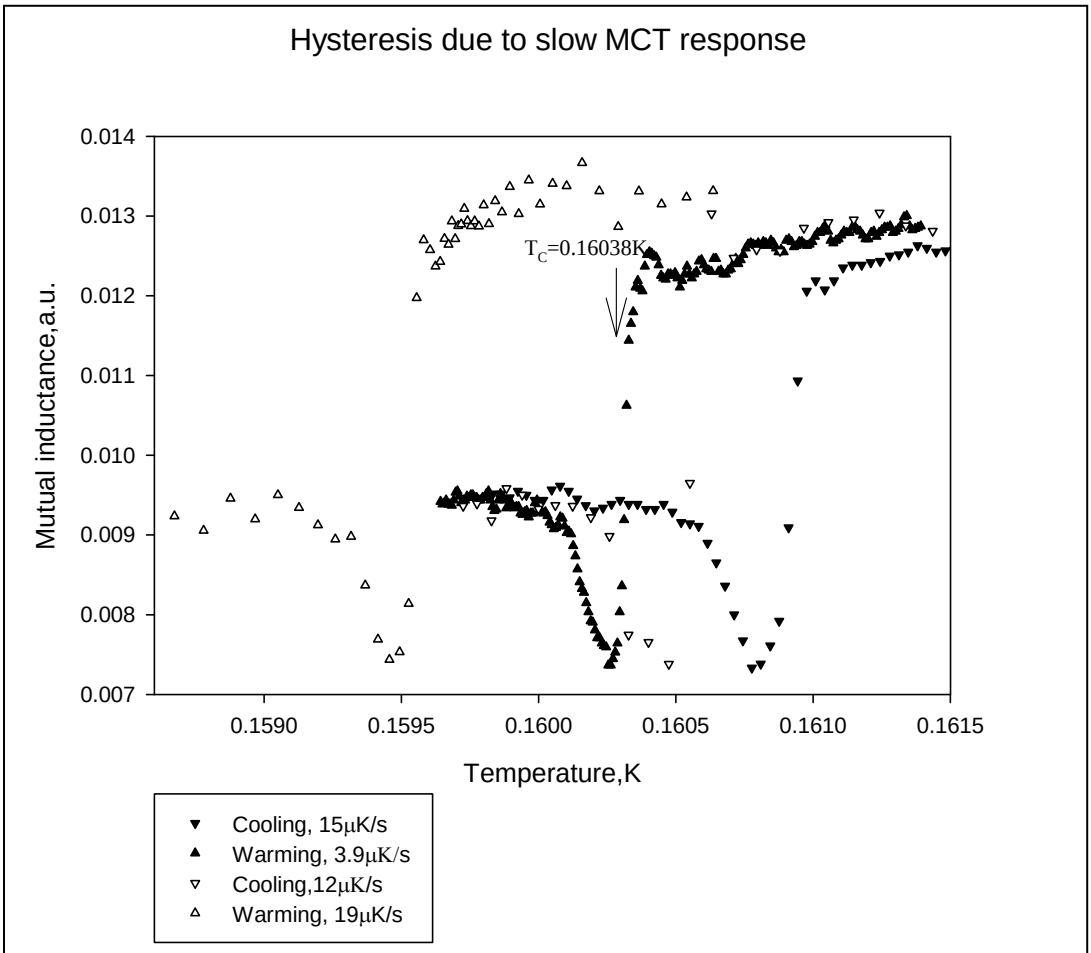

Fig. 36 Hysteresis in $AuAl_2$ transition due to slow MCT response

3.10 MCT time constant

Thermometer dynamic response is usually expressed in terms of the thermal time constant. It is commonly accepted to be the time that is needed for a signal to have an e-factor change or in other terms, to reach 63.2% of its asymptotical value. Time constant measurements were organized through an estimate of MCT temperature deviation from FPD temperature as was described in the previous paragraph.

In order to estimate time constant at 160mK, several $AuAl_2$ transition tracings were performed with different tracing speeds. As described before, the largest deviation occurred with the fastest tracing, 19μK/s. Transition temperature of 3.9μK/s warming was assumed to be an asymptotical value (Fig.36). Points were fitted with a single-parameter exponential function that gave τ of about 60s.

On basis of this we can conclude that the hysteresis of the Ir transition can be explained by the fast cooling tracing speed (5.6μK/s).

An estimate of the time constant at 22mK can be made from the analysis of the Be transition considered earlier. Cooling was made from the initial temperature of about 27mK with the constant circulation rate down to 16mK and the Be transition was swept with the speed of 2.3μK/s. Then the dilution unit was slowly warmed and Be transition was swept back with the rate of 2.4μK/s. As can be seen (Fig.31), the sweeping rates 2.4 and 2.3μK/s did not cause any hysteresis which is also contributed by supercooling. An exponential function needs $t \cong 3\tau$ to reach an asymptotical value. This means that the time constant at 22mK should be $\sim\frac{1}{3}$ of inverse tracing speed, hence τ is ~150s. At the same time, this means that the W (16.34mK) transition (Fig.34) was traced out not enough slow that caused the hysteresis.

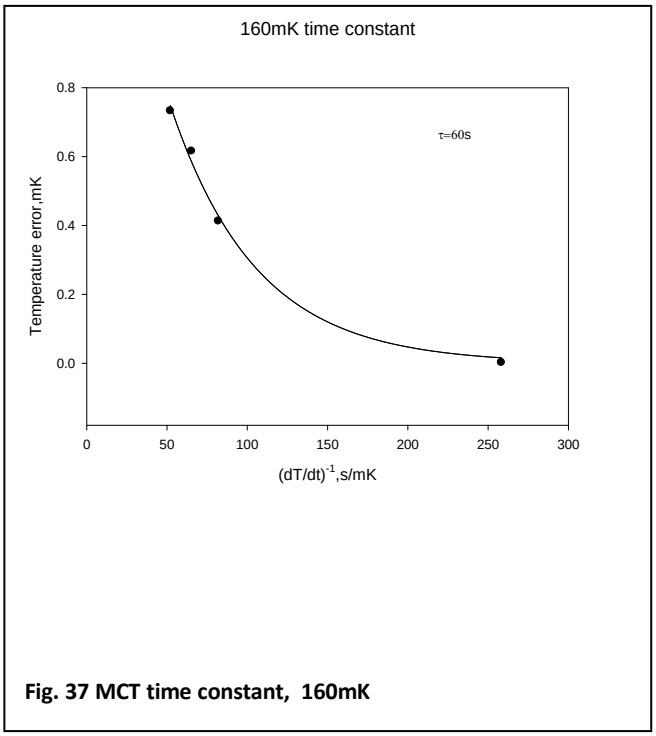

Fig. 37 MCT time constant, 160mK

3.11 Comparison between MCT and FPD.

The main aim of the experiment was to achieve coincidence or at least very small divergence between MCT and SRM-768 which allowed us to reliably calibrate resistance thermometers. Unfortunately we were unable to find the pressure minimum properly and make an appropriate systematic error correction of MCT alone. As a result, we had to rely on the FPD transition points which were used as a reference instead of pressure minimum. The finite transition reproducibility of a reference point specified by the manufacturer leads to uncertainty for other transition temperatures, ΔT_{ref}. Moreover, each transition also has an uncertainty in reproducibility (Table 3), ΔT_{rep}. There are also calibration uncertainties due to Digiquartz pressure transducer resolution: 0.005% of pressure: about 1.5mbar for p=30bars and frequency counter error, ΔT_{Dig}. The frequency counter we used measured frequency with 0.1Hz precision. This gives an instrumental

error of 0.5mbar which also should be taken into account, ΔT_{count}. The calibration error negligibly contributes to absolute error for low temperature points, whereas it increases for high temperature transitions due to change in dP/dT value.

The net error of MCT temperature should be estimated as

$$\Delta T = (\Delta T_{rep}^2 + \Delta T_{ref}^2 + \Delta T_{count}^2 + \Delta T_{Dig}^2)^{1/2}$$

The deviation between FPD and MCT temperatures is shown on Fig. 38. The relative deviation of MCT from FPD is shown on Fig. 39.

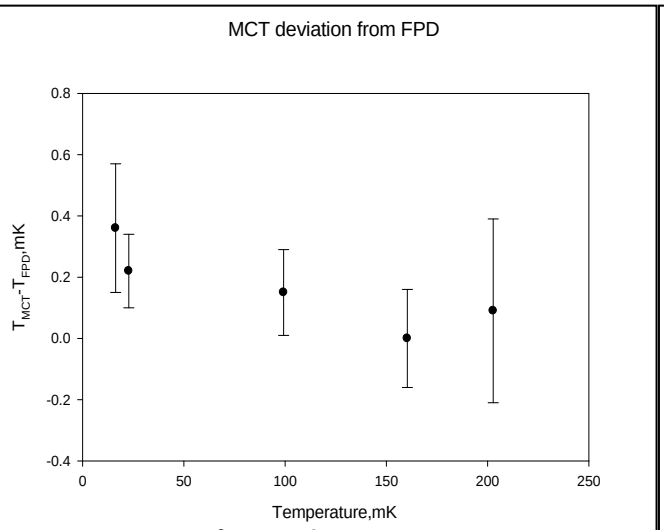

Fig. 38 Comparison of MCT and FPD

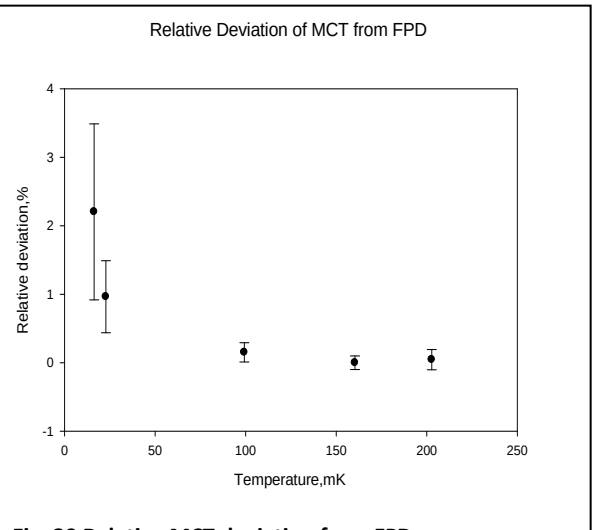

Fig. 39 Relative MCT deviation from FPD

The result allows us to claim that MCT and FPD coincide within uncertainty intervals for all fixed points except tungsten, ΔT_W=0.4mK. As a result, if no saturation effects occur, resistance thermometer can be reliably calibrated against MCT.

One should keep in mind errors which were not taken into account above: the uncertainty due to Digiquartz aging and MCT calibration drift during one run caused by the membrane inelastic deformation.

3.12 Performance of resistance thermometers

The evaluation of the resistance thermometer performance and their calibration against MCT was the most practically valuable part of this work. All sensors showed reliable performance and had similar R (T) dependencies in a high temperature range, at T>100mK. However, S_3 single-chip sensor had certain problems with wiring which were already observed at room temperature: it was very susceptible to touching and other manipulations. The resistance of this sensor was lower than that for other thermometers during the whole experimental run and it will not be studied further.

A certain divergence in the thermometer performance appeared at lower temperatures where problems with thermal contact and influence of RF-interference became more significant. Fig. 40 shows behavior of the sensors resistance as a function of temperature. The single-chip sensor, S_2,

was operable down to 35mK but then suffered from saturation. The 16-chip sensors remained non-saturated even at lower temperatures, down to about 30mK for S_0 and 20mK for S_1. Moreover, it was found that S_0 sensor was very sensitive to changes in the 0.1K plate temperatures where the filtering board was placed. The difference in their performance can be explained by different wiring. This means that the choice of a grounded I^- lead connection is preferable.

The Lakeshore sensor kept working down to 40mK. At lower temperatures its resistance approached 100KΩ that led to higher noise which can be overcome only by higher excitation. The latter led to overheating and saturation of the sensor.

Thus, our bare single-chip thermometer has the same operational range as the packaged commercial Lakeshore 102-A sensor. However, 16-chip sensors remained operable at substantially lower temperatures.

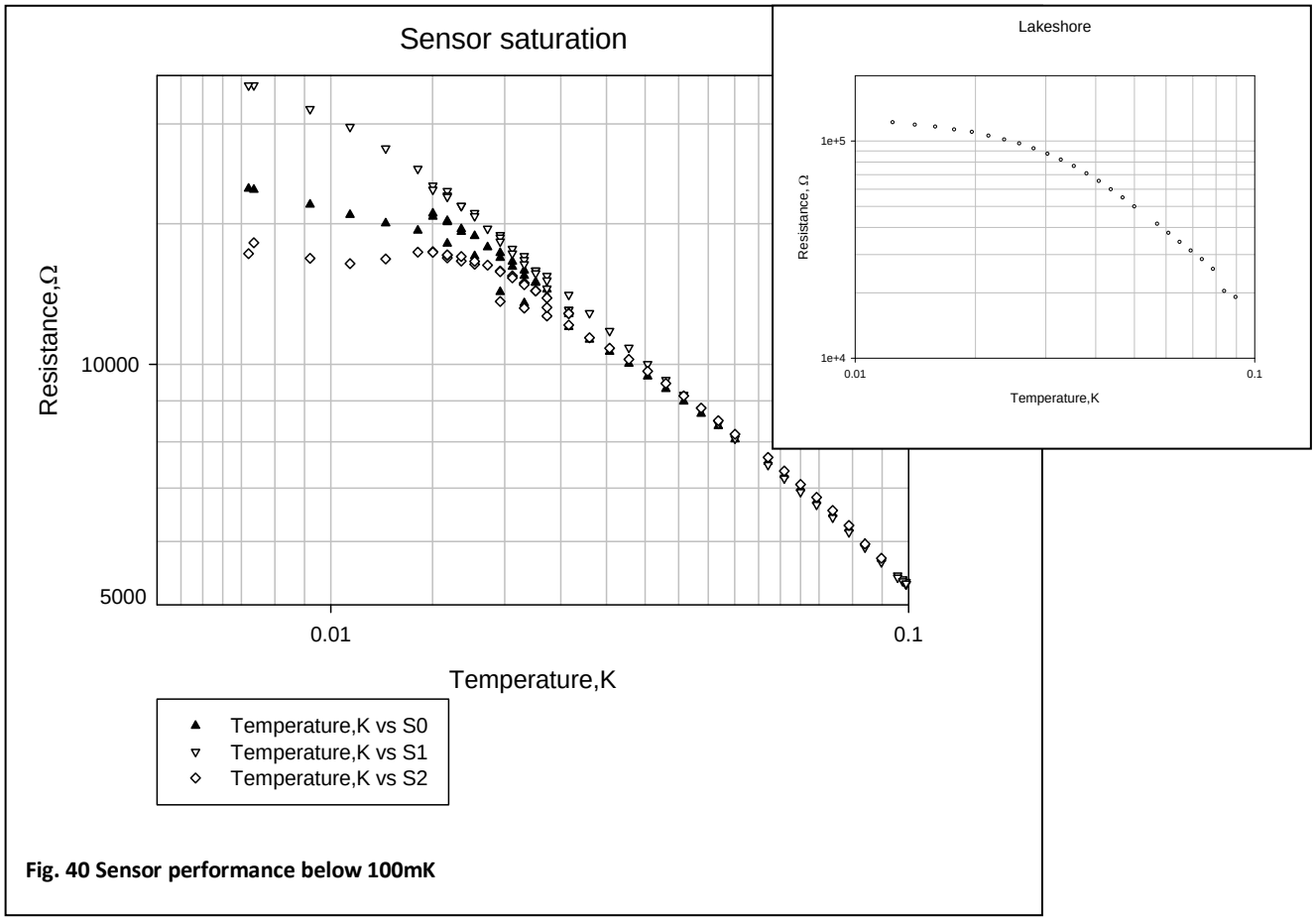

Fig. 40 Sensor performance below 100mK

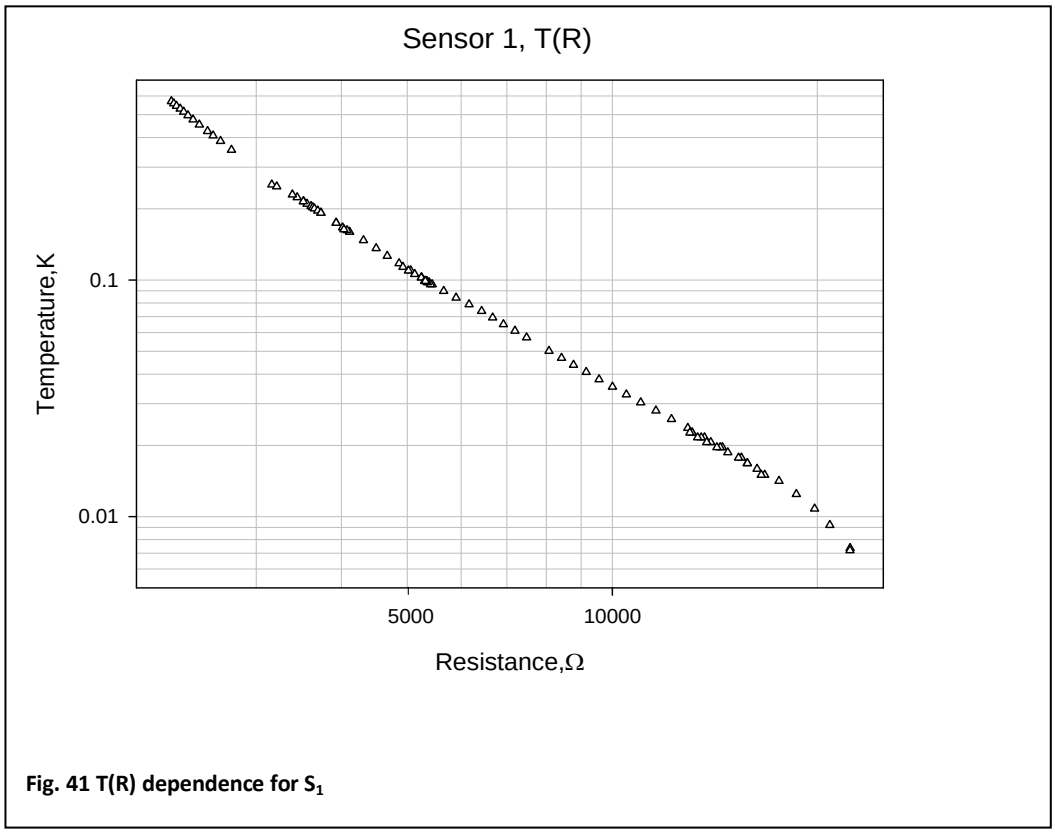

Fig. 41 T(R) dependence for S_1

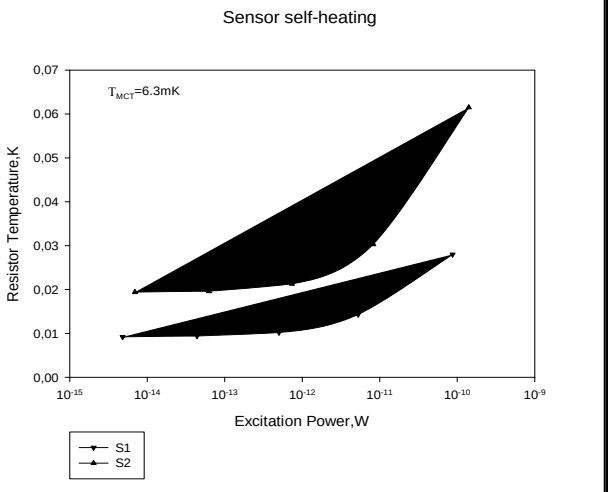

Fig. 42 Sensor excitation-heating test

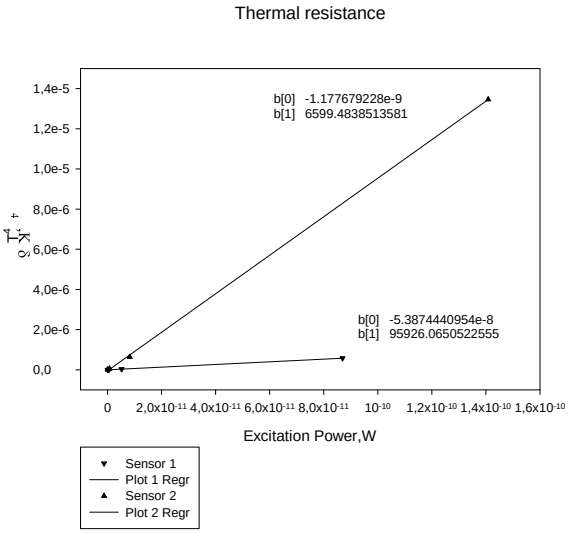

Fig. 43 Thermal resistance evaluation

3.13 Thermal contact

Thermal contact quality is the main factor that determines the possible working range of a resistance thermometer. Thermometers of different configurations were used in experiment in order to clarify which design provides better performance at low temperature. It was of practical importance to compare whether the use of 16 chips gives any advantage relatively to the simple single-chip design.

For these reasons, the best sensors, S_1 and S_2, were compared in the excitation-heating tests. The MC temperature was about 6.3mK according to MCT, the lowermost we have reached. However both sensors were already overheated to 10 and 20mK respectively.

Thermometers were step-by-step excited with 10, 30, 100, 300μV and 1mV voltage. Higher excitations led to enormous sensor overheating. Excitation was provided at 15Hz which was found to be the most optimal. The excitation-heating tests showed a larger overheating of S_2 thermometer

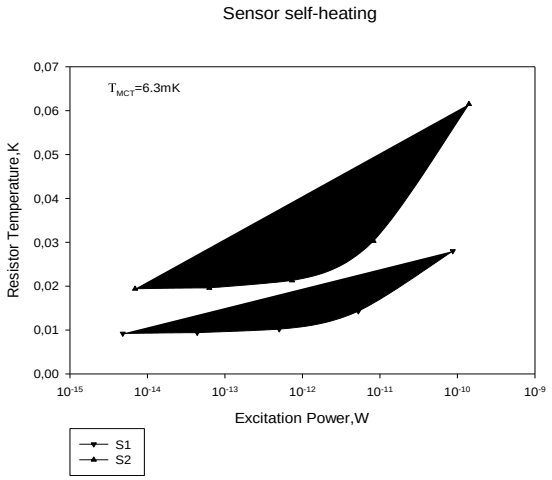

than that for S_1 by the same excitation power (Fig. **42**).

However an evaluation of the sensor thermal resistance gives more detailed information. Generally it can be found as $R_{th} = \frac{\delta T}{\delta Q}$ and is smaller for better thermal contact. This relation is usable only for infinitesimal changes of T. As far as R_{th} has a strong dependence on T a modified expression should be applied

$$R_{th} = \frac{\delta T^n}{\delta Q}$$

n is usually chosen to be from 4 to 6 for the thermal contacts between solids [14]. The dependence should be linear and the slopes make possible to estimate the ratio of the thermal resistances. A plot of δT^4 versus excitation power is shown on Fig. 43.

The slope ratio for the sensors S_1 and S_2 is about 15, which corresponds to 15 times better thermal contact for the S_1 thermometer. Thermal resistance is roughly proportional to inverse number of chips and therefore to sensor contact area. This means that thermal contact between sensor and copper base is established mainly through epoxy and glass cover of the chip while manganin wires do not play any significant role.

3.14 Study of the sensor interchangeability

A use of several thermometers allows judging about reproducibility of R (T) characteristics among chips from the same batch. For these purposes, S_0,S_1 and S_2 sensors were compared. Unfortunately S_3 performed unreliably even at room temperature and it should be kept out of consideration.

The resistances of the sensors were compared in a range between 0.1 and 0.6K in order to cancel any contributions of the saturation effects appearing at lower temperature (Fig. 44).

The relative deviation of the S_0 and S_2 from S_1 sensor is shown on the Fig. 45. The sensors have a slight difference in performance of order of 2% near 100mK due to different overheating for each of them. However the divergence almost vanishes at T=250mK and becomes observable at T>400mK. The discrepancy at high temperatures, where dR/dT becomes lower, may be attributed to the difference in the wire resistance. However, the R(T) divergence for sensors is not larger than 2% for the range of 0.1-0.6K (Fig.45).

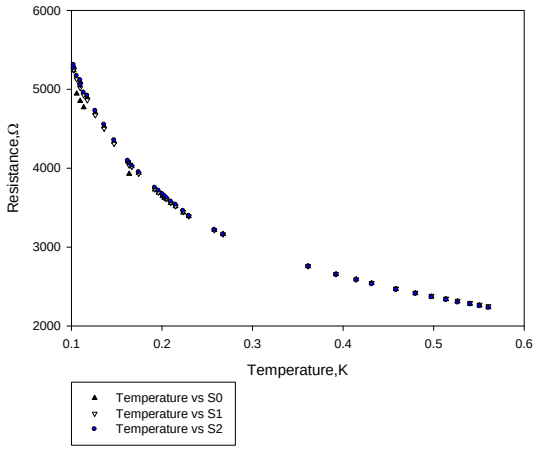

Fig. 44 Sensor resistances in a range of 0.1-0.6K

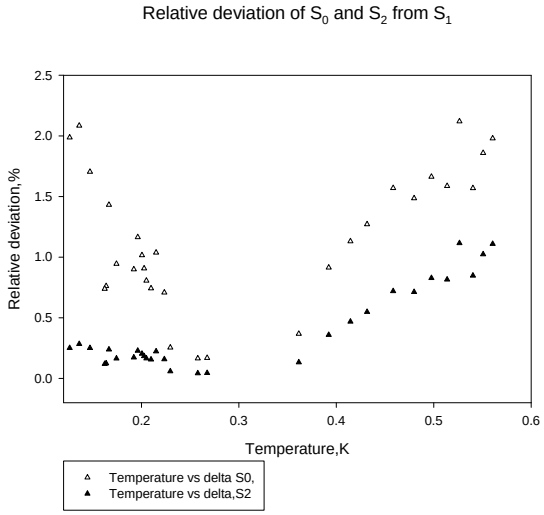

Fig. 45 Relative deviation (in temperature) of S_0 and S_2 from S_1

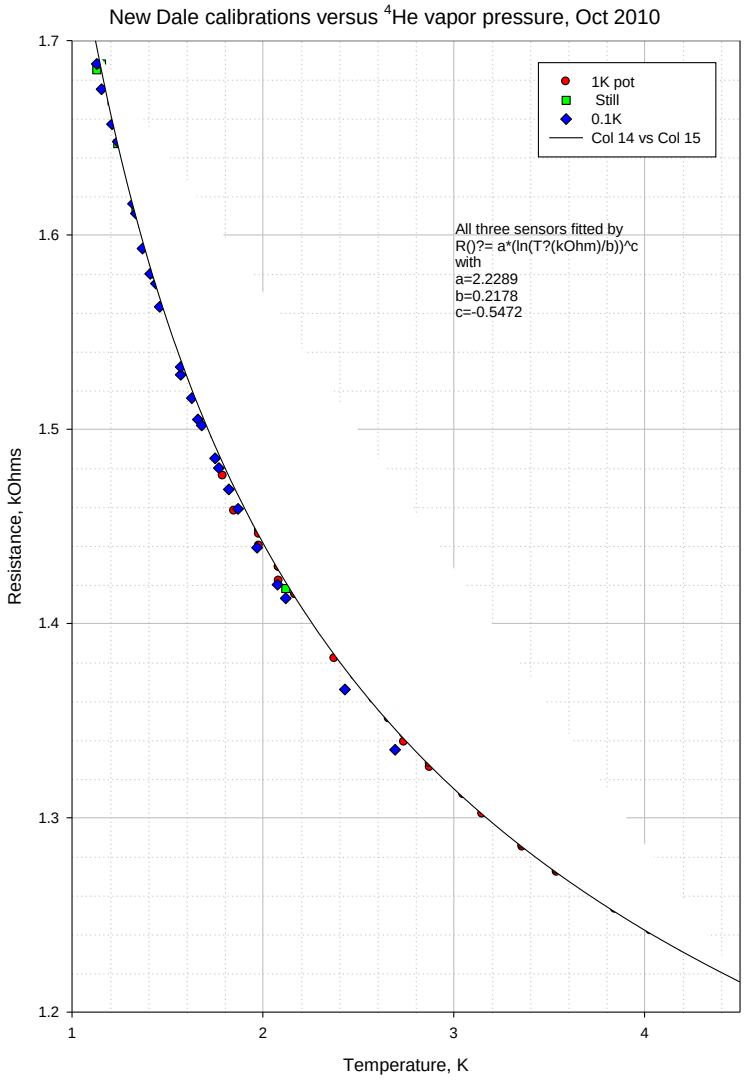

Fig. 46 RCW575 Dale chips from the same batch as the sensors in current experiment. Calibration against ^{4}He vapor pressure. Data from previous runs.

It is useful to compare the calibration of RuO2 chips for higher temperatures, performed during pre-cooling of the refrigerator. The data from previous runs are shown on Fig. 46. Sensors from the same batch as we used in the current experiment were calibrated. The thermometers were mounted at different levels of the dilution refrigerator and were calibrated against ^{4}He vapor pressure. The R (T) values of the sensors are in a good agreement: they almost coincide at temperatures from 1 to 2K and slightly diverge at higher temperatures that may be explained by a certain difference in the lead resistance.

An independent study of the resistance performance during thermal cycling was also carried out. Four previously unused RCW575 Dale chips from the same batch as described before were tested. All of them were prepared as single chip thermometers (Fig. 27) and each sensor was placed in a metal dipstick and then tested one-by-one. Sensors were bolted to the bottom of the dipstick for

better thermal contact; however the dipstick was not vacuum-tight and thermal contact was established mainly through helium vapors.

Chip resistances were as follows: R_1=1001Ω, R_2=1000Ω, R_3=1000Ω R_4=1000Ω. A certain difference appeared after wiring: R_1=1012Ω, R_2=1014Ω, R_3=1007Ω, R_4=1010Ω.

Dipstick was slowly immersed in liquid helium and sensor resistance was monitored with the SIM-921 resistance bridge. The whole procedure consumed about 10 minutes for each cooling. Warming was carried out by a rather slow (5-7 min) dipstick extracting from the dewar and then by heating with air gun (50-70'C). Values at 4.2K as well as at room temperature acquired after the thermal equilibrium had been established and resistance stopped changing.

Sensor R_1 was cycled 15 times, whereas R_2 and R_3 and R_4 only 5 times. All sensors have a good reproducibility upon thermal cycling of about 1Ω (20mK), however their absolute resistances had a noticeable difference: R_1=1258Ω, R_2=1245Ω, R_3=1233Ω and R_4=1251Ω. No trend in the sensor resistances during thermal cycling was noticed and all values fluctuated not more than 1Ω from that considered earlier.

Manganin resistivity changes only by 10% after cooling to 4.2K [74] and the difference between sensors arises mainly from wire resistance. However, difference between R_1 and R_2 (0.2K) which have almost the same room temperature resistances can be attributed only to constructional features of the chips. Room temperature values were stable within 0.2Ω for all sensors and did not change during cycling.

As a result, the study of possible sensor interchangeability showed that sensors have a very moderate difference in R(T) dependencies, at low temperatures T~2K, whereas it becomes more significant at higher temperatures due to certain wiring dissimilarities.

3.15 RuO_2 resistor calibration

High reproducibility of R(T) dependence among the sensors makes possible to utilize the calibration for all chips from the same batch with a very modest uncertainty.

On the first stage a range where the sensor to-be-calibrated remains sensitive to the temperature change should be defined. An increasing thermal resistance makes sensor more prone to RF-noise pick-up and overheating from excitation. As was found, 16-chip S_1 sensor performs better than other sensors and therefore should be used for calibration. The calibration correction for other sensors should include a certain difference in the lead resistance for high temperature range where it can cause an observable error due to decreasing sensitivity dR/dT.

In order to define temperatures where the saturation effects start depressing sensor's performance, calibration points from 100 to 40mK were fitted with 6-parameter exponential function. Afterwards

fitting function was extrapolated down to 5mK and experimental points were added to the plot (Fig. 48).

A certain deviation appeared from approximately 25mK which can be explained by saturation effects. The S_1 sensor overheating is plotted on Fig. 49 and Fig. 50. The thermometer overheating is $\approx$0.5mK at 25mK and $\approx$1mK at 20mK. At lower temperatures saturation effects are more significant which deflect sensor resistances from expected values. Nevertheless S_1 can still be used even below 20mK but with reduced accuracy.

Several fitting functions were tried: exponential, rational, inverse cubic and logarithmic. Logarithmic and rational fitting have the smallest error. However, it is more correct to use logarithmic or exponential fit as it is known from the physics of semiconductors. On the other hand if one simply needs a fitting curve to find R(T) function, a rational fit suits best.

The fitting errors have a certain maximum around 300mK which is caused by small MCT sensitivity around minimum leading to errors in temperature. A decrease of sensor resistance sensitivity dR/dT leads to larger errors at higher temperatures (Fig.51).

Although an appropriate pressure correction eliminated discrepancy between MCT and FPD, the uncertainty in the bridge balance measuring causes an error in the resistance thermometer calibration. As was mentioned before, the zero sensitivity of MCT around minimum allows even a small pressure uncertainty to provoke a large temperature error there. The 1μV accuracy in a bridge balance measuring we achieved corresponded to 7×10^{-7} of the ratio transformer dial. An error in the resistance thermometer calibration due to limited accuracy of the bridge balance measuring is shown on Fig. 47.

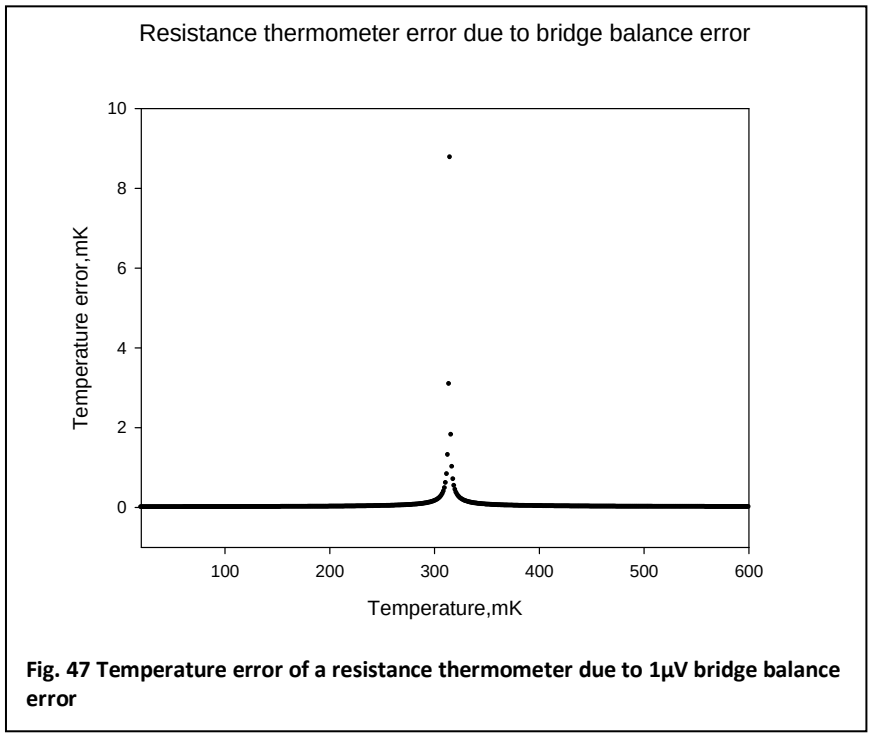

Fig. 47 Temperature error of a resistance thermometer due to 1μV bridge balance error

The R (T) dependence for a wider temperature range up to 28K is shown on Fig. 56. It contains the data acquired during several runs for the sensors from the same batch. The plot includes the calibration of our RCW575 Dale chips against ^{4}He vapor pressure (1-4K), H_2 vapor pressure and commercial Ge thermometer (4-28K). Points are fitted with a rational function and the fitting curve can be used for following temperature in the whole range 0.025-28K.

Sensors remain sensitive at higher temperatures up to 10-20K (Fig. 57). The sensitivity is 8Ω/K at 10K and 4Ω/K at 15K. Therefore, they can be used as thermometers in this range if a very high accuracy is not required.

Therefore, the RCW575 Dale chips by Vishay Co can serve as very cheap and reliable thermometers for measurements in a wide temperature range. Advanced 16-chip design greatly widens the operational range relative to a simple single-chip design due to superior thermal contact at lowest temperatures. Proper packaging and filtering allows one to measure temperature at least down to 25mK with an uncertainty of only 0.5mK and 1.5mK at 15mK (10%). Sensors can be effectively used up to several Kelvin but at the same time remain sensitive up to 30K. Good interchangeability and reproducibility upon thermal cycling for the sensors from the same batch allows utilizing calibration among sensors.

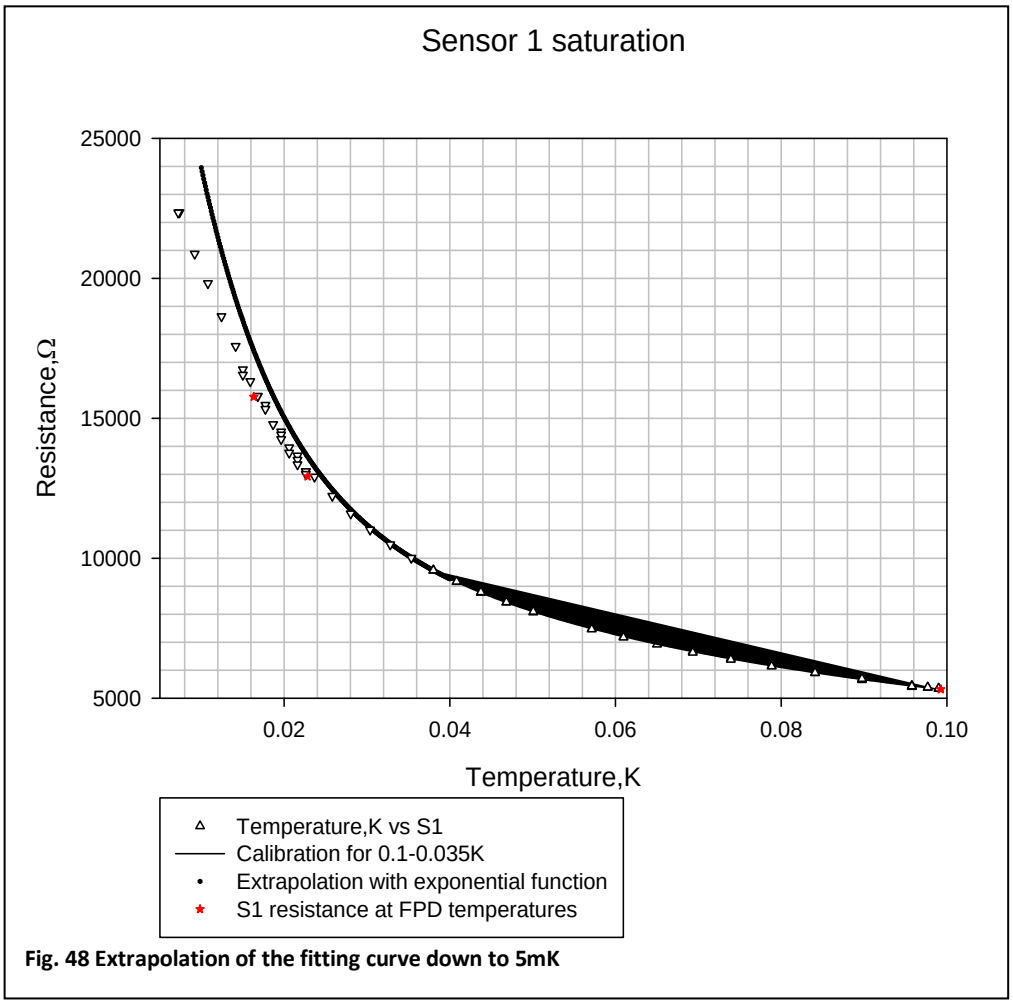

Fig. 48 Extrapolation of the fitting curve down to 5mK

The extrapolation function (Fig.48):
f=a*exp(-b*x)+c*exp(-d*x)+g*exp(-h*x),
a=3186.5878
b=5.6210e-005
c=33079.3433
d=103.7032
g=10629.5285
h=9.9801

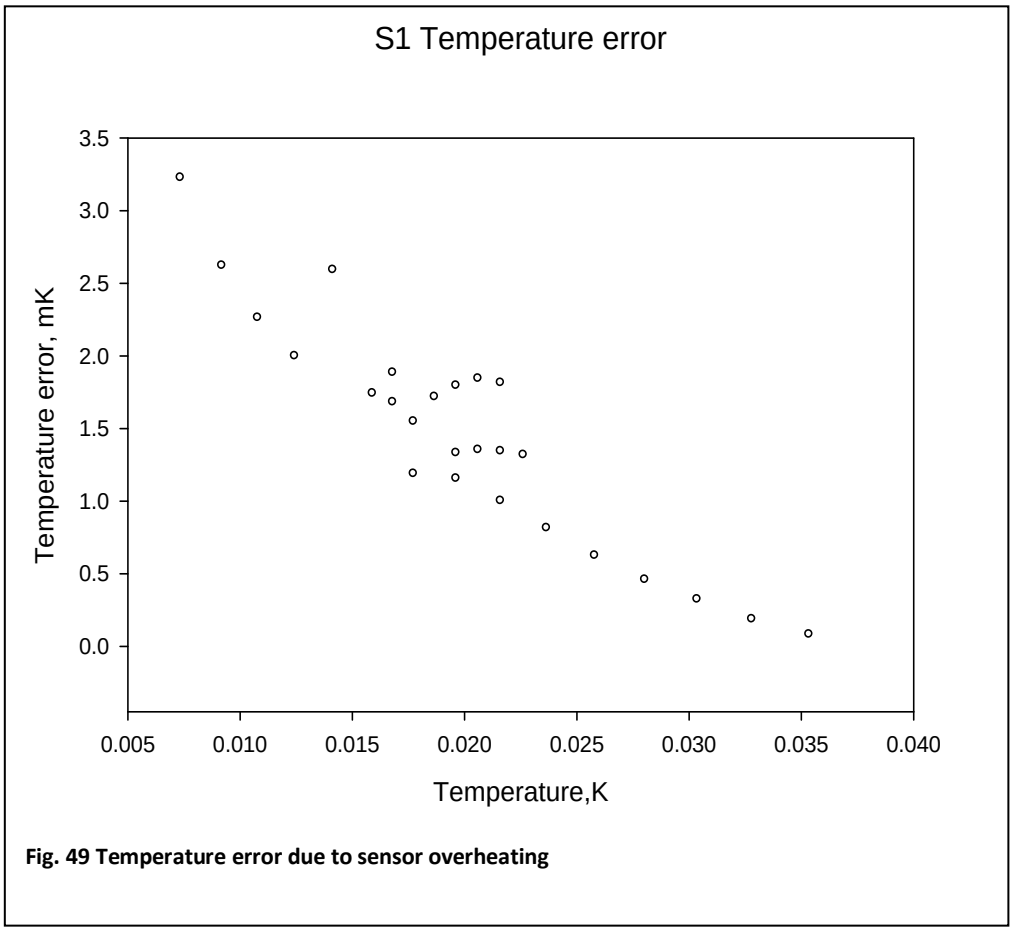

Fig. 49 Temperature error due to sensor overheating

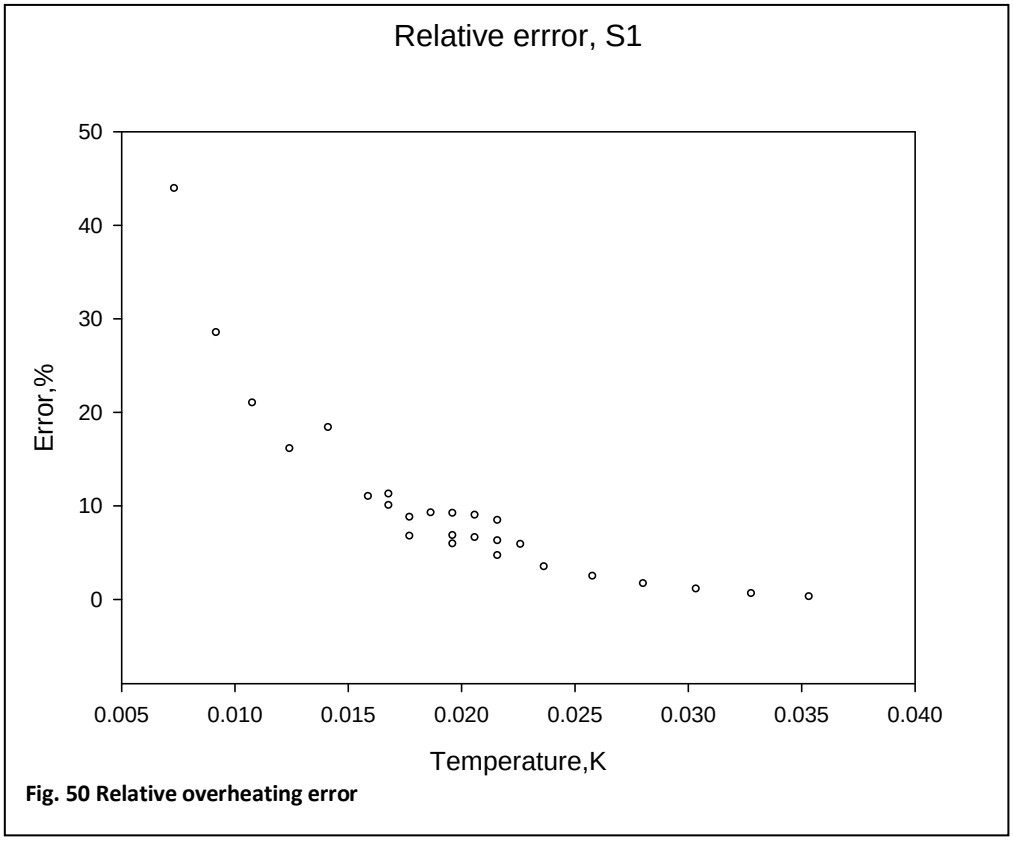

Fig. 50 Relative overheating error

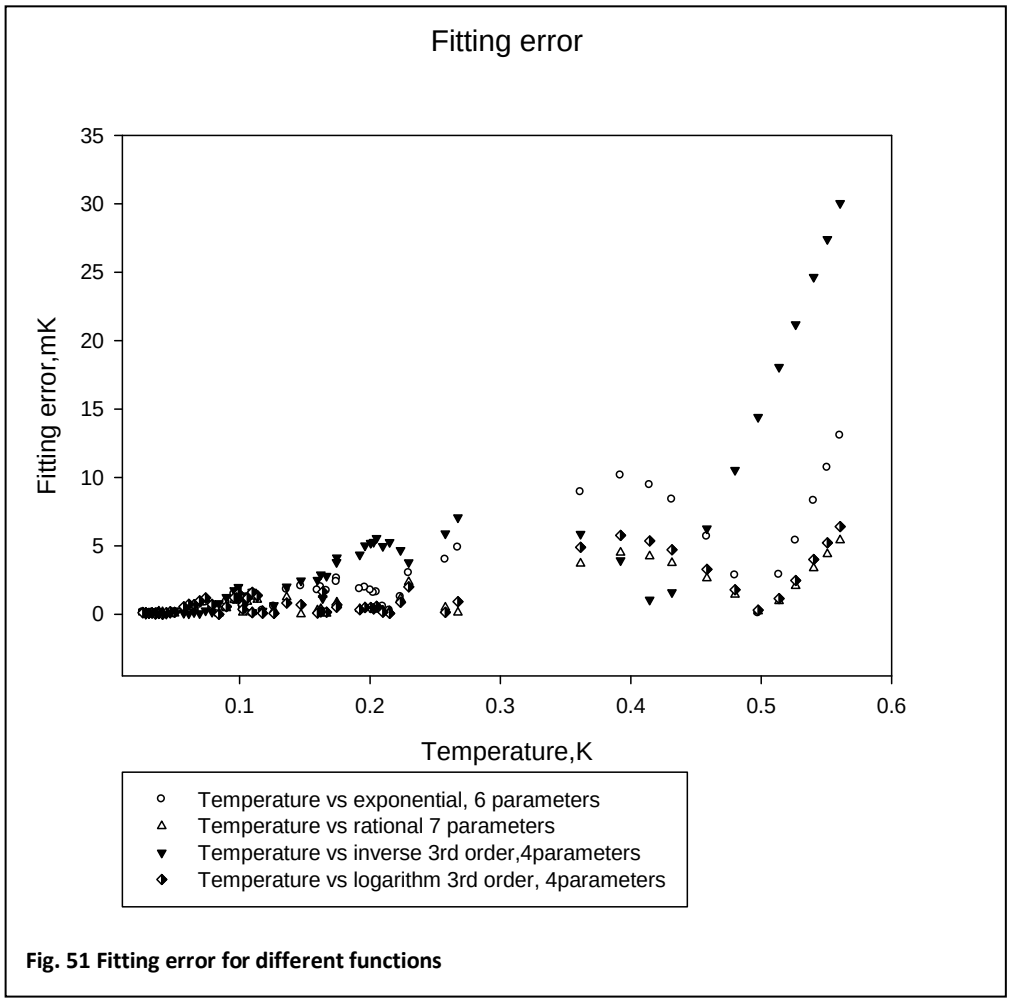

Fig. 51 Fitting error for different functions

The used fitting functions:

Exponential: R(T)= f=a*exp(-b*x)+c*exp(-d*x)+g*exp(-h*x)

a=16211.0204
b=67.9156
c=8093.4178
d=16.1843
g=4158.3202
h=1.1219

Rational (Fig.53): R(T)=(a+b*T+c*T^2+d*T^3)/(1+e*T+f*T^2+g*T^3),

a=41215.1035
b=105343.4142
c=-2359571.9679
d=-2021725.1162
e=110.7579
f=-524.7906
g=-1922.1234

Inverse 3rd order: R(T)=y0+(a/x)+(b/x^2)+(c/x^3)

y0=1551.5204
a=447.9011
b=-7.6811
c=0.0841

Logarithmic 3rd order (Fig.52): R(T)= ln(R)=y0+a*ln(abs(T))+b*(ln(abs(T)))^2+c*(ln(abs(T)))^3,

y0=7.5148
a=-0.3256
b=0.0716
c=5.1000e-3

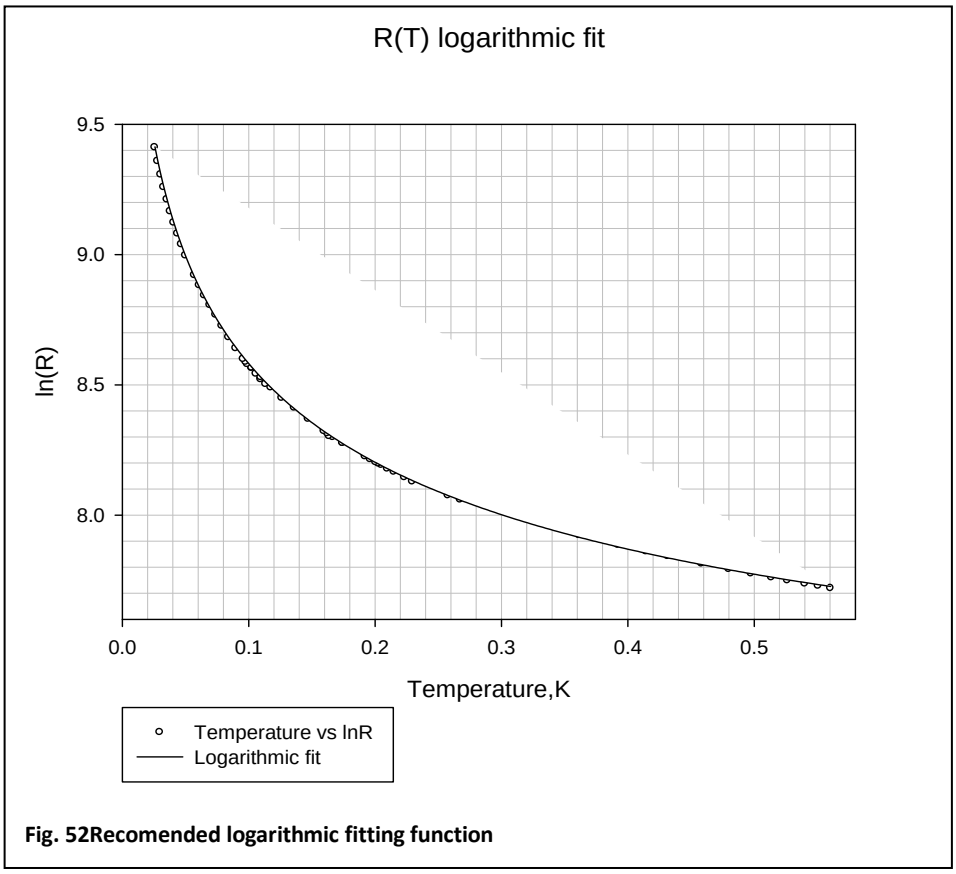

Fig. 52Recomended logarithmic fitting function

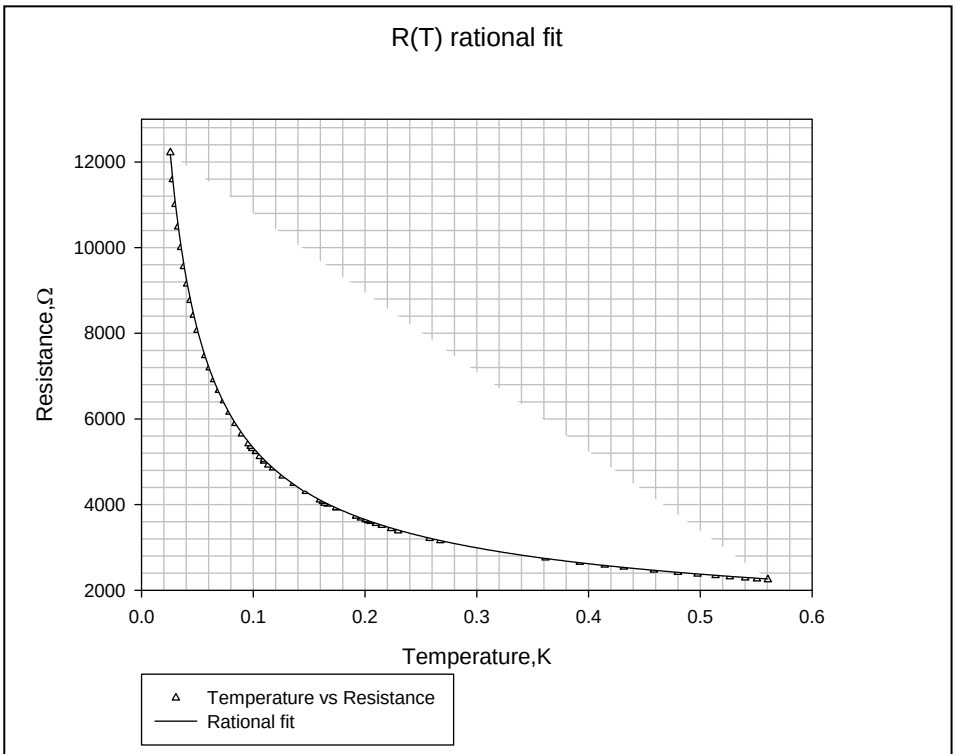

Fig. 53 Fitting with rational function

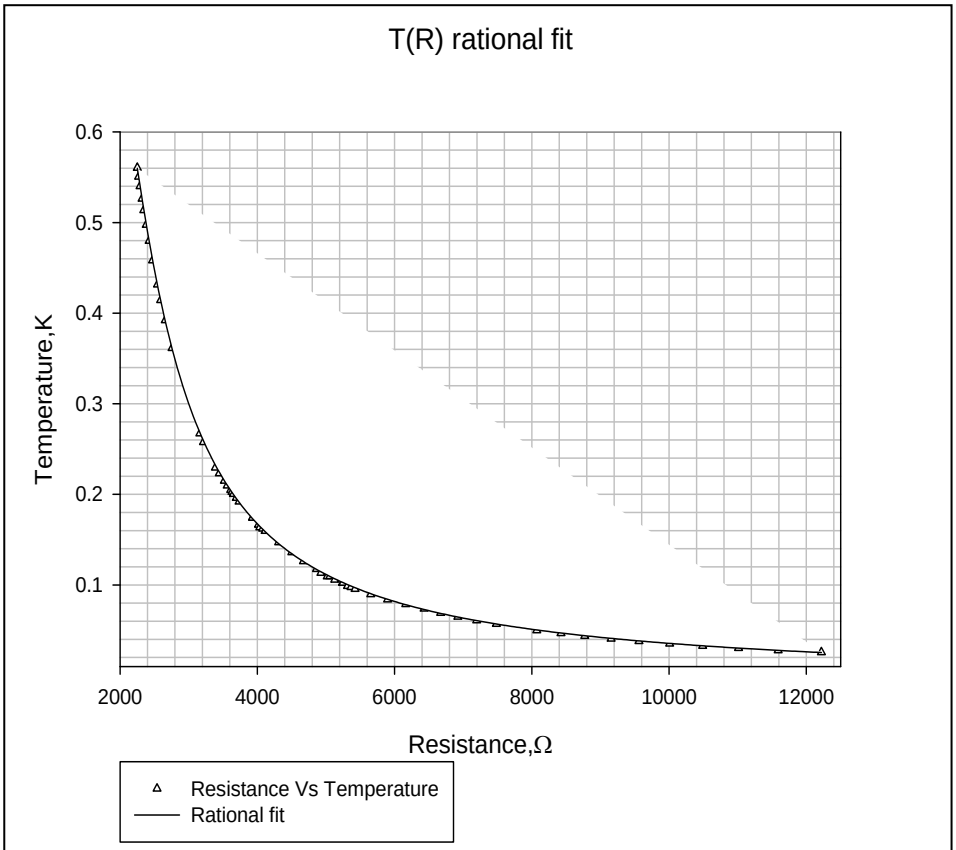

Fig. 54 Rational fit for T(R) dependence

The fitting function (Fig.54):
T(R)=(a+b*R+c*R^2+d*R^3)/(1+e*R+f*R^2+g*R^3),
a=-0.1258
b=2.0000e-4
c=-1.9590e-8
d=4.2671e-13
e=-1.2000e-3
f=4.8163e-7
g=-3.9302e-11

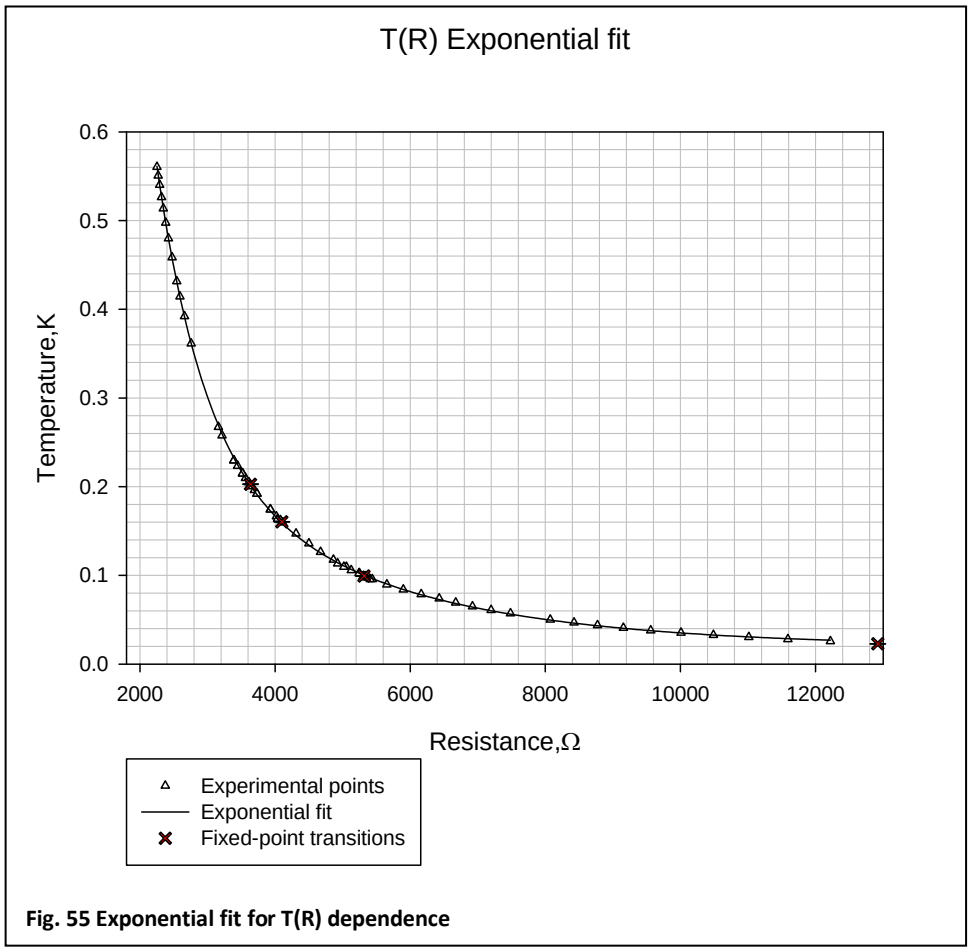

Fig. 55 Exponential fit for T(R) dependence

The fitting function (Fig.55):
f=y0+a*exp(-b*x)+c*exp(-d*x)+g*exp(-h*x),
y0=0.0197
a=0.4636
b=0.0003
c=12.1819
d=0.0014
g=-4.5872
h=0.0014

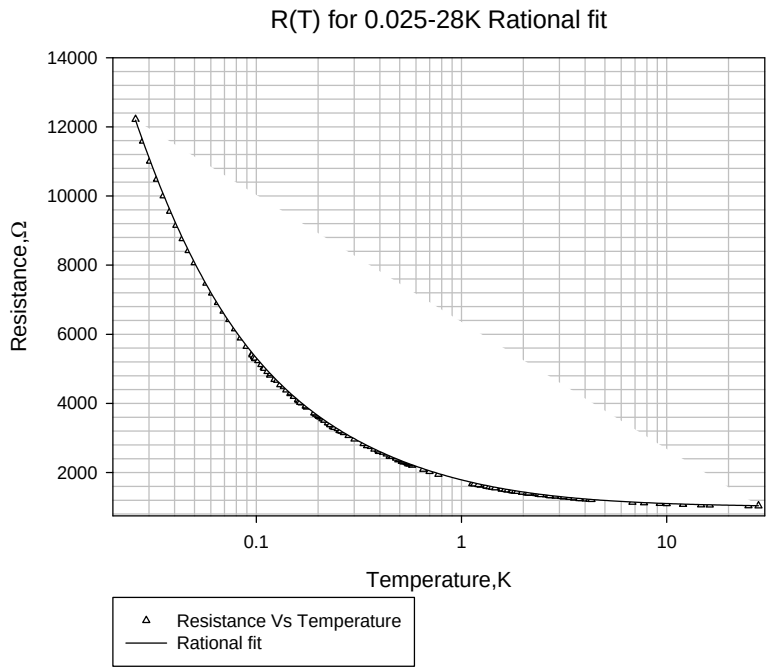

Fig. 56 RCW575 Dale chip performance in the range of 0.025-28K

The fitting function (Fig. 56):
R=(a+b*T+c*T^2)/(1+d*T+e*T^2+f*T^3),
a=43279.2290
b=427330.2061
c=317147.5039
d=126.4081
e=312.8131
f=0.0715

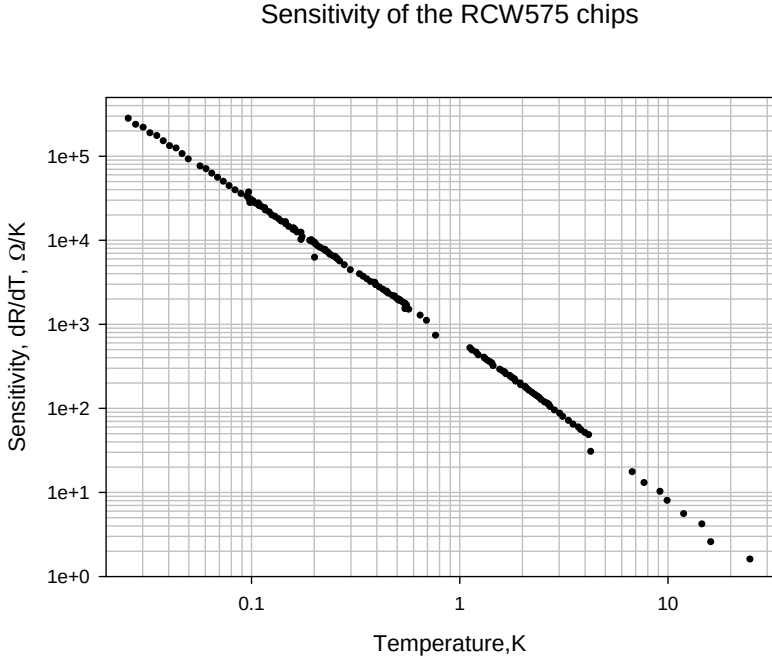

Fig. 57 Sensitivity of RCW575 chips

Conclusion

This work presents a detailed review of modern thermometry below 1K. The main emphasis was made on the recent progress in ^{3}He melting curve thermometry, superconducting fixed-point devices and resistance thermometry which were used in our experiments. The recently proposed novel methods, such as Coulomb blockade and Shot-noise thermometry as well as conventional primary methods, the nuclear orientation and Johnson noise thermometry, were also analyzed in the introductory part of the thesis.

In spite of recently developed nanofabricated primary thermometers, such as Coulomb blockade and shot noise devices, ^{3}He thermometer for almost 40 years serves as the compromise between reliability, accuracy and convenience. It is based on the $P_m(T)$ dependence for a ^{3}He two-phase mixture and defines the current provisional low-temperature scale, PLTS-2000. Although, MCT is too complicated for routine measurements, it can be utilized as a secondary standard for practically used resistance sensors.

Resistance thermometry and especially RuO_2 sensors are known to be the most suitable and popular for temperature measurements below 1K. They can operate down to 10-20mK, have a good reproducibility for the sensors from the same batch, moderate magnetoresistance and low price. At the same time, commercially available uncalibrated resistance thermometers cost about several hundred dollars for a bare chip whereas calibration increases their price up to one order.

In experimental part of the work, temperature measurement in a range from 600mK down to 6mK was carried out by three separate thermometers: ^{3}He melting curve thermometer, SRM 768 Fixed-point device and RuO_2 resistance thermometers of various design and packaging. A number of precautions were fulfilled in order to provide a proper performance for the thermometers such as magnetic shielding of FPD and electrical grounding and shielding for resistance sensors. A new perspective RuO_2 Dale RCW575-based resistance thermometer for application from several Kelvin down to 15mK was developed. The sensor can be also used even beyond this range up to 30K with a reduced efficiency. Low price, reliable thermal contact, ease of packaging and reproducibility for the sensors from the same batch make it a very convenient thermometer means for routine measurements. The thermometer was calibrated against ^{3}He melting curve thermometer and SRM-768 Fixed-point device. Calibration acquired by these two methods coincided in the whole range of measurement within error bars. As a result, our sensor can be used in a wide spectrum of low-temperature laboratories and successfully substitute available commercial resistance thermometers.

References

[1]. B. W. Mangum, G. T. Furukawa, Guidelines for Realizing the International Temperature Scale of 1990 (ITS-90)

[2]. R.L. Rusby, B. Fellmuth, J. Engert, W.E. Fogle, E.D. Adams, L. Pitre, M. Durieux, Realization of the ^{3}He Melting Pressure Scale, PLTS-2000, Journal of low temperature physics – 2007 – vol.149 – p.156 - 175

[3]. B.I.Verkin, Refrigeration and thermometry at low and ultra-low temperatures, Kiev, Naukova Dumka, 1987 (in Russian)

[4].J.Pekola, Trends in thermometry, Journal of low temperature physics – 2004 – vol. 135, nos.5/6 – p.723-744

[5]. E.D.Adams, The ^{3}He Melting Curve and Melting Pressure Thermometry, Progress in Low Temperature Physics – 2005 – vol.XV – p.423 – 45

[6]. R.L. Rusby, M.Durieux, A.L. Reesink, R.P.Hudson, G.Schuster, M.Kuhne, W.E.Fogle, R.J. Soulen, E.D. Adams, Journal of Low Temperature Physics – 2002 – vol.126 – Nos. 1/2 – p.633-642

[7]. R. Rusby, D. Head, D. Cousins, S. Schöttl, H. Godfrin, Yu.M. Bunkov, R.E. Rapp, F. Gay, M. Meschke, C. Lusher, J. Li, B. Cowan, J. Saunders, A. Casey, Dm. Shvarts, V. Mikheev, J. Pekola, K. Gloos, P. Hernandez, S. Triquenaux, M. de Groot, A. Peruzzi, R. Jochemsen, A. Chinchure, E. van Heumen, G.E. de Groot,W. Bosch, F. Mathu, J. Flokstra, D. Veldhuis, Y. Hermier, L. Pitre, A. Verge, F. Benhalima, B. Fellmuth, J. Engert, EU dissemination of the provisional ultra-low-temperature scale, PLTS-2000, Physica B – 2003 – vol. 329-330, p.1564-1565

[8]. J. Fischer and B. Fellmuth, Temperature metrology, Reports on Progress in Physics – 2005 – vol.68 – p.1043–1094

[9]. F.Pobell, Matter and Methods at Low Temperatures, 3rd rev. and exp. ed, Springer Verlag, 2007

[10]. W.Ni, J.S. Xia, E.D. Adams, P.S.Haskins, J.E.McKisson, ^{3}He Melting Pressure temperature Scale Below 25mK, Journal of Low Temperature physics – 1995 – vol.99 – Nos.1/2 – p.167 - 182

[11]. J.Fischer, M.de Podesta, K.D.Hill, M.Moldover, L.Pitre, R.Rusby, P.Steur, O.Tamura, R.White, L.Wolber, Present estimates of the Differences between thermodynamic temperatures and the ITS-90, International Jornal of Thermophysics – 2011 – vol.32 – p.12-25

[12]. J. Engert, B. Fellmuth and K.Jousten, A new ^{3}He vapour-pressure based temperature scale from 0.65 K to 3.2 K consistent with the PLTS-2000, Metrologia – vol.44 – p.40

[13]. W. D. Brewer, Recent developments in low-temperature nuclear orientation, Reports on Progress in Physics – 1990 – vol.53 – p.483 - 548

[14]. O.V.Lounasmaa, Experimental principles and methods below 1K, Academic press, London and New York, 1974

[15]. D. R. White, R. Galleano, A. Actis, H. Brixy, M. De Groot, J. Dubbeldam, A. L. Reesink, F. Edler, H. Sakurai, R. L. Shepard and J. C. Gallop, The status of Johnson noise thermometry, Metrologia, 1996 – vol. 33 – p.325-335

[16]. Kamper R. A., Zimmerman J. E., Noise Thermometry with the Josephson Effect, Journal of Applied Physics – 1971 – vol.42 – p.132 - 136

[17]. S. Menkel, D.Drung, C.Aumann and T.Schurig, A resistive d.c. SQUID noise thermometer, Applied Superconductivity – 1998 - Vol. 6 - Nos 7±9 - pp. 417±422

[18]. A.Webb, R.P.Giffard, and J.C.Wheatley, Noise thermometry at ultralow temperatures, Journal of Low temperature physics – 1973 - vol.13 - #3/4 – p.383 - 429

[19]. J. Li, V.A. Maidanov, H. Dyball, C.P. Lusher, B.P. Cowan, J. Saunders, Current sensing noise thermometry for millikelvin temperatures using a DC SQUID preamplifer, Physica B - 2000 – vol.280 – p.544 – 545

[20]. J. Engert, J. Beyer, D. Drung, A. Kirste, D. Heyer, A. Fleischmann, C. Enss and H.-J. Barthelmess, Practical noise thermometers for low temperatures, 25th International Conference on Low Temperature Physics (LT25), Journal of Physics: Conference Series – 2009 – vol.1501 - 012012

[21]. A.Netsch, E.Hassinger, C.Enss and A.Fleischmann, Novel, Non-contact Noise Thermometer for milli-kelvin temperatures, Low Temperature Physics: 24th International Conference on Low Temperature Physics – 2006

[22]. J.P.Pekola, K.P.Hirvi, J.P.Kauppinen, and M.A.Paalanen, Thermometry by arrays of tunnel junctions, Physical Review Letters – 1994 – vol.73 - #21 – p.2903 – 2906

[23]. T.Bergsten, C.Tord, P.Delsing, A fast primary Coulomb blockade thermometer, Applied physics letters – 2001 – vol.78 – issue 9 – p.1264 - 1266

[24]. Sh. Farhangfar, R. S. Poikolainen, D. S. Golubev , A. D. Zaikin, and J. P. Pekola, Coulomb blockade in one-dimensional arrays of high-conductance tunnel junctions, Physical Review B – 2001 – vol. 63 – p.075309

[25].T.Holmqvist, J.Pekola, M.Meschke, Influence of Environment on Tunneling Thermometry, Journal of Low Temperature Physics – 2009 – vol.154 – 172 – 178

[26]. http://www.aivon.fi, general CBT-brochure

[27].J. P. Kauppinen, K. T. Loberg, A. J. Manninen, and J. P. Pekola, Coulomb blockade thermometer: Tests and instrumentation, Review of scientific instruments – 1998 – vol.69,#12 – p.4166 - 4175

[28]. E. Isosaari, T. Holmqvist, M. Meschke, M. Heinonen, and J.P. Pekola, Thermometry by micro and nanodevices, The European Physical Journal Special Topics – 2009 – vol.172 – p.323 - 332

[29]. J.Pekola, T.Holmqvist, and M. Mescke, Primary Tunnel Junction Thermometry, Physical Review Letters – 2008 – vol.101 – p.206801

[30]. J.P.Pekola, J.K.Suoknuuti, J.P.Kauppinen, M.Weiss, P.v.d.Linden, and A.G.M.Jansen, Coulomb Blockade Thermometry in the Milli-Kelvin Temperature range in High Magnetic Fields, Journal of Low Temperature Physics – 2002 – Nos.5/6 – p.263 – 269

[31]. http://www.aivon.fi

[32]. L.Spietz, K.W.Lehnert, I.Siddiqi, R.J.Schoelkopf, Primary Electronic Thermometry Using the Shot Noise of a Tunnel Junction, Science – 2003 – vol.300 – p.1929-1932.

[33]. L.F.Spietz, The shot noise thermometer, Ph.D. thesis, Yale University, 2006, not published

[34]. L.Spietz, R.J.Schoelkopf, Shot noise thermometry down to 10mK, Applied physics letters – 2006 – vol.89 – 183123

[35]. L.Spietz, W.Tew, R.J.Schoelkopf, Systematic errors in shot noise thermometer measurements, Conference on Precision Electromagnetic Measurements Digest -2008 – p.702-703

[36]. R.L. Rosenbaum, Y. Eckstein and J. Landau, Thermometry using the osmotic pressure of mixtures of ^{3}He in superfluid ^{4}He, Cryogenics – 1974 – vol.14 – issue 1 – p.21-24

[37]. R.C.Richardson, The Pomeranchuk effect, Reviews of Modern Physics – 1997 – vol.69 - #3 – p.683 - 690

[38]. A. N. Ganshin, V. N. Grigor'ev, V. A. Maidanov, A. A. Penzev, E. Ya. Rudavski , A. S. Rybalko, and E. V. Syrnikov , Low Temperature Physics – 2001 – vol.27 - #6 – p.509 - 510

[39]. Schuster, D. Hechtfischer, W. Buck, A. Hoffmann, Physica B – 1990 – vol.165, 166 – p.31-32

[40]. L. P. Roobol, P. Remeijer, C. M. C. M van Woerkens, W. Oekers, S. C. Steel, R. Jochemsen and G. Frossati, ^{3}He melting curves in high magnetic fields, Physica B – 1994 – vol. 194-196 – p.741-742

[41]. D. S. Greywall and P. A. Busch, ^{3}He-Melting-Curve Thermometry, Journal of Low Temperature Physics – 1982 - Vol. 46, Nos. 5/6, p.451-465

[42]. V.A. Mikheev, N. Masuhara, Th. Wagner, G. Eska, P. Mohandas and J. Saunders, Cylindrical pressure gauge, Cryogenics – 1994 – Vol. 34 #2 - p.167 - 168

[43]. M.Karhunen, ^{3}He melting-curve thermometry and thermometer, Licentiate thesis, University of Turku, 1994, not published

[44]. A. Sebedash, J. T. Tuoriniemi, S. Boldarev, E. M. Pentti and A. J. Salmela, Melting Pressure Thermometry for Dilute ^{3}He-^{4}He Mixtures, AIP Conference Proceedings – 2006 - Vol. 850 - Issue 1 – p.1591-1592

[45]. A.P. Sebedash, J.T. Tuoriniemi, S.T. Boldarev, E.M.M. Pentti, A.J. Salmela, Adiabatic Melting of ^{4}He Crystal in Superfluid ^{3}He at Sub-millikelvin Temperatures, Journal of Low Temperature Physics – 2007 – vol.148 – p.725–729

[46]. A. Sebedash, J. Tuoriniemi, E. Pentti, and A. Salmela, Improved Capacitive Melting Curve Measurements, Journal of Physics: Conference Series – 2009 - vol.150 – p.012043

[47]. Dm. Shvarts, A. Adams, C.P. Lusher, R. Korber, B.P. Cowan, P. Noonan, J. Saunders, V.A. Mikheev, A self-contained ^{3}He melting curve thermometer for dissemination of the new provisional low-temperature scale, Physica B – 2003 – vol.329–330 - 1566–1567

[48] C.T.Van Degrift, Tunnel diode oscillator for 0.001ppm measurements at low temperatures, Review of Scientific Instruments – 1975 – vol.46 - #5 – p.599 - 607

[49]. V. Keith and M.G. Ward, A recipe for sintering submicron silver powders, Cryogenics – 1984 – vol.24 – issue 5 – p.249 – 250

[50]. I.Shinkoda, ^{3}Helium Melting Curve Thermometer, Master Degree Thesis – University of British Columbia – 1983, not published

[51]. J. Pollanen, H. Choi, J.P. Davis, B.T. Rolfs and W.P. Halperin, Low Temperature thermal resistance for a new design of silver sinter heat exchanger, Journal of Physics: Conference Series – 2009 – vol.150 – p.012037

[52]. Yu.N. Ovchinnikov, B.I. Ivlev, R.J.Soulen Jr., J.H. Claassen, W.E. Fogle, J.W. Colwell, Temperature and magnetic field dependence of the induced magnetization in macroscopic samples due to proximity effect, Physical Review B – 1997 – vol.56 - #14 – 9036 - 9051

[53]. J.H. Colwell, W.E. Fogle and R.J. Soulen Jr, LT-17 (Contributed Papers) – 1984 – p.395 – 396.

[54]. R.A.Buhrman and W.P.Halperin, The Elimination of Supercooling in Superconductors by the Proximity Effect: New Bounds on T_c for Mg, Ag, And Au, Journal of Low Temperature Physics – 1974 – vol.16 – Nos.5/6 – p.409 - 415

[55]. R.J.Soulen Jr., R.B. Dove, SRM 768: Temperature Reference Standard for Use below 0.5K, NBS, 1979

[56]. A.J.Storm, W.A.Bosch, M.J. de Groot, R. Jochemsen, F. Mathu, G.Nieuwenhuys, A new superconducting reference device for thermometry below 100mK, Physica B – vol.284 - 288 – p.2008 - 2009

[57]. SRD1000 System User's Manual, version: 06.02.2006

[58]. http://www.xs4all.nl/~hdleiden/srd1000/

[59]. W.A. Bosch, J.J.M. van der Hark, J.Pöll, and R.Jochemsen, SRD1000 with improved reference points for thermometry, Journal of Low Temperature Physics – 2005 – vol.138 – Nos. 3/4 – p. 935 - 940

[60]. S.Shöttl, R.Rusby, H.Godfrin, M.Meschke, V.Goudon, S.Triqueneaux, A.Peruzzi, M.J.de Groot, R.Jochemsen, W.Bosch, Y.Hermier, L.Pitre, C.Rives, B.Fellmuth and J.Engert, Evaluation of SRD1000 Superconductive Reference Devices, Journal of Low Temperature Physics – 2005 – vol.138 – Nos.3/4 – p.941-946

[61]. http://www.leidencryogenics.com/accessories.php

[62]. N. Samkharadze, A. Kumar, G. A. Csáthy, A New Type of Carbon Resistance Thermometer with Excellent Thermal Contact at Millikelvin Temperatures, Journal of Low Temperature Physics – 2010 – vol.160 – p.246-253

[63]. R.G. Goodrich, Donavan Hall, Eric Palm and Tim Murphy, Magnetoresistance below 1 K and temperature cycling of ruthenium oxide– bismuth ruthenate cryogenic thermometers, Cryogenics – 1998 – vol.38 – p.221–225

[64]. D. Zak, A. Dziedzic, A. Kolek, A. W. Stadler, K. Mleczko, P. Szałanski and Z.Zawislak, Meas.Sci.Technol. – 2006 – vol.17 – p.22-27

[65]. http://www.lakeshore.com/temp/sen/rrtdts.html

[66]. M. Barucci, G. Bianchini, E. Gottardi, I. Peroni, G. Ventura, Dielectric properties of Stycast 1266 over the 0.07±300 K temperature range, Cryogenics - 1999, vol.39 – p.963 – 966

[67]. S. S. Courts and J. K. Krause, A Commercial Ruthenium Oxide Thermometer for Use to 20 Millikelvin, CP985, Advances in Cryogenic Engineering: Transaction of the Cryogenic Engineering Conference – CEC- 2008 – vol.53 – p.947 – 954

[68]. http://www.lakeshore.com/temp/sen/rrtdoi.html

[69].AVS-47 AC-resistance bridge, Instruction manual, 1996

[70]. R.Richardson, E.Smith, Experimental Techniques in Condensed Matter Physics at Low Temperatures, Addison-Wesley Publishing Company Inc., 1988

[71]. C. J. Yeager and S. S. Courts, A Review of Cryogenic Thermometry and Common Temperature Sensors, IEEE SENSORS JOURNAL – 2001 – vol.1, # 4 – p.352-360

[72]Professional address: P.L.Kapitza Institute for Physical Problems, 2 Kosygina str., 119334, Moscow, Russia

[73]. Paroscientific Inc., http://www.paroscientific.com/pdf/2000.pdf

[74]. M.P.Malkov, Reference book on cryogenics, Energoatomizdat, Moscow, 1985 (in Russian)